Physical, chemical and electrical properties of experimental composite materials based on amorphous calcium phosphate

Par, Matej

University of Zagreb

School of dental medicine

Matej Par

PHYSICAL, CHEMICAL AND ELECTRICAL PROPERTIES OF EXPERIMENTAL COMPOSITE MATERIALS BASED ON AMORPHOUS CALCIUM PHOSPHATE

DOCTORAL THESIS

Zagreb, 2017.

University of Zagreb

School of dental medicine

Matej Par

PHYSICAL, CHEMICAL AND ELECTRICAL PROPERTIES OF EXPERIMENTAL COMPOSITE MATERIALS BASED ON AMORPHOUS CALCIUM PHOSPHATE

DOCTORAL THESIS

Supervisors:
prof. dr. sc. Zrinka Tarle
assist. prof. dr. sc. Ozren Gamulin

Zagreb, 2017.

University of Zagreb

Stomatološki fakultet

Matej Par

FIZIKALNA, KEMIJSKA I ELEKTRIČNA SVOJSTVA EKSPERIMENTALNIH KOMPOZITNIH MATERIJALA TEMELJENIH NA AMORFNOM KALCIJEVOM FOSFATU

DOKTORSKI RAD

Mentori:
prof. dr. sc. Zrinka Tarle
doc. dr. sc. Ozren Gamulin

Zagreb, 2017.

This thesis was made at the Department of Endodontics and Restorative Dentistry, School of Dental Medicine, University of Zagreb, Croatia; Department of Physics and Biophysics, School of Medicine, University of Zagreb, Croatia; Institute of Physics, University of Zagreb, Croatia and at the Glass Laboratory (now Laboratory for Functional Materials), Ruđer Bošković Institute, Zagreb, Croatia.

The research was supported by the project led by prof. dr. Zrinka Tarle, "Evaluation of new bioactive materials and procedures in restorative dental medicine" (Project 08/31) funded by the Croatian Science Foundation.

Commission for evaluation of doctoral thesis:

prof. dr. sc. Vlatko Pandurić
prof. dr. sc. Andrea Moguš-Milanković
assist. prof. dr. sc. Danijela Marović
assist. prof. dr. sc. Eva Klarić Sever
prof. dr. sc. Silvana Jukić Krmek

Commission for doctoral thesis defense:

prof. dr. sc. Vlatko Pandurić
prof. dr. sc. Andrea Moguš-Milanković
assist. prof. dr. sc. Danijela Marović
assist. prof. dr. sc. Eva Klarić Sever
prof. dr. sc. Silvana Jukić Krmek
assist. prof. dr. sc. Bernard Janković

Date of thesis defense: Sep 27th 2017

Supervisors: prof. dr. sc. Zrinka Tarle
Department of Endodontics and Restorative Dentistry
School of Dental Medicine
University of Zagreb
Croatia

assist. prof. dr. sc. Ozren Gamulin
Department of Physics and Biophysics
School of Medicine
University of Zagreb
Croatia

Lector of English language: Domagoj Valjak, prof.

Lector of Croatian language: Sanela Vrbos Moslavac, prof.

The dissertation contains: 111 pages
21 figures
10 tables
1 CD

SUMMARY

Composite materials with amorphous calcium phosphate (ACP) release remineralizing ions that can be deposited in demineralized dental hard tissues and thus aid in the prevention of secondary caries. The main shortcomings of this class of experimental biomaterials are insufficient mechanical properties and fast degradation in the oral environment. The ACP-composites can be admixed with reinforcing fillers to improve mechanical properties and durability

The aim of this study was to investigate various properties of experimental ACP-composites that are important for their clinical applicability. Specifically, the effect of 10 wt% of reinforcing fillers comprising of barium glass and silica on the degree of conversion (DC), depth of cure, optical properties, and temperature rise during light curing were investigated. Additionally, a novel approach using impedance spectroscopy was used to explore the polymerization kinetics and microstructural characteristics of ACP-composites.

ACP-composites attained very high DC (about 80%), and the DC was not considerably diminished by the addition of inert fillers. Curing efficiency at depth for ACP-composites was comparable to that of conventional composites, with depths of cure of 2-3 mm. Temperature rise that was produced during light curing of ACP-composites was no more harmful to dental pulp than that of conventional composites. Light transmittance of ACP-composites was in the range of conventional composites. Real-time light transmittance measurements were shown to provide useful information on polymerization kinetics. ACP-composites have shown different polymerization kinetics than the materials that contain only reinforcing fillers, with possible consequences on polymerization shrinkage and polymeric network structure. Impedance spectroscopy was demonstrated as a valuable tool for investigating various characteristics of ACP-composites. Impedance data used for describing the extent of polymerization correlated well with the DC data obtained by Raman spectroscopy. Kinetic parameters obtained by impedance measurements correlated well with light transmittance. Impedance measurements proved to be useful for quantifying the amount of water introduced to the composite by ACP fillers.

Keywords: amorphous calcium phosphate, remineralizing composite, degree of conversion, light transmittance, temperature, impedance spectroscopy

PROŠIRENI SAŽETAK

Svrha rada

Eksperimentalni kompozitni materijali temeljeni na amorfnom kalcijevom fosfatu (amorphous calcium phosphate – ACP) otpuštaju kalcijeve i fosfatne ione i omogućavaju remineralizaciju tvrdih zubnih tkiva. Po mehaničkim svojstvima i trajnosti zaostaju za komercijalnim kompozitnim materijalima zbog visokog udjela topljivih čestica ACP-a koje nisu silanizirane i ne mogu se povezivati sa smolastom matricom. Dodatkom ojačavajućih silaniziranih punila od barijevog stakla i silike moguće je poboljšati mehanička svojstva, bez negativnog učinka na otpuštanje iona i remineralizirajuća svojstva. Svrha ovog rada bila je ispitati svojstva važna za kliničku primjenjivost ACP-kompozita: stupanj konverzije i njegovu ovisnost o debljini sloja i trajanju svjetlosne aktivacije polimerizacije, svjetlosnu transmisiju i porast temperature tijekom polimerizacije. Dodatno, pomoću impedancijske spektroskopije ispitana su električna svojstva ACP-kompozita koja su omogućila detaljniji uvid u mikrostrukturu materijala.

Materijali i postupci

Kompozitni materijali pripremljeni su miješanjem smole temeljene na bisfenol-A-etilmetakrilatu te punila sastavljenog od 40% ACP i 10% ojačavajućih punila od barijevog stakla i silike u različitim omjerima. Svi sastojci kompozita pomiješani su u dvostruko asimetričnoj centrifugalnoj miješalici. Stupanj konverzije određen je Ramanovom spektroskopijom na cilindričnim uzorcima promjera 3 mm i visine 6 mm. Ramanovi spektri su prikupljeni neposredno nakon svjetlosne aktivacije polimerizacije tijekom 20 ili 40 s s površine i zatim nakon 24 sata s pet mjernih dubina: površina, 1 mm, 2 mm, 3 mm i 4 mm. Svjetlosna transmisija izmjerena je u vidljivom spektru tijekom svjetlosne aktivacije polimerizacije uzoraka promjera 6 mm i debljine 2 mm u stvarnom vremenu. Temperatura tijekom polimerizacije izmjerena je termočlankom T-tipa u stvarnom vremenu na uzorcima iste geometrije. Električna svojstva izmjerena su impedancijskom spektroskopijom pri fiksnoj frekvenciji od 1 kHz i u frekvencijskom rasponu od 0,05 Hz do 1 MHz tijekom 24 sata. Iz kompleksne impedancije izračunata je električna provodnost, a impedancijski spektri su analizirani modeliranjem ekvivalentnog kruga.

Rezultati

ACP-kompoziti su postigli visok stupanj konverzije (oko 80%), a učinak ojačavajućih punila na stupanj konverzije bio je zanemariv. Učinkovitost polimerizacije ACP-kompozita u ovisnosti o debljini sloja bila je usporediva onoj kod konvencionalnih kompozita, s dubinom polimerizacije od 2-3 mm. Porast temperature tijekom svjetlosne aktivacije polimerizacije ACP-kompozita u rasponu je vrijednosti izmjerenih kod komercijalnih kompozita. Svjetlosna transmisija ACP-kompozita bila je također u rasponu konvencionalnih kompozita. Mjerenja svjetlosne transmisije u stvarnom vremenu omogućila su prikupljanje korisnih informacija o kinetici polimerizacije. ACP-kompoziti su pokazali drukčiju kinetiku polimerizacije od konvencionalnih materijala koji sadržavaju samo ojačavajuća punila, s mogućim posljedicama na razvoj polimerizacijskog skupljanja i strukturu polimerne mreže. Demonstrirana je primjenjivost impedancijske spektroskopije kao vrijednog alata za ispitivanje različitih svojstava ACP-kompozita. Pomoću promjene električnih svojstava tijekom polimerizacije opisana je kinetika polimerizacije, a rezultati su dobro korelirali s vrijednostima stupnja konverzije izmjerenim Ramanovom spektroskopijom. Kinetički parametri dobiveni mjerenjem električnih svojstava pokazali su dobru korelaciju sa svjetlosnom transmisijom. Mjerenja impedancije su se pokazala korisnim za kvantifikaciju količine vode unesene ACP-punilima u kompozitni materijal.

Zaključak

Istraživana svojstva eksperimentalnih ACP-kompozita (stupanj konverzije, dubina polimerizacije, svjetlosna transmisija, porast temperature tijekom polimerizacije) povoljna su za njihovu potencijalnu kliničku primjenu. Daljnjim istraživanjima potrebno je poboljšati mehanička svojstva kako bi se ACP-kompoziti mogli koristiti kao restaurativni materijali.

Ključne riječi: amorfni kalcijev fosfat, remineralizirajući kompozit, stupanj konverzije, svjetlosna transmisija, temperatura, impedancijska spektroskopija

The list of abbreviations

ACP	Amorphous calcium phosphate
ANOVA	Analysis of variance
Bis-EMA	Ethoxylated bisphenol-A dimethacrylate
Bis-GMA	Bisphenol-A glycidyl dimethacrylate
CCD	Charge-coupled device
CNLLSQ	Complex non-linear least square
CPE	Constant phase element
CQ	Camphorquinone
DC	Degree of conversion
DX511	Proprietary modified urethane dimethacrylate resin
EBPADMA	Ethoxylated bisphenol-A dimethacrylate
FTIR	Fourier-transform infrared
FT-Raman	Fourier-transform Raman
HEMA	2-hydroxyethyl methacrylate
IS	Impedance spectroscopy
LED	Light-emitting diode
Lucirin TPO	Ethyl-2, 4, 6 trimethylbenzoylphenyl phosphinate
MDPB	12-methacryloyloxydodecylpyridinium bromide
Nd:YaG	neodymium-doped yttrium aluminum garnet
PET	polyethylene terephthalate
PPD	1-phenyl-1,2-propanedione
SEM	Scanning electron microscope
TCD-DI-HEA	Bis-(acryloyloxymethyl)tricyclo(5.2.1.02,6)decane
TEGDMA	Triethylenglycol-dimethacrylate
UDMA	Urethane dimethacrylate

CONTENTS

1. Introduction 1

1.1 Dental composite materials 2

1.1.1 Composition 2

1.1.2 Properties 4

1.1.3 Composite restorations and secondary caries 6

1.2 Bioactive composite materials 7

1.2.1 Antibacterial composites 7

1.2.2 Remineralizing composites 7

1.3 Remineralizing composite materials based on amorphous calcium phosphate 8

1.3.1 Bioactive properties, ion release 9

1.3.2 Degree of conversion 9

1.3.3 Mechanical properties 10

2. General and specific aims 11

3. Conversion and temperature rise of remineralizing composites reinforced with inert fillers 13

3.1 Abstract 14

3.2 Introduction 15

3.3 Materials and methods 17

3.3.1 Composite materials 17

3.3.2 Degree of conversion 18

3.3.3 Temperature rise 19

3.3.4 Scanning electron microscopy (SEM) 20

3.3.5 Statistical analysis 20

3.4 Results 20

3.5 Discussion 25
3.6 Conclusions 29
3.7 Acknowledgments 30
3.8 References 30

4. Light transmittance and polymerization kinetics of amorphous calcium phosphate composites 35
4.1 Abstract 36
4.2 Introduction 37
4.3 Materials and methods 39
4.3.1 Composite materials 39
4.3.2 Light transmittance and temperature 41
4.3.3 Degree of conversion 42
4.3.4 Scanning electron microscopy (SEM) 42
4.3.5 Statistical analysis 43
4.4 Results 43
4.5 Discussion 50
4.5.1 The effect of composition on light transmittance 50
4.5.2 Polymerization kinetics 51
4.6 Conclusions 54
4.7 Acknowledgments 54
4.8 References 55

5. Impedance changes during setting of amorphous calcium phosphate composites 59
5.1 Abstract 60
5.2 Introduction 61
5.3 Materials and methods 62
5.3.1 Composite materials 62
5.3.2 Impedance spectroscopy 64

5.3.3 Gravimetric analysis 64
5.3.4 Light transmittance 65
5.3.5 Scanning electron microscopy (SEM) 65
5.3.6 Raman spectroscopy 65
5.3.7 Statistical analysis 66
5.4 Results 66
5.4.1 Short-term setting - impedance measurements at fixed frequency 69
5.4.2 Long-term setting - impedance measurements in a wide frequency range 70
5.4.3 SEM studies 73
5.5 Discussion 74
5.5.1 Short-term setting and kinetics of the polymerization reaction 74
5.5.2 Long-term setting 76
5.5.3 Degree of conversion and correlation with change of resistivity 78
5.6 Conclusions 79
5.7 Acknowledgments 80
5.8 References 80

6. General discussion 84

7. Conclusions 96

8. Literature 98

9. Curriculum vitae 109

1. INTRODUCTION

An extensive research in the field of dental composites in past decades has led to the development of sophisticated materials which are suitable for any restorative indication [1]. Versatility of composites and the current trend of abandoning amalgam as a restorative material have made them an indispensable part of everyday clinical work. Mechanical properties of contemporary composites are comparable to that of amalgam, and their aesthetic properties greatly surpass all other direct restorative materials [1, 2]. However, the shortcomings inherent to the composite material, arising from polymerization shrinkage, have not yet been completely overcome. Although mitigated to a certain extent by immense improvements in the technology of dental adhesives, the polymerization shrinkage and its consequences still remain one of the main causes for the failure of composite restorations [3]. Besides some problems that do not directly jeopardize the service life of a restoration (e.g. postoperative sensitivity, marginal staining, enamel fractures), the major issue related to polymerization shrinkage is the development of secondary caries [4]. The approaches to address the issue of secondary caries range from developing new low-shrinkage monomer systems [5, 6] and introducing composites with antibacterial agents [7] to the investigations of bioactive, ion-releasing composites with remineralizing properties [8]. Such materials have the potential to remineralize dental hard tissues adjacent to the restoration and possibly even seal the marginal gap with the hydroxyapatite precipitate [9]. Although the remineralizing composites are still in the experimental phase, they appear very promising and have a great potential to reach clinical applicability in the future.

1.1 Dental composite materials

1.1.1 Composition

Composite materials are generally composed of inorganic filler particles dispersed in a polymer matrix. The filler particles are coated with silane which enables chemical bonding of their surface with the methacrylate network [10]. Filler particles are most commonly composed of various types of glass, silicon dioxide (silica) and zirconium oxides [2]. A wide variety of particle geometries and size distributions allows the formulation of composite materials with distinctive properties and clinical indications [11]. For example, material viscosity, mechanical properties and handling characteristics can be tailored by adjusting the filler load and particle size distribution. The wide range of existing composites materials makes it difficult to classify them into groups with similar properties. The common

classification relies on the filler size, but it is not indicative of material properties, as high heterogeneity of properties exists within each material category [2]. In the classification by the filler size, the only distinguishable material class consists of microfill composites, characterized by significantly lower mechanical properties than other classes of contemporary composites [12].

The development of dental composites included a progressive decrease in filler size, resulting in contemporary hybrid composites containing filler particles of two distinguishable orders of magnitude – the smaller particles of about 40 nm and the larger of about 1 μm [1]. The terms "microhybrid", "submicrohybrid" and "nanohybrid" have little practical relevance and are more related to the advertising and marketing purposes than to the actual material properties. There are also "true" nanofill composites which are filled only with nano-sized particles [13]. However, they also contain both solitary nanoparticles and clusters of these particles, and, in regards to the particle size, they can be considered as hybrid. A relatively recent class of composites that appeared in the last decade, bulk-fill composites, features larger particles than those commonly present in contemporary composites [14, 15]. Thus the development of bulk-fill composites reversed the continuous trend of decreasing particle size in order to increase the translucency and improve the depth of cure [16].

Unlike the filler particle size, which experienced a considerable evolution since the inception of dental composites, the resin component has not changed much [17]. Despite the fact that many new promising monomer chemistries were introduced and investigated, practically all of the commercially available composites are still based on methacrylates [18]. Even if some of the novel monomer systems are used (e.g. ormocers or dimer-acid monomers), they still have to be combined with the methacrylates-based resin [19]. The most common base monomers are bifunctional methacrylates: Bis-GMA, Bis-EMA, and UDMA, while TEGDMA is the most common diluent monomer [17]. A monofunctional hydrophilic monomer HEMA is sometimes added to control the resin hydrophilicity and polymer network structure, although it is more commonly found in adhesive systems [20]. An alternative low-shrinkage monomer system based on siloranes appeared promising but was never successfully commercialized [6]. Another alternative low-shrinkage monomer is based on dimer-acid and is admixed to methacrylate monomers in one brand of commercial composites [21]. Other commercially employed "modified" monomers include the modified UDMA, termed DX511, and urethane monomer TCD-DI-HEA [1].

Most of the contemporary restorative composites are visible light-curable [22]. The classic photoinitiator system comprising of camphorquinone and a tertiary amine is still dominant, although some new photoinitiator chemistries are used as adjuncts to the camphorquinone-amine system [23]. Lucirin-TPO and PPD are used in very bright shades [24], and a germanium-based Ivocerin is used in one brand of bulk-fill composites [25].

Additional ingredients include inhibitor systems that improve composite's chemical stability and shelf life, photostabilizers for color stability, and pigments for fine-tuning of various composite shades.

1.1.2 Properties

Properties of a composite material are a function of its composition. Each compositional feature (filler type, load and surface treatment, particle geometry, resin composition, composite paste viscosity, photoinitiator system and its concentration, rheological properties, composite shade and optical properties) has an effect on final properties of the cured material [2]. Many of these features are inter-dependent, and their fine-tuning is essential for the formulation of a composite with optimal properties. A large number of adjustable compositional variables enable a diverse range of composites that can be found on the contemporary dental market.

Mechanical properties generally improve with higher filler load, thus highly filled composite pastes are stronger, stiffer, and tougher than flowable composites which contain less filler [26]. However, the relationship between the filler load and the mechanical properties is not as straightforward, since the increase of the filler load beyond a certain level might act to reduce mechanical properties [27]. In a study of 72 commercial composites, the threshold level was determined around 60 vol% and it was suggested that increasing the filler load beyond this value introduces more structural defects and, in turn, diminishes mechanical properties [2]. With regard to the mechanical properties, modern composites are no longer inferior to the amalgam, as both materials present comparable strength and toughness [1]. However, composite materials are subject to a slow degradation, as during the service life water penetrates the resinous matrix and hydrolyzes the siloxane bonds between the filler and resin [28]. Also, plasticization of the polymeric network contributes to the diminishment of mechanical properties [29]. The effects of water-induced degradation on the clinical success

or failure of a composite restoration are difficult to assess, but appear to be negligible in comparison to the clinically more relevant degradation of the restoration's adhesive interface [30, 31]. Considering the aging of the bonded restoration as a whole, a more detrimental effect of aging in water is exerted on the marginal seal than on the composite bulk itself. This leads to the issue of secondary caries, as will be presented in the next paragraph.

The degree of conversion (DC) is the ratio of C=C methacrylate bonds that were converted to C-C single bonds during polymerization and represents a fundamental property of a cured composite that influences all other properties [14, 26, 32, 33]. The DC of dental composites never reaches 100%, as diffusional limitations stop the polymerization reaction before all monomer molecules could be added to the polymeric network [34]. Thus the DC of conventional composites generally ranges from 50% to 80% [14, 35, 36]. Many factors affecting the DC pertain to either the material's composition (monomer composition, viscosity, filler load, and optical properties) or the curing conditions (curing unit type, output wavelength range, radiant energy, and layer thickness) [37]. Most of the monomer conversion occurs during light curing. However, a considerable part of the polymerization continues to occur "in the dark", after the light curing is over [38]. This post-cure polymerization commonly completes within the 24 hours after curing, but in some materials it may continue up to 7 days [25]. Due to the attenuation of the curing light passing through the composite, the DC of a composite layer is always heterogeneous to a certain extent [37]. Therefore, there is always a gradient of other properties throughout a composite restoration, which should be minimized in clinical work by assuring optimal curing conditions. A property inseparably linked to the DC is the polymerization shrinkage. Since the polymerization shrinkage is a linear function of the amount of consumed double bonds [39], the composites with higher DC shrink more and might create higher shrinkage stress [40]. The relationship between the DC and shrinkage stress is, however, very complex and depends on cavity configuration and the dynamic development of elastic modulus during the light curing [41-43]. Thus high DC values only indicate the possibility of increased shrinkage stress but do not necessarily imply it.

Optical properties of dental composites are crucial for their aesthetic appearance and also for the curing efficiency through a composite layer [16]. The amount of transmitted light (light transmittance) can be controlled by adjusting the filler size distribution and the refractive index mismatch between the filler and the resin [44]. The light transmittance commonly

changes as the composite polymerizes, which can affect the aesthetic properties in clinical work but can also be used to monitor the polymerization kinetics in laboratory studies [45].

Water sorption and solubility of dental composites depend on the filler/resin ratio, as the organic part of the composite has the affinity to absorb water and can release unreacted monomer molecules [46]. The water sorption of composites can be adjusted by balancing the amount of hydrophobic and hydrophilic monomers, as well as the filler load [47]. Water sorption is accompanied with a small volumetric expansion, which is commonly smaller than the polymerization shrinkage and thus unable to compensate for its effects.

Electrical properties of composite materials are not routinely investigated, as they lack direct clinical relevance. Unlike amalgam, composites are electrical insulators and cannot produce an electrical stimulus to the dental pulp. However, investigating electrical properties through impedance spectroscopy can be useful for gaining an array of useful information about composite materials [48, 49].

1.1.3 Composite restorations and secondary caries

Secondary caries occurs at the tooth/restoration interface and has traditionally been related to the phenomenon of marginal microleakage [50]. The classical etiopathogenesis of secondary caries includes the formation of a gap which is penetrated by oral microorganisms and allows the inflow of substrates needed for microbial acidogenic activity [51]. Due to the absence of buffering systems, the pH value inside the gap decreases and causes mineral loss that ultimately leads to caries. Although the cause-and-effect relationship between the microleakage and the occurrence of secondary caries has recently been challenged [52], there is no question that sufficiently large marginal gap becomes colonized by acidogenic bacteria and plays a role in the development of the recurrent (secondary) caries [51].

Secondary caries has often been quoted as one of the main reasons for the failure of composite restorations [1, 3, 52]. This fact motivates the development of various strategies to create composites with anticariogenic activity. This can be attained by two different approaches: lowering the polymerization shrinkage or formulating composites with bioactive properties. While low-shrinkage composites aim to prevent secondary caries by reducing the marginal leakage, the bioactive composites aim to mitigate the consequences of the leakage after it occurs, as no composite restoration demonstrates a perfect marginal sealing [53]. The

term “bioactive composites” encompasses a very heterogeneous group of materials that show either antimicrobial or remineralizing activity [54]. Also, these two effects can be combined in a single material [55].

1.2 Bioactive composite materials

1.2.1 Antibacterial composites

Composite materials tend to accumulate more bacterial plaque than other restorative materials due to several causes: surface roughness, the stimulatory effect of some methacrylate monomers on bacterial growth, and the lack of antibacterial effect [56]. This issue is currently being addressed by investigations of experimental antibacterial composites. Various antibacterial compounds were examined as additives to composites, such as chlorhexidine, fluoride, silver nanoparticles, zinc oxide nanoparticles, quaternary ammonium compounds, and MDPB monomer [1, 54]. The antimicrobial composites seem promising, but their effect lasts for a limited amount of time as most of the antibacterial compounds become depleted within several months.

1.2.2 Remineralizing composites

Remineralizing composites feature soluble calcium phosphate fillers and sufficient hydrophilicity to allow the diffusion of calcium and phosphate ions from the cured material [57]. The released ions can be incorporated into the tooth structure to remineralize it [58], or, alternatively, they can be deposited in the form of the hydroxyapatite layer on the composite surface and contribute to the sealing of the marginal gap [9]. Various calcium phosphates have been successfully admixed to methacrylate resins to produce remineralizing composites. Monocalcium phosphate [59], dicalcium phosphate [60], tricalcium phosphate [61], tetracalcium phosphate [62], amorphous calcium phosphate (ACP) [63], and hydroxyapatite [64] are all being investigated as fillers in bioactive composites. The solubility of a certain calcium phosphate depends on its composition and environmental conditions [65]. As the solubility of calcium phosphates typically increases at lower pH values, this group of materials may offer a “smart” response to pH fluctuations during the day [62]. This would

allow the activation of the ion release during the acid attack and the preservation of the remineralizing ions reserve when the ion release is not needed.

1.3 Remineralizing composite materials based on amorphous calcium phosphate

ACP is a calcium orthophosphate salt that lacks the long-range crystalline order. Even though there is no long-range order of the crystalline lattice, ACP appears to have a well-defined local structural unit known as the Posner's cluster, with the chemical composition of $Ca_9(PO_4)_6$, and the same stoichiometry as tricalcium phosphate [66]. ACP is thermodynamically unstable and susceptible to transformation into a more stable crystalline structure of hydroxyapatite [67]. Depending on the solution pH, various other crystalline calcium orthophosphates may also form in addition to or instead of hydroxyapatite [68]. The transformation process includes a combination of ionic rearrangement, ionic clusters rearrangement and dissolution-reprecipitation process [69]. The latter phenomenon is important for the bioactive effect of ACP, as it includes a gradual dissolution of solid ACP particles with the release of calcium and phosphate ions into its immediate environment, followed by the reprecipitation of these ions into hydroxyapatite on the surface of the ACP particles [70]. This process can be exploited in the experimental dental composites filled with ACP to provide them with the remineralizing ability [47].

Bioactive ACP-composites are based on similar resins and photoinitiator systems that are used in conventional composites [57]. In this regard, the only "new" ingredient is the ACP itself, as all other components (reinforcing fillers, resinous matrix, and photoinitiator system) are already commonly employed in commercial composites. Much investigation has been conducted on experimental ACP-based composites, evaluating the composition-structure-property relationship for different modifications of ACP fillers [71], filler particle size [72], silanization of filler surface [63], different resin compositions [73], addition of self-adhesive monomers [74], addition of reinforcement fillers [75], and transition to nano-sized ACP fillers [76].

The development of ACP- composites is still in an experimental phase. Until now, only a single commercial ACP-based material intended for use as an orthodontic adhesive had appeared on the dental market but was soon discontinued due to its poor mechanical properties [77]. There are currently no commercial ACP-containing composites available, but, as new investigations are performed, the base of knowledge continues to increase, and

the properties of ACP-composites are progressively refined. Continuing efforts in this field could lead to a clinically applicable material in the future.

1.3.1 Bioactive properties, ion release

The most distinguishable property of ACP-composites is their ion-releasing ability. This effect is a result of the metastability of the ACP phase which, in the aqueous environment, tends to release calcium and phosphate ions while converting into a more stable hydroxyapatite [65]. The concentration of calcium and phosphate ions reaches supersaturated levels with respect to hydroxyapatite, suggesting that the released ions can be spontaneously deposited in the demineralized tooth structure. In addition to multiple laboratory studies that reported high concentrations of released ions [8, 70, 72, 75], the ACP-composites were demonstrated to remineralize enamel in vitro [58] and in situ [78]. Also, the study that used the rat cavity model demonstrated the remineralizing effect and stimulation of the tertiary dentin formation by ACP-composites in vivo [79].

Although high concentrations of remineralizing ions are attainable, the ion-releasing effect only lasts for as long as the ACP-to-hydroxyapatite conversion takes place [80]. Thus the bioactive effect of early ACP-composites was limited to the maximum of several months [68]. By retarding the intracomposite ACP conversion, the ion release can be prolonged. This can be attained by stabilizing the ACP particles by zirconia [71]. Since the conversion of ACP is irreversible, the “recharging” ability, as seen in glassionomers, cannot be achieved. However, by introducing a novel resin that is capable of binding calcium and phosphate ions from externally applied remineralizing solution, ACP-composites capable of recharging have recently been developed [81]. This shows that combining several technologies may be used to achieve interesting synergistic effects in bioactive materials and warrants further studies.

1.3.2 Degree of conversion

ACP-composites typically reach DC values higher than those commonly found in commercial composites. DC values measured in ACP composites can reach up to 94% [82] and are probably due to the presence of unsilanized filler particles that do not form chemical bonds with the methacrylate network, thus allowing better mobility of the reaction medium

during polymerization [83]. Although beneficial for biocompatibility, high DC necessarily implies higher polymerization shrinkage that may have unwanted effects [84]. However, as the shrinkage stress depends both on the volumetric shrinkage and the dynamic development of the elastic modulus, decreasing the modulus or modifying the polymerization kinetics may mitigate negative consequences of high polymerization shrinkage [41]. It should be noted that the polymerization kinetics seems to be affected by the high amount of unsilanized ACP particles in the sense of diminishing the effect of autoacceleration and decreasing the overall reaction rate [85]. This may be beneficial for marginal integrity, as the slower development of shrinkage forces may allow more stress relaxation due to viscous flow.

1.3.3 Mechanical properties

Mechanical properties of ACP-composites are, unsurprisingly, weaker than those of commercial composites, as their unsilanized filler particles are unable to provide structural reinforcement [86]. This has been addressed by the addition of the reinforcing glass fillers that are compositionally similar to those found in the commercial composites. Theddition of the reinforcing fillers improves mechanical properties without impairing ion release and bioactivity [70, 75]. However, a rather high weight ratio of ACP fillers (about 40%) is required for adequate bioactivity, thus leaving little space for reinforcing fillers. In those "traditional" ACP formulations filled with ACP particles with a wide particle size distribution, only 10wt% of additional reinforcing fillers can be added before the viscosity becomes too high for appropriate handling [87]. The recent development of nano-sized ACP particles should resolve this issue, as these particles yield bioactive properties at much lower amounts due to their extremely high surface area [76]. Thus higher loads of reinforcing fillers are possible, which considerably improves mechanical properties [88]. Additionally, nano-ACP particles leave comparatively smaller defects compared to the traditional ACP after the dissolution-reprecipitation process [89], which is favorable for the long-term improvement of mechanical properties.

2. GENERAL AND SPECIFIC AIMS

The aim of this study was to investigate various properties of experimental ACP-composites that are important for their clinical applicability. Specifically, the effect of 10 wt% of reinforcing fillers comprising of barium glass and silica on the DC, optical properties and temperature rise during light curing were investigated. Additionally, a novel approach using impedance spectroscopy was used to explore the polymerization kinetics and microstructural characteristics of ACP-composites.

The individual aims of this study were to investigate the following aspects of experimental ACP-composites:

- the maximum attainable DC
- the effect of the addition of inert fillers on the DC
- influence of different radiant exposures on the DC
- dependence of DC on layer thickness
- temperature rise during light curing
- optical properties (light transmittance) as a prerequisite for efficient curing at depth
- dynamic changes in light transmittance during light curing
- real-time light transmittance measurements as a possible indicator of the polymerization reaction rate
- polymerization kinetics by simultaneous transmittance and temperature measurements
- differences in polymerization kinetics caused by the addition of reinforcing fillers
- impedance spectroscopy as a means to characterize both short-term and long-term setting
- kinetic parameters of the polymerization reaction by real-time impedance measurements
- correlation of impedance data with the DC, light transmittance and microstructural features
- usability of impedance measurements to determine the amount of water present in the ACP filler
- possibility to separate the electrical contributions of different phases within the material structure by means of equivalent circuit modeling

3.

CONVERSION AND TEMPERATURE RISE OF REMINERALIZING COMPOSITES REINFORCED WITH INERT FILLERS

Matej Par, Ozren Gamulin, Danijela Marovic, Hrvoje Skenderovic, Eva Klaric, Zrinka Tarle

Published in Journal of Dentistry 2016;48:26-33, doi: 10.1016/j.jdent.2016.03.008

3.1 Abstract

Objectives: Remineralizing experimental composites based on amorphous calcium phosphate (ACP) were investigated. The impact of curing time (20 and 40 s), curing depth (1, 2, 3 and 4 mm) and addition of inert fillers (barium glass and silica) on the conversion and temperature rise during curing were examined.

Methods: Five ACP-composites and two control composites were prepared based on the light-curable EBPADMA-TEGDMA-HEMA resin. For temperature measurements, a commercial composite was used as an additional control. Conversion was assessed using FT-Raman spectroscopy by comparing the relative change of the band at 1640 cm^{-1} before and after polymerization. The temperature rise during curing was recorded in real-time using a T-type thermocouple.

Results: At 1 mm depth, the ACP-composites attained significantly higher conversion (77.8-87.3%) than the control composites based on the same resin (60.5-66.3%). The addition of inert fillers resulted in approximately 5% lower conversion at clinically relevant depths (up to 2 mm) for the curing time of 40 s. Conversion decline through depths depended on the added inert fillers. Conversion values higher than 80% of the maximum conversion were observed for all of the ACP-composites at depths up to 3 mm, when cured for 40 s. Significantly higher total temperature rise for the ACP-composites (11.5-13.1 °C) was measured compared to the control composites (8.6-10.8 °C) and the commercial control (8.7 °C).

Conclusions: The admixture of inert fillers represents a promising strategy for further development of ACP-composites, as it reduced the temperature rise while negligibly impairing the conversion.

Clinical significance: High conversions of ACP-composites are favorable in terms of mechanical properties and biocompatibility. However, high conversions were accompanied with high temperature rise, which might present a pulpal hazard.

3.2 Introduction

Composite materials based on amorphous calcium phosphate (ACP) represent an experimental class of remineralizing materials envisioned as a possible solution for combating secondary caries, one of the main causes of composite restoration failure (1). When exposed to an aqueous environment, composite materials incorporating ACP release calcium and phosphate ions in concentrations that are supersaturated with respect to hydroxyapatite, allowing the remineralization of dental hard tissues (2). Remineralizing effects of ACP-composites have been reported *in vitro* (3), *in situ* (4) and *in vivo* (5), rendering them a promising future alternative to conventional composites. However, the clinical applicability of ACP-composites is limited by insufficient mechanical properties; their flexural strength ranges from 20-70 MPa (6-8), while at least 80 MPa is required for placement in load-bearing areas (9). The less than optimal mechanical properties are explained by the agglomeration of ACP particles, high water sorption of ACP-composites, intra-composite conversion of ACP to hydroxyapatite and lack of chemical bonding between the resinous matrix and ACP particles (2, 6).

The issue of low mechanical properties has been addressed by introducing the ACP-composites with reinforcing silanized fillers similar to those used in commercial composites (7, 8, 10). This approach yields a "hybrid" material, whose filler consists of a bioactive part (ACP) and an inert part (barium glass or silica). Since the ACP filler compromises mechanical properties, its load should be reduced to a minimal level which is sufficient for the remineralizing effect. This has led to the optimization of the composition to 40 wt% of ACP (11). By adding up to 10 wt% of silanized barium glass or silica fillers, the flexural strength of ACP-composites was improved for up to 46 % (from 22 to 32 MPa),while the ion release capability was unaffected (7, 8). Despite the improvements, the flexural strength of the ACP-composites was still insufficient for use in load-bearing areas (7, 8). Fine-tuning of the filler size, increasing the load of inert fillers and incorporating the nano-sized ACP particles may further improve mechanical properties (10), possibly leading to a remineralizing composite that would be able to withstand masticatory forces (12).

Adequate conversion is a basic prerequisite for a composite material, since it underlies virtually every property of the cured material, including its biocompatibility and mechanical features. ACP composites formulated with ethoxylated bisphenol A dimethacrylate (EBPADMA)-based resin attain high conversions (around 80%), as previously reported (6,

13, 14). Since high temperature rise might be a consequence of high conversion (15), this otherwise favorable property implies a potential hazard to pulpal health. However, the temperature rise does not depend simply on the conversion, but is affected by other factors, such as sample geometry, thermal capacity, translucency and polymerization kinetics (16). Thus it was of interest to examine the temperature rise that occurs during curing of ACP composites, as a possible side-effect of their high conversion.

Temperature rise due to the composite polymerization presents a continuing concern for pulpal health (17, 18). There is currently no consensus regarding the maximum allowed intrapulpal temperature (17, 19), nor the maximum temperature in the bulk of polymerizing composite material (15, 16, 20-27). In a classic and frequently cited study performed on monkey teeth, an intrapulpal temperature rise of 5 °C was proposed as critical for pulpal recovery (28). The findings of this study were critically evaluated (26, 29), pointing out that the pulpal tolerance to temperature rise may have been underestimated. During that experiment, the heat source was kept in contact with the tooth for a predetermined time (5-20 s). Upon reaching a desired time point, the intrapulpal temperature was recorded. At this time, there was a temperature gradient from the point of application of heat source on the tooth surface towards the pulp, the temperature at the tooth surface being much higher than recorded in the pulp. The intrapulpal temperature continued to rise after its value was recorded in the experiment. It is thus likely that the intrapulpal temperature rise required for irreversible damage is higher than the reported 5.5 °C. Another study (30) evaluated the pulpal response in premolar teeth scheduled for orthodontic extraction and found no histological changes indicative of pulpal damage upon the temperature increase up to 11 °C. However, the study was performed on young intact teeth and the findings may not apply to teeth whose pulp is already traumatized by caries and restorative procedures. Moreover, the temperature recorded in the bulk of the composite cannot be simply translated into the intrapulpal temperature. In the absence of reliable reference values for maximum allowed temperature rise, the researchers often resort to comparison with the temperature rise produced by existing commercial composite materials, for which there is clinical evidence of being tolerated by the pulp (16, 17).

This study is a sequel to our investigations of ACP-composites modified with inert fillers (7, 8, 31). The impact of curing time, curing depth and addition of inert fillers on the conversion of ACP-composites is examined and the temperature rise during curing was recorded in real-time and compared to that of a commercial composite. The hypotheses tested were: (I) ACP-

composites attain higher conversion than the control composites based on the same resin and photoinitiator; (II) conversion of ACP-composites is influenced by the following factors: curing time (20 and 40 s), curing depth (1, 2, 3 and 4 mm) and addition of inert fillers (5 formulations); (III) ACP-composites can be adequately cured up to 3 mm depth; (IV) high conversion of ACP-composites is accompanied with a high temperature rise; (V) ACP-composites produce higher temperature during curing than a commercial composite.

3.3 Materials and methods

3.3.1 Composite materials

The synthesis of zirconia-hybridized ACP (Zr-ACP) fillers followed the procedure by Skrtic et al. (13). Briefly, Zr-ACP precipitated from a water solution upon mixing of $Ca(NO_3)_2$, Na_2HPO_4, $Na_4P_2O_7$ and $ZrOCl_2$. The suspension was filtered, the solid phase washed with ice-cold ammoniated water and acetone and then lyophilized.

The experimental resin contained 67 wt% of EBPADMA (Esstech, Essington, PA, USA), 23 wt% of tri-ethylene glycol dimethacrylate (TEGDMA; Esstech) and 10 wt% of 2-hydroxyethyl methacrylate (HEMA; Esstech). The resin was rendered photosensitive by the addition of 0.2 wt% of the photo oxidant camphorquinone (CQ; Aldrich, Milwaukee, WI, USA) and 0.8 wt% of photo reductant ethyl-4- (dimethylamino) benzoate (4E; Aldrich). The monomers and photoactivators were mixed in the lightproof container using a magnetic stirrer for 48 hours in order to assure a homogeneous mixture.

The resin was blended with fillers in lightproof containers using a dual asymmetric centrifugal mixing system (Speed Mixer TM DAC 150 FVZ, Hauschild & Co KG, Hamm, Germany) at 2700 rpm. The mixing was performed in five one-minute intervals separated by one-minute breaks. After mixing, the obtained composite pastes were deaerated in vacuum for 12 hours. Seven experimental materials were prepared: five were ACP-based, while two materials were based on conventional inert fillers and served as a control (Table 1).

Table 1. Composition of the experimental composite materials.

	Material	Filler (wt%)	Resin (wt%)	Filler load (vol%)
ACP-based materials	**ACP40**	40% Zr-ACP	60	27.6
	ACP40-Ba10	40% Zr-ACP, 10% Ba-fillers	50	35.1
	ACP40-Si10	40% Zr-ACP, 10% Si-fillers	50	36.6
	ACP40-Ba5Si5	40% Zr-ACP, 5% Ba-fillers, 5% Si-fillers	50	35.9
	ACP40- Ba9Si1	40% Zr-ACP, 9% Ba-fillers, 1% Si-fillers	50	35.3
control materials	**Ba40**	40% Ba-fillers	60	22.0
	Ba40Si10	40% Ba-fillers, 10% Si-fillers	50	31.5

Barium-fillers (Ba): SiO_2 55.0%, BaO 25.0%, B_2O_3 10.0%, Al_2O_3 10.0%, F 2.00%, particle size (d50/d99 (µm)) 0.77/2.28, silanization 6 wt%, product name/manufacturer: GM39923/Schott, Germany.

Silica-fillers (Si): SiO2 ≥ 99.8, primary particle size: 12 nm, silanization 4-6 wt%, product name/manufacturer: Aerosil DT/Evonik Degussa, Germany.

3.3.2 Degree of conversion

Five cylindrical samples (d=3 mm, h=5 mm) were made for each composite and each curing time using a custom-made stainless steel split-mold. Uncured composite was placed into the mold, both mold apertures were covered with a polyethylene terephthalate (PET) film and curing was performed for 20 s or 40 s through the upper aperture with a LED curing unit (Bluephase G2, Ivoclar-Vivadent, Schaan, Liechtenstein; wavelength range 380–515 nm, irradiance 1200 mW/cm^2). The curing unit tip was positioned directly on top of the PET film covering the sample. The samples were cured at 21±1°C and transferred to the incubator (Cultura, Ivoclar-Vivadent, Schaan, Liechtenstein) for dark storage at 37±1°C. After 24 h, Raman spectra were collected from four depths: 1, 2, 3 and 4 mm.

FT-Raman spectroscopy measurements were performed using a Spectrum GX spectrometer (PerkinElmer, Waltham, USA). The excitation was an NdYaG laser at 1064 nm wavelength, with laser power of 400 mW and resolution of 4 cm^{-1}. The samples were mounted on a universal holder that enabled translation along the axis of cylindrical sample thereby exposing

different depths to the excitation laser light. The exposed sample surface was 0.5 mm in diameter. For each spectrum, 100 scans were recorded. Spectra of the uncured composites (n=5) were recorded in the same manner. The spectra were processed with the Kinetics add-on for Matlab (Mathworks, Natick, Massachusetts, USA).

Degree of conversion (DC) calculation was performed by comparing the relative change of the band at 1640 cm^{-1}, representing the aliphatic C=C stretching mode to the aromatic C=C band at 1610 cm^{-1}, before and after polymerization. Peak heights of aliphatic C=C and aromatic C=C bands were used for DC calculation by the following equation: $DC = 1 - R_{polymerized}/R_{unpolymerized}$, where R = (aliphatic C=C peak height) / (aromatic C=C peak height) (32).

3.3.3 Temperature rise

Uncured composite materials were cast into cylindrical Teflon molds (d=6 mm, h=2 mm), covered from both sides with PET film (0.05 mm thick) and sandwiched between two glass plates (h=1 mm). The curing unit tip was positioned immediately below the glass plate, i.e. at 1.05 mm distance from the sample surface. At the opposite side of the sample, T-type thermocouple was positioned centrally between the PET film and glass plate. This assembly was held together by a custom-made brass holder. The sample was enclosed by the Teflon mold and PET films, so that it was not in direct contact with the brass holder. Five repeats were made for each material (n=5).

Curing was performed using the Bluephase G2 curing device (1200 mW/cm^2) for 30 seconds and a custom-made computer program was used to record the temperature change at the rate of 20 points per second. Two minutes after the end of curing, temperature returned to the baseline and the curing device was activated again for 30 seconds. Two illuminations were performed to separate the heating effect of the curing unit from the reaction exotherm. Preliminary experiments showed that the second illumination did not significantly increase the conversion, thus it was assumed that the polymerization was completed during the first illumination.

Additionally, Tetric EvoCeram (Ivoclar Vivadent, Schaan, Liechtenstein) of shade A2, LOT: S26173, EXP: 06/2017 was used as a commercial control for temperature measurements.

3.3.4 Scanning electron microscopy (SEM)

The light-cured (30 s), disc-shaped samples of 1 mm thickness, unpolished and uncoated were examined with FE-SEM JSM 7000 (JEOL, Peabody, MA, USA).

3.3.5 Statistical analysis

Results of DC were compared by means of mixed model ANOVA and a multivariate analysis was used to test the influence of parameters "material", "curing depth" and "curing time" on the DC values within the group of ACP-composites The DC values among curing depths within a material and curing time were compared using a repeated measures ANOVA with Bonferroni correction. For a given curing depth, DC values among the materials and curing times were compared using ANOVA with Tukey correction.

Results of temperature rise were compared using ANOVA with Tukey correction, while the temperature rises during first and second illumination for a given material were compared by a repeated samples t-test. Statistical analysis was performed in SPSS 20 (IBM, Armonk, NY, USA) with α=0.05.

3.4 Results

Mean DC values and results of statistical analysis are shown in Table 2. For the group of ACP-composites, a significant influence ($p<0.001$) was found for all three factors: "material" ($\eta^2=0.628$), "curing depth" ($\eta^2=0.980$) and "curing time" ($\eta^2=0.925$). Significant interactions were observed between the factors "material" and "curing depth" ($p<0.001$) and "curing depth" and "curing time" ($p<0.001$). At all curing depths, ACP40 showed significantly higher DC than the ACP-composites with inert fillers. DC values among the ACP-composites with inert fillers were mostly statistically similar for a given depth and curing time. The control composites showed about 20% lower DC than the ACP-composites at the clinically relevant depths (up to 2 mm). Increasing the curing time from 20 to 40 s significantly improved DC at all depths except at 1 mm. For 40 s curing time, there was no significant difference in DC between the depths of 1 mm and 2 mm.

Table 2. Mean values (s. d.) of degree of conversion (%).

	curing depth	curing time (s)					
	(mm)	20			40		
ACP40	1	85.7 (1.3)	AB		87.3 (0.7)	A	*
	2	75.7 (4.8)	HI		85.2 (2.3)	G	*
	3	52.4 (2.1)	Q		77.4 (4.2)	M	
	4	39.1 (1.7)	UV		56.9 (6,7)	S	
ACP40-Ba10	1	80.7 (2.7)	BCD		82.0 (1.9)	BCD	*
	2	71.8 (4.0)	IJ		81.0 (0.4)	GH	*
	3	48.0 (5.0)	QR		74.1 (1.5)	MNO	
	4	35.5 (2.8)	VW		54.6 (4.5)	S	
ACP40-Si10	1	78.9 (1.6)	CD		82.0 (0.4)	BCD	*
	2	70.2 (2.8)	IJ		79.8 (0.7)	GH	*
	3	47.0 (4.7)	QR		67.0 (1.6)	NOP	
	4	29.1 (4.0)	W		45.5 (3.1)	TU	
ACP40-Ba5Si5	1	79.8 (2.8)	CD		82.8 (0.8)	ABC	*
	2	65.7 (4.5)	JK		80.0 (3.7)	GH	*
	3	45.3 (3.7)	QR		75.1 (3.7)	MN	*
	4	31.4 (1.7)	VW		54.2 (6.9)	S	
ACP40-Ba9Si1	1	77.8 (1.7)	D		79.6 (2.1)	CD	*
	2	62.3 (4.0)	KL		80.9 (1.3)	GH	*
	3	43.2 (5.6)	R		72.1 (2.8)	MNOP	
	4	33.8 (2.5)	VW		52.4 (3.4)	ST	
Ba40	1	61.7 (1.8)	EF		66.3 (1.8)	E	*
	2	55.6 (2.7)	L		67.2 (2.2)	JK	*
	3	46.0 (3.4)	QR		66.0 (1.9)	OP	*
	4	31.8 (2.0)	VW		55.7 (3.7)	S	
Ba40Si10	1	60.5 (5.2)	F	*	65.8 (2.2)	E	*
	2	56.0 (6.5)	L	*	65.0 (3.1)	JK	*
	3	47.8 (6.1)	QR	*	64.3 (2.4)	P	*
	4	34.1 (4.4)	VW		59.2 (2.9)	S	

Asterisks (*) denote statistically homogeneous groups among depths for a given material and curing time.

Letters denote homogeneous groups among materials and curing times for a given depth.

As a useful representation of the curing efficiency at depth (33), the ratio of DC at given depth and maximum DC (measured at 1 mm depth) is shown in Figure 1. The requirement of at least 80% of the maximum DC (33) was fulfilled at depths up to 2 and 3 mm for 20 s and 40 s curing time, respectively.

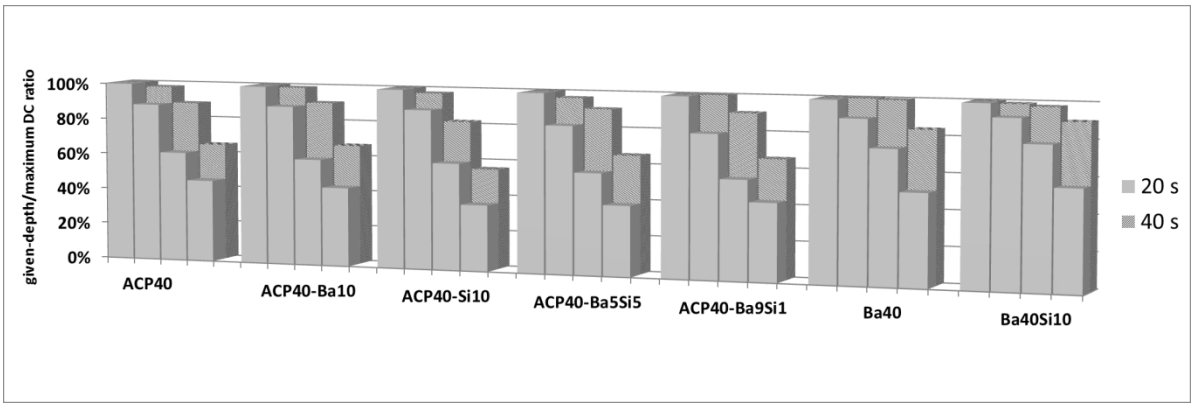

Figure 1. The given-depth/maximum DC ratio for different depths and curing times. For a given material, bars from left to right represent the curing depths of 1, 2, 3 and 4 mm.

A representative curve of temperature rise during curing is shown in Figure 2. The first temperature peak represents the total temperature rise (T_{total}), while the second peak corresponds to the temperature rise due to the heating from the curing unit (T_{curing}). The difference between these values is the temperature rise of reaction exotherm ($T_{reaction}$).

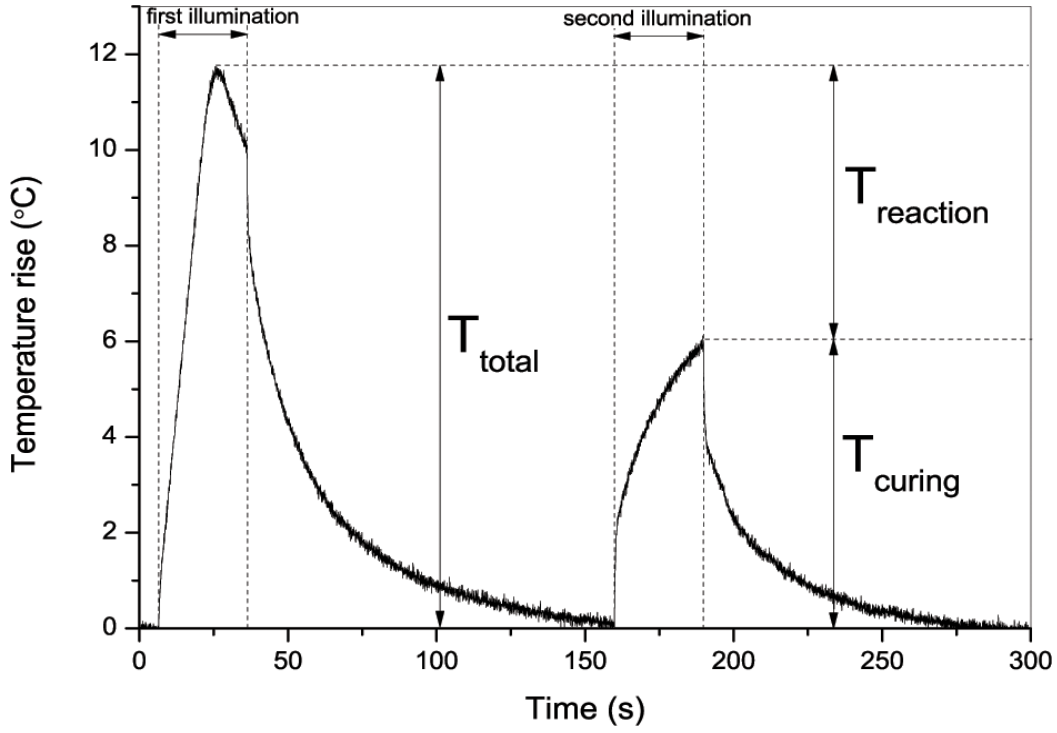

Figure 2. Curve of temperature rise during curing for ACP40-Ba5Si5. Two illuminations of 30 s were performed. The first temperature peak represents the total temperature rise, while the second peak is due to the heating effect of the curing unit.

Results of temperature measurements are presented in Table 3. ACP40 had the highest T_{total}, ACP-composites with inert fillers had intermediary T_{total}, while the control composites presented the lowest values of T_{total}. All of the ACP-composites showed similar $T_{reaction}$, which was significantly higher than that of the controls.

Figure 3 shows the SEM micrograph of ACP40. The particle size of ACP agglomerates was approximately 2-5 μm, as reported in previous studies using the same preparation protocol (13).

Table 3. Mean values (s. d.) of temperature rise.

	T_{total} / °C		T_{curing} / °C		$T_{reaction}$= T_{total} - T_{curing} / °C	
ACP 40	13.05 (0.50)	A	6.32 (0.20)	A	6.73 (0.34)	A *
ACP40-Ba10	12.13 (0.21)	B	5.72 (0.28)	A	6.41 (0.24)	AB *
ACP40-Si10	11.53 (0.41)	BC	6.08 (0.17)	A	5.45 (0.37)	C *
ACP40-Ba5Si5	12.12 (0.40)	B	6.20 (0.25)	A	5.92 (0.27)	BC *
ACP40-Ba9Si1	12.57 (0.51)	AB	6.23 (0.52)	A	6.34 (0.31)	AB *
Ba40	10.80 (0.32)	C	8.52 (0.41)	B	2.28 (0.31)	D *
Ba40Si10	8.58 (0.12)	D	7.45 (0.29)	C	1.13 (0.36)	E *
Tetric EvoCeram	8.73 (0.25)	D	7.31 (0.42)	C	1.42 (0.30)	E *

Same letters indicate statistically homogeneous groups within a column.

Asterisks (*) denote the statistically significant difference between T_{total} and T_{curing}.

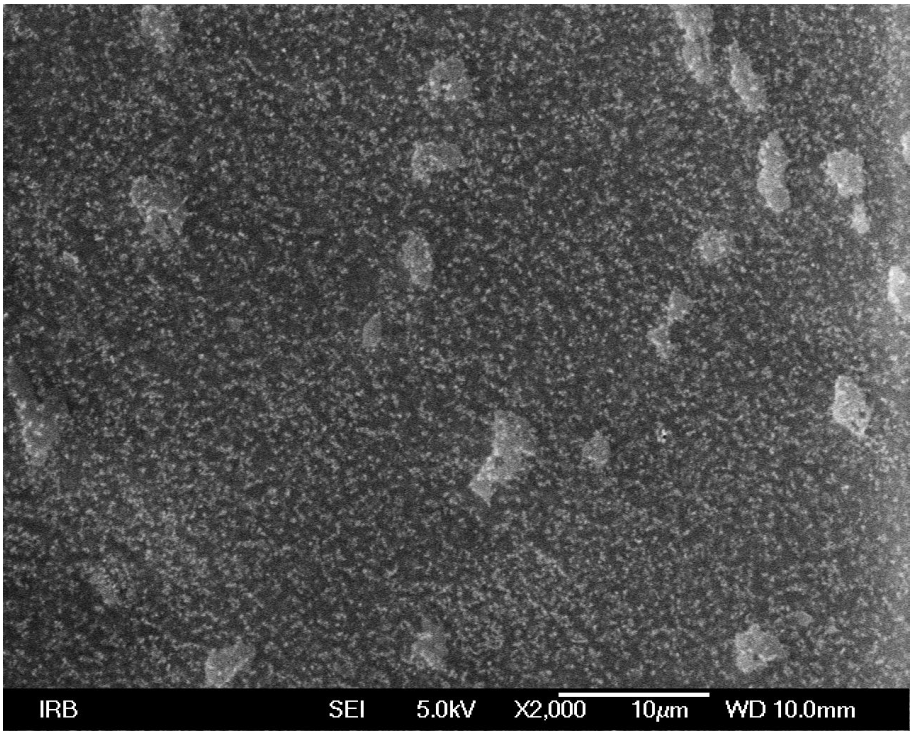

Figure 3. SEM micrograph of the sample surface for ACP40.

3.5 Discussion

This study examined the influence of curing time, curing depth and admixture of inert fillers on the conversion of ACP-composites. Additionally, the temperature rise during curing was recorded in real-time in order to examine if high conversions of ACP-composites were accompanied by high temperature increase.

At 1 mm depth, the ACP-composites presented significantly higher DC (77.8-87.3%) than the control composites (60.5-66.3%), thus confirming the first hypothesis. For a given resin-photoinitiator composition, conversion is expected to depend on the filler load (34, 35) and filler size (36). These factors determine the particle surface area which is in contact with the resin. Higher particle surface area increases local viscosity, thus reducing monomer mobility and leading to lower conversion. The ACP-composites had slightly higher filler vol% (27.6-36.6%) than the control composites (22.0-31.5%), however, the filler mostly consisted of comparatively larger ACP agglomerates of 2-5 μm (Figure 3). Thus the ACP-composites had lower filler surface area and consequently higher DC than the control composites. Factors such as larger particle size (36) and lower filler vol% (34) are known to increase conversion, however this does not sufficiently explain very high DC of ACP-composites in our study. Composites in the cited studies (34, 36) had the particle size and vol% similar to those in our study, while their conversions were only about 61% and 73%, respectively. Moreover, commercial composites with a wide variety of filler and resin compositions usually attain DC in the range of 50-70% (37). This suggests that there may be an additional factor other than filler size and load that contributed to the considerable difference between the ACP- and control composites. Since the unsilanized ACP particles comprised the largest part of the filler in the ACP-composites, their inability to chemically bond with polymeric matrix may be responsible for high conversion. The literature data is ambiguous regarding the effect of surface-silanization on conversion of dental composites – some studies (35, 38) found no difference among materials with silanized and unsilanized filler, while others (34, 39) have shown that fillers with unreactive surfaces enhance resin mobility during curing and improve the final conversion. The comparison of materials containing silanized and unsilanized fillers is also complicated by the fact that unreacted C=C double bonds in silane molecules contribute to apparently lower DC (38). Based on the data from the filler and resin manufacturers, we calculated the percentage of C=C bonds originating from silane in the total amount of C=C bonds. Since control materials Ba40 and Ba40Si10 respectively contained only 3.1% and 4.4% double bonds from silane, this probably did not cause the observed 20%

difference in DC between the ACP- and control composites. Thus, it appears that the lack of silanization is indeed a contributing factor for the high conversion of the ACP-composites.

The addition of different combinations of inert fillers to the ACP-composites slightly decreased their DC (Table 2). This is attributed to higher total filler volume and the previously discussed effect of silanized fillers on conversion (35, 40). Moreover, small silica particles with high surface area significantly increase the viscosity, suggesting lower molecular mobility and consequently lower DC (35). Although all of the ACP-composites with inert fillers consistently showed lower DC than ACP40 at all depths, these differences were rather small and can be considered clinically negligible. For example, the ACP-composites with inert fillers showed about 5% lower conversion than ACP40 at depths up to 2 mm, for 40 s curing time. Moreover, the DC of ACP-composites with inert fillers around 80% at depths up to 2 mm was above the common DC range of commercial composites (37). This shows that the modification of ACP-composites with conventional fillers results in only minor sacrifice in conversion and that inert filler load may be further increased, in efforts to improve mechanical properties (7, 8).

The conversion at depth is limited by curing light attenuation caused by scattering and absorption (41). Due to these phenomena, deeper layers of the sample receive lower number of photons that initiate polymerization. This can be partly compensated by extending the curing time and thus increasing the radiant energy delivered to a particular depth (33). A significant interaction ($p<0.001$) between the factors “curing depth” and “curing time” shows that the decline of DC through depths can be mitigated by longer curing times. Considering the main factor “curing time”, a significant influence on the conversion of ACP-composites was observed at depths of 2 mm and above. This suggests that at 1 mm the maximum DC was attained with 20 s curing time, while the conversion at higher depths benefited from prolonged curing time. For ACP-composites, the greatest DC improvement due to the longer curing was observed at 3 mm, while the beneficial effect of longer curing diminished at 4 mm. Since the light intensity decreases exponentially with depth (42), it appears that light penetration was very restricted at the depth of 4 mm, thus limiting the DC improvement by means of longer curing. In contrast, the more translucent control-composites (Ba40 and Ba40Si10) presented the highest improvement at 4 mm.

Since the DC was significantly influenced by the factors “material”, “curing depth” and “curing time”, the second hypothesis was confirmed. For the ACP-composites, mixed model

ANOVA detected a significant interaction between the factors "material" and "depth" ($p<0.001$), indicating that the admixture of different combinations of inert fillers caused these materials to behave differently at depth. The ACP-composites with inert fillers had similar filler volume ratios (35-37%), thus the differences in their behavior regarding conversion at depth should be due to the particle size and refractive index of inert fillers. The refractive indices of Si and Ba fillers were 1.46 and 1.52, respectively. Since HEMA, TEGDMA and EBPADMA had refractive indices of 1.45, 1.46 and 1.54 respectively, the comonomer refractive index should be in the range of 1.45-1.54. This approximation does not allow the precise evaluation of refractive index mismatch between filler and resin. However, as the Rayleigh scattering is a function of the refractive index mismatch raised to the first power, and the particle size raised to the third power (43), the latter exerts much stronger effect on light scattering. The effect of particle size was the most noticeable for the ACP40-Si10 material, which presented more pronounced DC decline through depths than the other ACP-composites. The Si fillers were originally 12 nm in diameter, causing negligible scattering of the curing light, but due to agglomeration some of the secondary particles may have dimensions close to half the wavelength of the curing light and cause considerable light scattering (44, 45). The contribution of Ba fillers to the DC decline at depth was less pronounced, since their dimensions were outside the critical range for light scattering. Finally, large ACP agglomerates of approximately 2-5 μm caused only moderate scattering, allowing high conversions of all ACP formulations at depths up to 3 mm. It should be noted that the light scattering of unsilanized ACP particles may be higher if composites are cured in constrained conditions, due to the occurrence of gaps at filler-resin interface (46).

Depth of cure is defined as a maximum thickness of a composite that attains clinically acceptable conversion (33). The bottom/top ratio of microhardness or DC (47) higher than 80% is considered to indicate clinically acceptable conversion. It should be noted that the 80% threshold for both microhardness and DC is chosen arbitrarily and has no underlying physical or chemical meaning, but it may serve as a convenient indicator of the polymerization efficiency at depth (32, 33, 47). Since our preliminary study showed that there was no significant difference between the DC at surface and 1 mm depth, the DC values at 1 mm were considered maximum and used to calculate the given-depth/maximum DC ratio (Figure 1). The "adequate cure" (ratio above 80%), was attained for all ACP-composites at depths up to 2 mm and 3 mm for the curing times of 20 s and 40 s, respectively. The third hypothesis of adequate cure up to 3 mm is thus confirmed only for the 40 s curing time. The

capability of ACP-composites to be efficiently cured at depth is comparable to that of conventional commercial composites that are usually placed in layers of 2-3 mm. Although the "adequate cure" at 2 mm was attained with 20 s curing time, it must be noted that the DC difference at 2 mm between 20 s/40 s was statistically significant for all of the materials and amounted to 9.0-18.6%. This finding demonstrates the benefit of longer curing time to assure optimal mechanical properties and biocompatibility at the restoration bottom.

Significantly higher total temperature rise for the ACP-composites (11.5-13.1 °C) was measured compared to the control composites (8.6-10.8 °C), confirming the fourth hypothesis that the high conversion of ACP-composites is accompanied with higher temperature rise. The fifth hypothesis was also confirmed, as the temperature rise of ACP-composites was significantly higher than that of the commercial control, Tetric EvoCeram (8.7 °C). However, the impact of these results on pulpal response is questionable, given that some of the commercial composites were reported with much higher temperatures (15). Comparison of temperature rises across different studies is difficult for several reasons. Since the sample size differs among studies and the thermal insult to dental pulp is a function of both the temperature rise and the amount of material, the pulpal hazard is not adequately represented by the temperature values alone. Additionally, results obtained from different experimental setups are not directly comparable, as evidenced by the great variation of temperature rise reported for commercial composites. For example, Al-Qudah et al. reported the extreme values of total temperature rise for a commercial composite of up to 43 °C using the infrared scanning system (15). Some studies used the gypsum molds (22) and water circulation from water bath (25, 26) to emulate heat dissipation in the pulp and reported the total temperature rises of 11.2-16.2 °C, 2.4-7.1 °C and 6.9-11.0 °C, respectively. The studies that used a rather simple setup and sample geometry similar to ours (16, 27), reported the total temperature rise of 6.6-14.1 °C and 5.8-14.0 °C, respectively. Therefore their results are comparable to the values recorded for ACP-composites. Thus, although the temperature rise of ACP-composites was higher than that of the commercial control in our study, it falls within the range reported previously for several commercial composites in similar experimental conditions (16, 27). It should be noted that the ACP-composites with the addition of inert fillers showed the trend towards the lower temperature rise, as a result of the lower resin allotment (15). Since the development of ACP-composites is directed towards incorporating higher total filler loads, the temperature rise is expected to further decrease.

Total temperature rise during curing is the result of the polymerization reaction exotherm and heat produced by the curing unit. Previous studies have reported different relative contributions of these factors (17, 20) which is related to the characteristics of the curing unit and composite formulation. In our study, the control composites presented a relatively small $T_{reaction}$ (1-2 °C) compared to T_{curing} (7-9 °C). Conversely, the ACP-composites showed significantly higher $T_{reaction}$ (5-7 °C), with magnitude similar to that of T_{curing} (6 °C). The reaction exotherm is directly related to the number of converted double bonds, which is determined by the resin ratio and final conversion (24). In our study conversion had a decisive influence on the magnitude of reaction exotherm, as exemplified by Ba40 having significantly lower $T_{reaction}$ compared to the ACP-composites, despite its higher resin allotment (78 vol% vs. 63-72 vol%). Additionally, Ba40Si10 had resin allotment similar to the ACP-composites, but presented a significantly lower $T_{reaction}$. Thus it seems that the conversion was more important determinant for reaction exotherm than the resin vol%. Moreover, the values of $T_{reaction}$ may be affected by polymerization kinetics, since higher polymerization rates allow less time for heat dissipation, resulting in higher temperature buildup. Since no parameters of reaction rate were measured, it can only be speculated that unsilanized filler in the ACP-composites enabled better monomer mobility and consequently higher reaction rates. It should be noted that the transfer of heat produced by the curing unit slightly differed between the first and the second illumination due to the change of light transmittance that occurred during curing. However, these differences were neglected and the temperature difference between the first and the second illumination was considered to represent the heating effect of reaction exotherm.

3.6 Conclusions

Experimental ACP-composites prepared with a light-curable EBPADMA-based resin showed very high conversions, up to 87.3%. Introduction of 10 wt% of inert fillers comprised of silanized barium glass and/or silica caused a minor decline in conversion. Given the sufficient curing time, all of the ACP-composites showed conversions higher than 80% of the maximum conversion up to the depth of 3 mm. High conversions of ACP-composites were accompanied with the temperature rise higher than that of the controls, reaching up to 13.1 °C. The measured values of temperature rise fall within the range reported for commercial composites in the literature, suggesting that they should be no more harmful to dental pulp than the

established composites used widely in clinical practice. The admixture of inert fillers represents a promising strategy for further development of ACP-composites, as it reduced the temperature rise while negligibly impairing the conversion.

3.7 Acknowledgments

We thank Mira Ristić and Marijan Marciuš from the Division of Materials Chemistry, Ruđer Bošković Institute for the SEM micrographs. We also gratefully acknowledge Drago Skrtic for providing us with the zirconia-hybridized ACP. This investigation was supported by Croatian Science Foundation (Project 08/31 Evaluation of new bioactive materials and procedures in restorative dental medicine). The authors declare no conflict of interest.

3.8 References

1. Sarrett DC. Clinical challenges and the relevance of materials testing for posterior composite restorations. Dent Mater 2005;21(1):9-20.
2. Skrtic D, Antonucci JM. Bioactive polymeric composites for tooth mineral regeneration: physicochemical and cellular aspects. J Funct Biomater 2011;2(3):271-307.
3. Langhorst SE, O'Donnell JN, Skrtic D. In vitro remineralization of enamel by polymeric amorphous calcium phosphate composite: quantitative microradiographic study. Dent Mater 2009;25(7):884-91.
4. Melo MA, Weir MD, Rodrigues LK, Xu HH. Novel calcium phosphate nanocomposite with caries-inhibition in a human in situ model. Dent Mater 2013;29(2):231-40.
5. Li F, Wang P, Weir MD, Fouad AF, Xu HH. Evaluation of antibacterial and remineralizing nanocomposite and adhesive in rat tooth cavity model. Acta Biomater 2014;10(6):2804-13.
6. Skrtic D, Antonucci JM, Eanes ED. Amorphous calcium phosphate-based bioactive polymeric composites for mineralized tissue regeneration J Res Natl Inst Stand Technol 2003;108(3):167-82.
7. Marovic D, Tarle Z, Hiller KA, Muller R, Ristic M, Rosentritt M, et al. Effect of silanized nanosilica addition on remineralizing and mechanical properties of

experimental composite materials with amorphous calcium phosphate. Clin Oral Investig 2014;18(3):783-92.

8. Marovic D, Tarle Z, Hiller KA, Muller R, Rosentritt M, Skrtic D, et al. Reinforcement of experimental composite materials based on amorphous calcium phosphate with inert fillers. Dent Mater 2014;30(9):1052-60.
9. Heintze SD, Zimmerli B. Relevance of in vitro tests of adhesive and composite dental materials, a review in 3 parts. Part 1: Approval requirements and standardized testing of composite materials according to ISO specifications. Swiss Dent J 2011;121(9):810-6.
10. Xu HH, Moreau JL, Sun L, Chow LC. Nanocomposite containing amorphous calcium phosphate nanoparticles for caries inhibition. Dent Mater 2011;27(8):762-9.
11. O'Donnell JN, Langhorst SE, Fow MD, Antonucci JM, Skrtic D. Light-cured dimethacrylate-based resins and their composites: comparative study of mechanical strength, water sorption and ion release. J. Bioact Compat Polym 2008;23(3):207-26.
12. Xu HH, Weir MD, Sun L, Ngai S, Takagi S, Chow LC. Effect of filler level and particle size on dental caries-inhibiting Ca-PO(4) composite. J Mater Sci Mater Med 2009;20(8):1771-9.
13. Skrtic D, Antonucci JM, Liu DW. Ethoxylated bisphenol dimethacrylate-based amorphous calcium phosphate composites. Acta Biomater 2006;2(1):85-94.
14. Tarle Z, Knežević A, Matošević D, Škrtić D, Ristić M, Prskalo K, et al. Degree of vinyl conversion in experimental amorphous calcium phosphate composites. J Mol Struct 2009;924-926:161-65.
15. Al-Qudah AA, Mitchell CA, Biagioni PA, Hussey DL. Thermographic investigation of contemporary resin-containing dental materials. J Dent 2005;33(7):593-602.
16. Atai M, Motevasselian F. Temperature rise and degree of photopolymerization conversion of nanocomposites and conventional dental composites. Clin Oral Investig 2009;13(3):309-16.
17. Hannig M, Bott B. In-vitro pulp chamber temperature rise during composite resin polymerization with various light-curing sources. Dent Mater 1999;15(4):275-81.

18. Knezević A, Tarle Z, Meniga A, Sutalo J, Pichler G, Ristić M. Degree of conversion and temperature rise during polymerization of composite resin samples with blue diodes. J Oral Rehabil 2001;28(6):586-91.
19. Martins GR, Cavalcanti BN, Rode SM. Increases in intrapulpal temperature during polymerization of composite resin. J Prosthet Dent 2006;96(5):328-31.
20. Al-Qudah AA, Mitchell CA, Biagioni PA, Hussey DL. Effect of composite shade, increment thickness and curing light on temperature rise during photocuring. J Dent 2007;35(3):238-45.
21. Asmussen E, Peutzfeldt A. Temperature rise induced by some light emitting diode and quartz-tungsten-halogen curing units. Eur J Oral Sci 2005;113(1):96-8.
22. Kleverlaan CJ, de Gee AJ. Curing efficiency and heat generation of various resin composites cured with high-intensity halogen lights. Eur J Oral Sci 2004;112(1):84-8.
23. Masutani S, Setcos JC, Schnell RJ, Phillips RW. Temperature rise during polymerization of visible light-activated composite resins. Dent Mater 1988;4(4):174-8.
24. McCabe JF. Cure performance of light-activated composites by differential thermal analysis (DTA). Dent Mater 1985;1(6):231-4.
25. Shortall AC, Harrington E. Temperature rise during polymerization of light-activated resin composites. J Oral Rehabil 1998;25(12):908-13.
26. Stewardson DA, Shortall AC, Harrington E, Lumley PJ. Thermal changes and cure depths associated with a high intensity light activation unit. J Dent 2004;32(8):643-51.
27. Uhl A, Mills RW, Jandt KD. Polymerization and light-induced heat of dental composites cured with LED and halogen technology. Biomaterials 2003;24(10):1809-20.
28. Zach L, Cohen G. Pulp response to externally applied heat. Oral Surg Oral Med Oral Pathol 1965;19:515-30.
29. Lloyd CH, Joshi A, McGlynn E. Temperature rises produced by light sources and composites during curing. Dent Mater 1986;2(4):170-4.
30. Baldissara P, Catapano S, Scotti R. Clinical and histological evaluation of thermal injury thresholds in human teeth: a preliminary study. J Oral Rehabil 1997;24(11):791-801.

31. Marović D, Tarle Z, Ristić M, Musić S, Škrtić D, Hiller KA, et al. Influence of different types of fillers on the degree of conversion of ACP composite resins. Acta Stomatol Croat 2011;45:231-8.
32. Par M, Gamulin O, Marovic D, Klaric E, Tarle Z. Raman spectroscopic assessment of degree of conversion of bulk-fill resin composites--changes at 24 hours post cure. Oper Dent 2015;40(3):E92-101.
33. Tarle Z, Attin T, Marovic D, Andermatt L, Ristic M, Taubock TT. Influence of irradiation time on subsurface degree of conversion and microhardness of high-viscosity bulk-fill resin composites. Clin Oral Investig 2015;19(4):831-40.
34. Ferracane JL, Berge HX, Condon JR. In vitro aging of dental composites in water - effect of degree of conversion, filler volume, and filler/matrix coupling. J Biomed Mater Res 1998;42(3):465-72.
35. Halvorson RH, Erickson RL, Davidson CL. The effect of filler and silane content on conversion of resin-based composite. Dent Mater 2003;19(4):327-33.
36. Turssi CP, Ferracane JL, Vogel K. Filler features and their effects on wear and degree of conversion of particulate dental resin composites. Biomaterials 2005;26(24):4932-7.
37. Van Landuyt KL, Nawrot T, Geebelen B, De Munck J, Snauwaert J, Yoshihara K, et al. How much do resin-based dental materials release? A meta-analytical approach. Dent Mater 2011;27(8):723-47.
38. Musanje L, Ferracane JL. Effects of resin formulation and nanofiller surface treatment on the properties of experimental hybrid resin composite. Biomaterials 2004;25(18):4065-71.
39. Wilson KS, Zhang K, Antonucci JM. Systematic variation of interfacial phase reactivity in dental nanocomposites. Biomaterials 2005;26(25):5095-103.
40. Atai M, Watts DC. A new kinetic model for the photopolymerization shrinkage-strain of dental composites and resin-monomers. Dent Mater 2006;22(8):785-91.
41. Leprince JG, Palin WM, Hadis MA, Devaux J, Leloup G. Progress in dimethacrylate-based dental composite technology and curing efficiency. Dent Mater 2013;29(2):139-56.
42. Emami N, Sjodahl M, Soderholm KJ. How filler properties, filler fraction, sample thickness and light source affect light attenuation in particulate filled resin composites. Dent Mater 2005;21(8):721-30.

43. Masotti AS, Onofrio AB, Conceicao EN, Spohr AM. UV-vis spectrophotometric direct transmittance analysis of composite resins. Dent Mater 2007;23(6):724-30.
44. dos Santos GB, Alto RV, Filho HR, da Silva EM, Fellows CE. Light transmission on dental resin composites. Dent Mater 2008;24(5):571-6.
45. Clewell DH. Scattering of Light by Pigment Particles. J Opt Soc Am 1941;31:512-7.
46. Feng L, Suh BI, Shortall AC. Formation of gaps at the filler-resin interface induced by polymerization contraction stress: Gaps at the interface. Dent Mater 2010;26(8):719-29.
47. Bouschlicher MR, Rueggeberg FA, Wilson BM. Correlation of bottom-to-top surface microhardness and conversion ratios for a variety of resin composite compositions. Oper Dent 2004;29(6):698-704.

4.

LIGHT TRANSMITTANCE AND POLYMERIZATION KINETICS OF AMORPHOUS CALCIUM PHOSPHATE COMPOSITES

Matej Par, Danijela Marovic, Hrvoje Skenderovic, Ozren Gamulin, Eva Klaric, Zrinka Tarle

Published in Clinical Oral Investigations 2017;21(4):1173-82,

doi: 10.1007/s00784-016-1880-6

4.1 Abstract

Objectives: This study investigated light transmittance and polymerization kinetics of experimental remineralizing composite materials based on amorphous calcium phosphate (ACP), reinforced with inert fillers.

Materials and methods: Light-curable composites were comprised of Bis-EMA-TEGDMA-HEMA resin and ACP, barium glass and silica fillers. Additionally, a commercial composite Tetric EvoCeram was used as a reference. Light transmittance was recorded in real-time during curing and transmittance curves were used to assess polymerization kinetics. To obtain additional information on polymerization kinetics, temperature rise was monitored in real-time during curing and degree of conversion was measured immediately and 24 h post-cure.

Results: Light transmittance values of 2 mm thick samples of uncured ACP-composites (2.3-2.9%) were significantly lower than those of the commercial composite (3.8%). The ACP-composites presented a considerable transmittance rise during curing, resulting in post-cure transmittance values similar to or higher than those of the commercial composite (5.5-7.9% vs. 5.4%). The initial part of light transmittance curves of experimental composites showed a linear rise that lasted for 7-20 s. Linear fitting was performed to obtain a function whose slope was assessed as a measure of polymerization rate. Comparison of transmittance and temperature curves showed that the linear transmittance rise lasted throughout the most part of the pre-vitrification period.

Conclusions: The linear rise of light transmittance during curing has not been reported in previous studies and may indicate a unique kinetic behavior, characterized by a long period of nearly-constant polymerization rate.

Clinical relevance: The observed kinetic behavior may result in slower development of polymerization shrinkage stress, but also inferior mechanical properties.

4.2 Introduction

Composites containing amorphous calcium phosphate (ACP) filler are capable of releasing calcium and phosphate ions, thus having the potential to prevent secondary caries (1-3). Mechanical properties of ACP-composites are generally lower than that of their commercial counterparts (1,4), but can be enhanced by the admixture of reinforcing fillers, such as silanized barium glass and silica (5,6). This approach improves the material's strength, while maintaining its favorable properties, i.e. remineralizing effect and high degree of monomer conversion (5-7). By fine-tuning the ACP particle size and composition of reinforcing fillers, mechanical properties similar to these of commercial composites may be attained (8). A more complete understanding and further improvement in mechanical properties of this class of biomaterials may lead to their clinical applicability in the future.

Optical properties of light-curable composites determine not only their aesthetic appearance, but also curing depth and polymerization kinetics (9,10). Light transmittance of composite materials is determined by absorption and complex light scattering on filler particles of various geometries and refractive indices (11). During polymerization, light transmittance changes due to a series of events. First, the resin matrix undergoes a change in optical properties due to its rising refractive index and changes in light scattering that occur during gelation and vitrification (12). Second, the consumption of camphorquinone (CQ) during polymerization (13) reduces light absorption, which in turn increases light transmittance. Third, the exothermic nature of polymerization reaction causes a transient decrease in refractive index of resin due to the density reduction (10). Fourth, the capability of material to scatter light is positively related to the refractive index mismatch between the polymer and the filler. The refractive index of polymer increases during curing due to the increase in density and reduced polarizability (10) while the refractive index of the filler remains constant, thus their mismatch either increases or decreases, depending on the initial values. If the initial refractive index of the monomer is lower than that of the filler, the refractive index mismatch diminishes during curing, resulting in a gradual increase in light transmittance (14). However, if the refractive index of monomer is initially higher than that of the filler, curing further increases the refractive index mismatch, progressively decreasing transmittance (15,16). It is also possible that the initially lower refractive index of the resin becomes equal to that of the filler at some point of conversion and continues to rise afterwards (17). Therefore, the change of transmittance during curing is a complex material-dependent phenomenon, influenced by several simultaneously occurring processes.

The changes in light transmittance during polymerization can be used to gain information on polymerization kinetics. Harrington et al. proposed light transmittance monitoring during light curing as a means of determining the optimal irradiation times, suggesting a cessation of light transmittance change as an indicator of complete cure (14). Howard et al. described how light transmission profile during curing relates to the initiator concentration, filler load and irradiance (10). Changes in light transmittance were used to assess how the reaction kinetics is affected by various photoinitiators (15) and refractive index mismatch and monomer reactivity (17). Rosentritt et al. compared light transmittance, differential scanning calorimetry and dielectrical analysis as a means of cure monitoring (18) and Ilie et al. used mathematical modeling to compare the real-time measurements of conversion and light transmittance during polymerization (19). These studies established that changes in light transmittance allow tracking of the curing progress, however the quantitative relation between the transmittance changes and the fundamental process of polymerization is poorly understood and recorded changes in transmittance cannot be directly translated into conversion kinetics (17). Despite the change of light transmittance during curing is to a certain extent convoluted by other factors (e.g. CQ consumption), the most part of light transmittance change is considered to be due to the changing refractive index of polymerizing resin, which in turn affects light scattering at filler/resin interface (16). In this regard, transmittance curves reflect the progress of monomer conversion and are considered suitable for assessing polymerization kinetics (19).

Photopolymerization of dental composites is characterized by rapidly increasing viscosity and follows three distinct kinetic regimes: (I) initial phase in which polymeric chains grow without restriction, with kinetics determined by the concentrations of monomer and free radicals, (II) the phase in which rapidly increasing viscosity restricts the termination of free radicals, resulting in an overall increased reaction rate (gel phase), and (III) the phase of extreme viscosity which limits propagation rate and finally ends the reaction (glass phase) (20). Ilie et al. were able to identify the latter two phases by fitting the real-time conversion data to two exponential functions, each representing one phase (19). They applied the same approach to the real-time light transmittance data and found transmittance curves less discriminative, able to address only the beginning of the glass phase. Although several other studies used the real-time light transmittance monitoring (10,14-18), none of them has attempted a mathematical analysis of the transmittance curves as a means of obtaining the polymerization rate.

This paper is one in the series of our investigations on ACP-composites reinforced with inert fillers (5-7,21). The aims of this study were to: (I) assess the light transmittance of ACP-composites with reinforcing fillers, (II) use the real-time light transmittance monitoring to obtain a measure of the polymerization rate, (III) compare the light transmittance, conversion and temperature data to gain information about polymerization kinetics and (IV) explore the relationship between the polymerization rate and light transmittance.

4.3 Materials and methods

4.3.1 Composite materials

Five ACP-based and two control composites were prepared, as described in our previous study (21). The composition of experimental composites is given in Table 1. For light transmittance and temperature measurements, Tetric EvoCeram (Ivoclar Vivadent, Schaan, Liechtenstein) of shade A2, LOT: S26173, EXP: 06/2017 was used as a reference. Personal communication with the manufacturer indicated that Tetric EvoCeram of shade A2 does not contain any alternative initiators besides CQ.

Table 1. Composition of the experimental composite materials.

	Material	Filler (wt%)	Resin (wt%)		Filler load (vol%)
ACP-based materials	**ACP40**	40% Zr-ACP	60 wt%	67%	27.6
	ACP40-Ba10	40% Zr-ACP, 10% Ba-fillers	50 wt%	EBPADMA 23% TEGDMA 10% HEMA	35.1
	ACP40-Si10	40% Zr-ACP, 10% Si-fillers	50 wt%		36.6
	ACP40-Ba5Si5	40% Zr-ACP, 5% Ba-fillers, 5% Si-fillers	50 wt%	photoinitiator: 0.2% CQ photoreductant: 0.8% 4E	35.9
	ACP40- Ba9Si1	40% Zr-ACP, 9% Ba-fillers, 1% Si-fillers	50 wt%		35.3
control materials	**Ba40**	40% Ba-fillers	60 wt%		22.0
	Ba40Si10	40% Ba-fillers, 10% Si-fillers	50 wt%		31.5

Barium-fillers (Ba): SiO_2 55.0%, BaO 25.0%, B_2O_3 10.0%, Al_2O_3 10.0%, F 2.00%, particle size (d50/d99 (µm)) 0.77/2.28, silanization 6 wt%, product name/manufacturer: GM39923/Schott, Germany.

Silica-fillers (Si): $SiO2 \geq 99.8$, primary particle size: 12 nm, silanization 4-6 wt%, product name/manufacturer: Aerosil DT/Evonik Degussa, Germany.

EBPADMA: ethoxylated bisphenol A dimethacrylate, Esstech, PA, USA; TEGDMA: tri-ethylene glycol dimethacrylate, Esstech; HEMA: 2-hydroxyethyl methacrylate, Esstech; CQ: camphorquinone, Aldrich, WI, USA; 4E: ethyl-4- (dimethylamino) benzoate, Aldrich.

4.3.2 Light transmittance and temperature

Uncured composite materials were cast into cylindrical Teflon molds (d = 6 mm, h = 2 mm), covered from both sides with a polyethylene terephthalate (PET) film (h = 0.05 mm) and sandwiched between two glass plates (h = 1 mm), as shown in Figure 1. Five samples were made per material. The curing unit tip was positioned immediately below the glass plate and the spectra were taken from the opposite side of the sample by a charge-coupled device array fiber spectrometer HR4000 (Ocean Optics, Dunedin, FL, USA). Light transmittance was recorded at the wavelength of 468 nm, corresponding to the CQ absorption peak (22). The ratio of the light intensity passing through the sample and the light intensity passing through the empty sample compartment was calculated as the light transmittance (%). Temperature was monitored simultaneously with light transmittance, using a T-type thermocouple positioned centrally between the PET film and glass plate at the side opposite to the curing unit.

Curing was performed for 30 s with Bluephase G2 (Ivoclar-Vivadent, Schaan, Liechtenstein; wavelength range 380–515 nm, intensity 1185 mW/cm^2, as measured with integrating sphere, IS, Gigahertz Optik GmbH, Puchheim, Germany). After 120 s, an additional illumination (30 s) was performed (Figure 2). The measurements were performed at the rate of 20 points per second and five samples were made for each composite. The environmental temperature was 25 ± 1 °C.

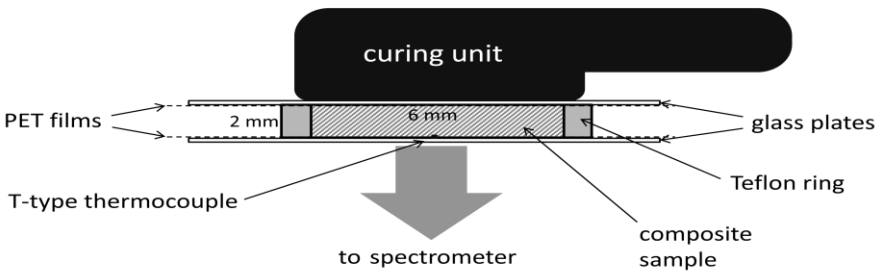

Figure 1. Cross-sectional scheme of the experimental setup

4.3.3 Degree of conversion

For each material, five discoid samples (d = 3 mm, h = 2 mm) were made using a stainless steel mold. Uncured composite was cast into the mold, the mold apertures were covered with a PET film and curing was performed for 30 s through the upper aperture with the Bluephase device. The curing unit tip was positioned at the angle of 90°, immediately adjacent to the mold aperture, contacting the PET film covering the sample. Curing was performed at 25 ± 1 °C. Raman spectra were recorded from the center of upper sample surface immediately after curing (a single measurement lasted for 15 minutes) and after 24 h of dark storage in the incubator (Cultura, Ivoclar-Vivadent) at 37 ± 1°C.

FT-Raman spectroscopy measurements were performed using a Spectrum GX spectrometer (PerkinElmer, Waltham, USA). The excitation was an Nd:YaG laser at 1064 nm wavelength, with laser power of 400 mW, resolution of 4 cm^{-1} and the exposed sample surface of 0.5 mm in diameter. For each spectrum, 100 scans were recorded. Spectra of the uncured composites (n = 5) were recorded in the same manner. The spectra were processed with the Kinetics add-on for Matlab (Mathworks, Natick, Massachusetts, USA).

Degree of conversion (DC) calculation was performed by comparing the relative change of the band at 1640 cm^{-1}, representing the aliphatic C=C stretching mode to the aromatic C=C band at 1610 cm^{-1}, before and after polymerization. Peak heights of aliphatic C=C and aromatic C=C bands were used for DC calculation by the following equation: $DC = 1 - R_{polymerized}/R_{unpolymerized}$, where R = (aliphatic C=C peak height) / (aromatic C=C peak height). A previous study by our group (21) showed that the DC values measured at sample surfaces were statistically similar to those measured at depths up to 2 mm, thus the surface DC values were considered representative for the samples used in transmittance measurements, despite different geometry.

4.3.4 Scanning electron microscopy (SEM)

The light-cured (30 s), disc-shaped samples of 1 mm thickness, unpolished and unsputtered were examined with FE-SEM JSM 7000 (JEOL, Peabody, MA, USA).

4.3.5 Statistical analysis

Normality of distribution and homogeneity of variances were confirmed using Shapiro-Wilk's and Levene's test, respectively. Light transmittance values at the start of curing (T1), end of curing (T2) and during an additional illumination (T3) were compared among composites by one-way ANOVA and Tukey post-hoc test. Within a given material, T1, T2 and T3 values were compared using repeated measurements ANOVA and Bonferroni post-hoc test.

Mean values of the variables used to describe polymerization kinetics (duration of the linear transmittance rise, time of the temperature peak, slope of the linear transmittance rise and DC) were compared among materials by one-way ANOVA and Tukey post-hoc test. Additionally, paired t-test was used to compare the duration of the linear transmittance rise and time of the temperature peak within each composite. Paired t-test was also used to compare the DC values immediately after curing and 24 h post-cure.

Pearson's correlation analysis was used to correlate the slope of the linear part of transmittance rise and transmittance values at three time points (T1, T2 and T3). Statistical analysis was performed in SPSS 20 (IBM, Armonk, NY, USA) with $\alpha = 0.05$.

4.4 Results

The light transmittance and temperature curves are exemplified in Figure 2. A linear transmittance rise can be observed in the initial part of the curve, followed by an exponential-like behavior towards the end of illumination. The temperature curve during the first illumination features a distinct peak that was used to approximate the onset of vitrification (23). Light transmittance values used in calculations were taken from transmittance curves at three time points: start of curing (T1), end of curing (T2) and during an additional illumination (T3). These values and results of statistical analysis are presented in Figure 3.

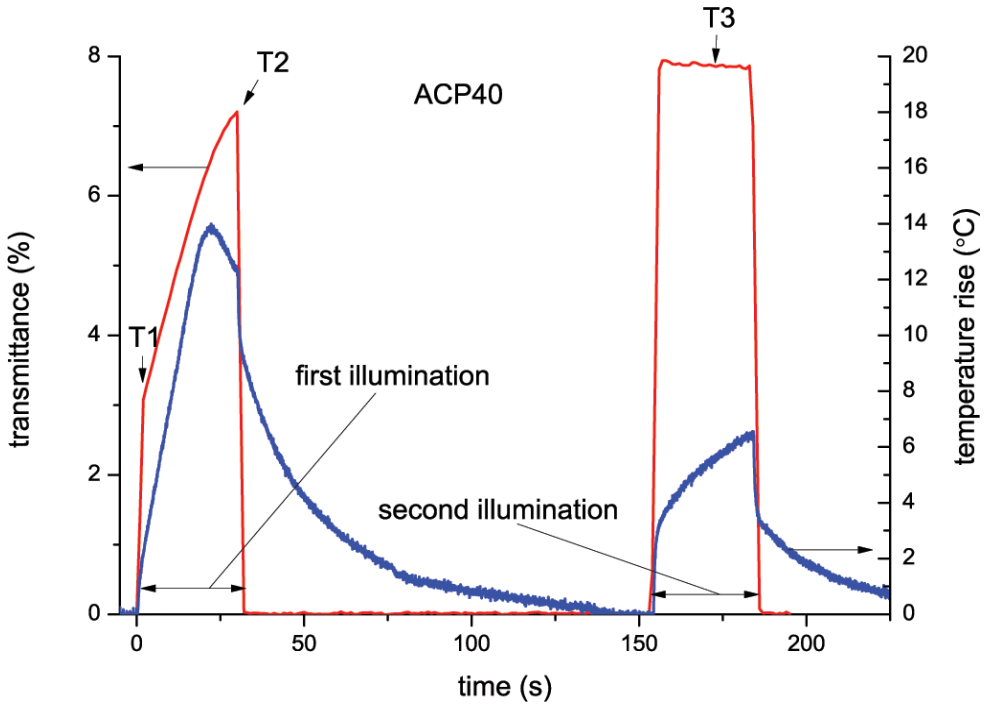

Figure 2. An example of simultaneously recorded light transmittance and temperature curves. Transmittance values at the start of curing (T1), end of curing (T2), and during an additional illumination (T3).

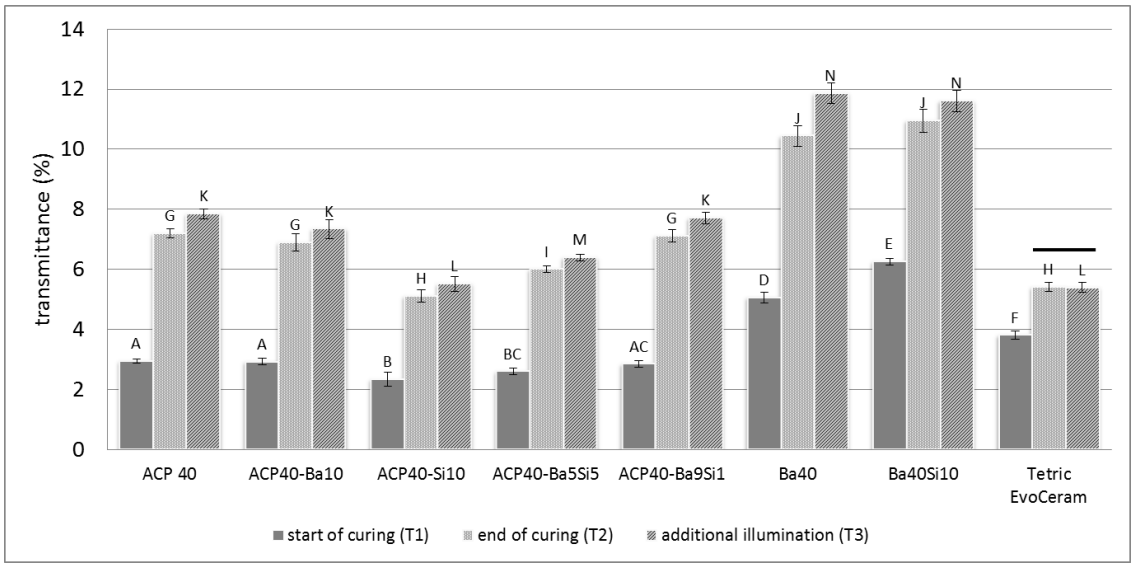

Figure 3. Light transmittance (%) at three time points. Same uppercase letters denote statistically homogeneous groups. Error bars represent ± one standard deviation. Horizontal line above the bars denotes statistical homogeneity between different time points, which was found only between T2 and T3 for Tetric EvoCeram.

Figure 4 shows light transmittance curves representative for the ACP-composites (a), control composites (b) and Tetric EvoCeram (c). To describe polymerization kinetics, an initial linear part of light transmittance curves was fitted to a linear function in the range for which R^2>0.98 could be obtained and its slope (Table 2) was assessed as a measure of the polymerization rate. Each curve was normalized to its transmittance change during curing (T2-T1), so that the slope represents the rate at which transmittance increases in terms of % of the total transmittance change during 30 s of curing. The slope values were plotted against transmittance values for each sample (total n = 35) and analyzed by Pearson correlation. A significant correlation and high r values were observed (Figure 5). Since the linear transmittance rise was not detectable for Tetric EvoCeram (Figure 4c), it was excluded from further kinetic analysis.

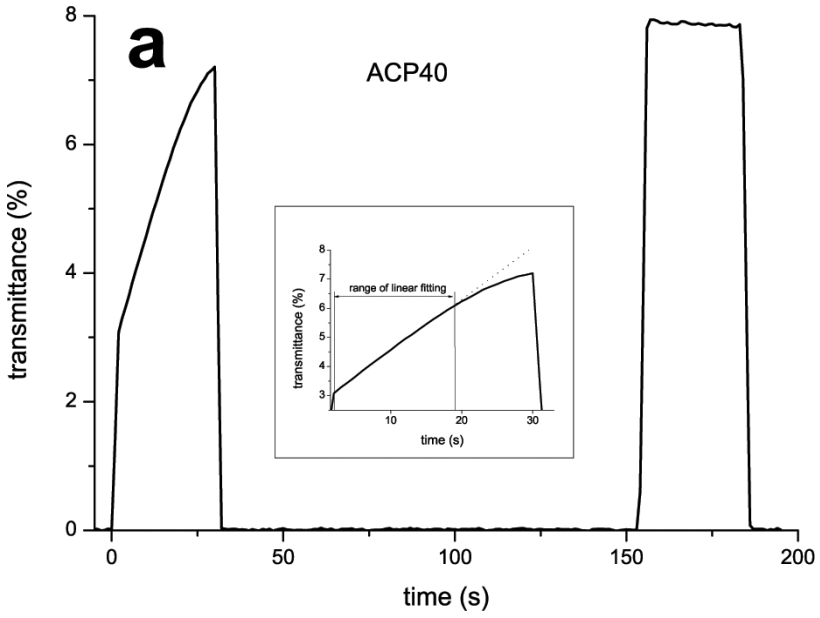

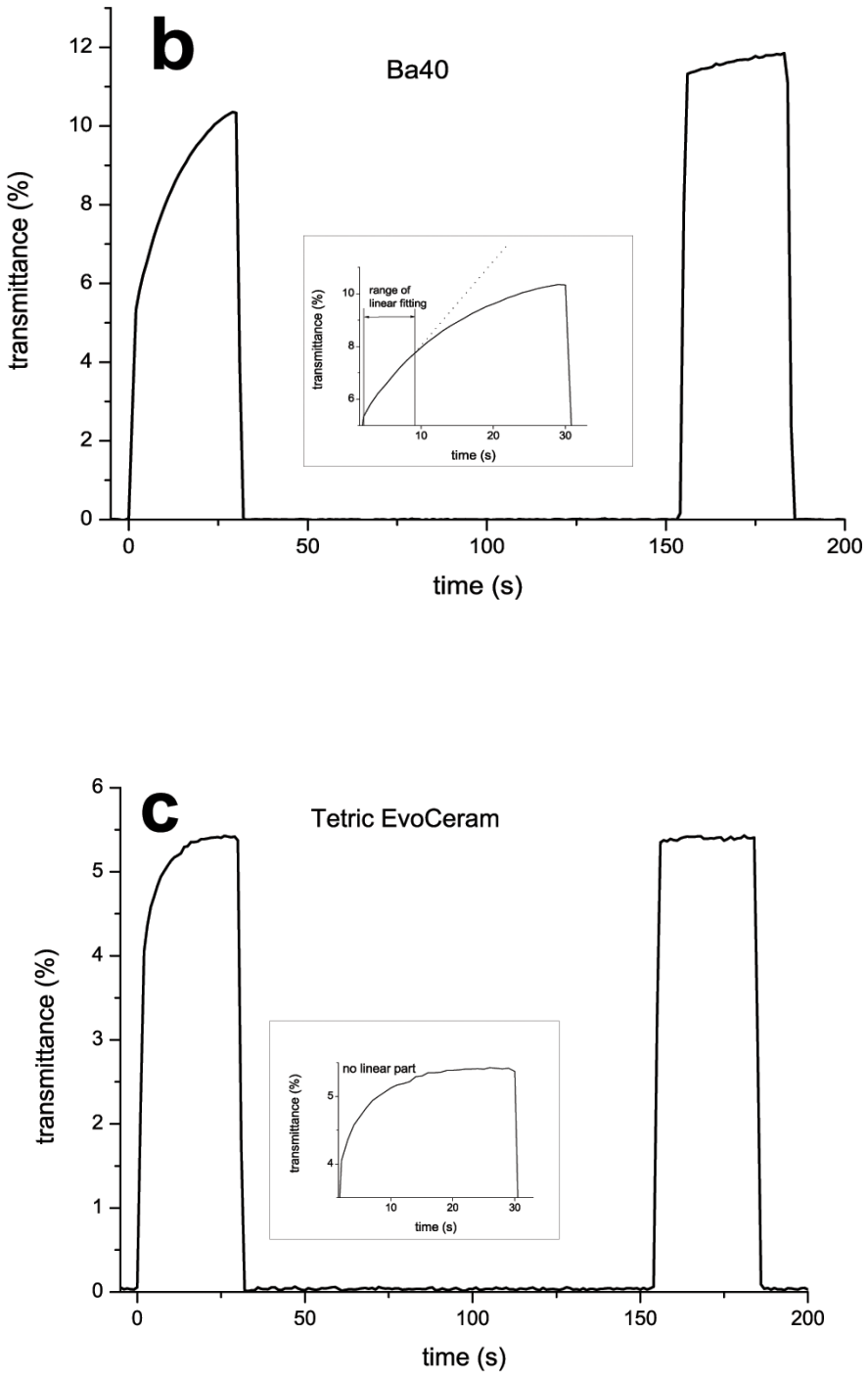

Figure 4. Averaged light transmittance curves for materials ACP40 (a), Ba40 (b) and Tetric EvoCeram (c). The insets show a magnified part of curves during the light-curing, range of linear fitting (R^2>0.98) and fit result (dotted line).

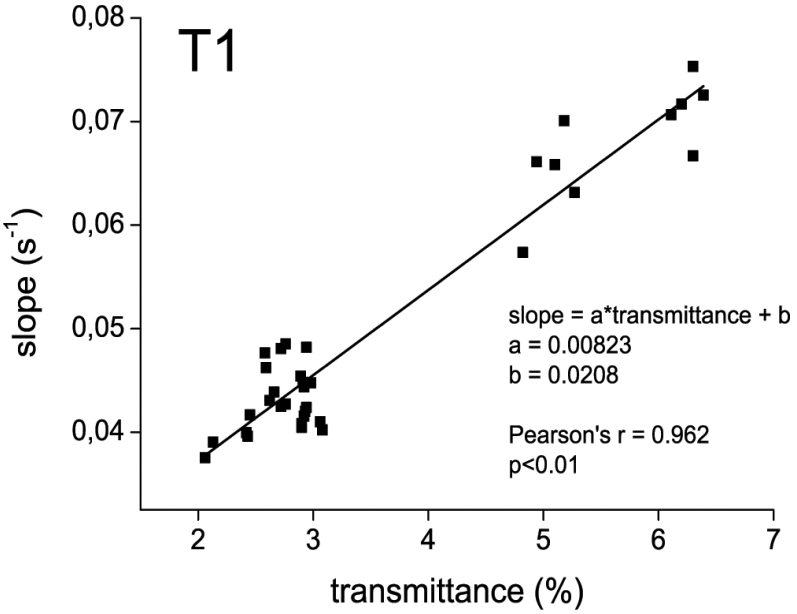
T1
slope (s-1)
transmittance (%)
slope = a*transmittance + b
a = 0.00823
b = 0.0208
Pearson's r = 0.962
p<0.01

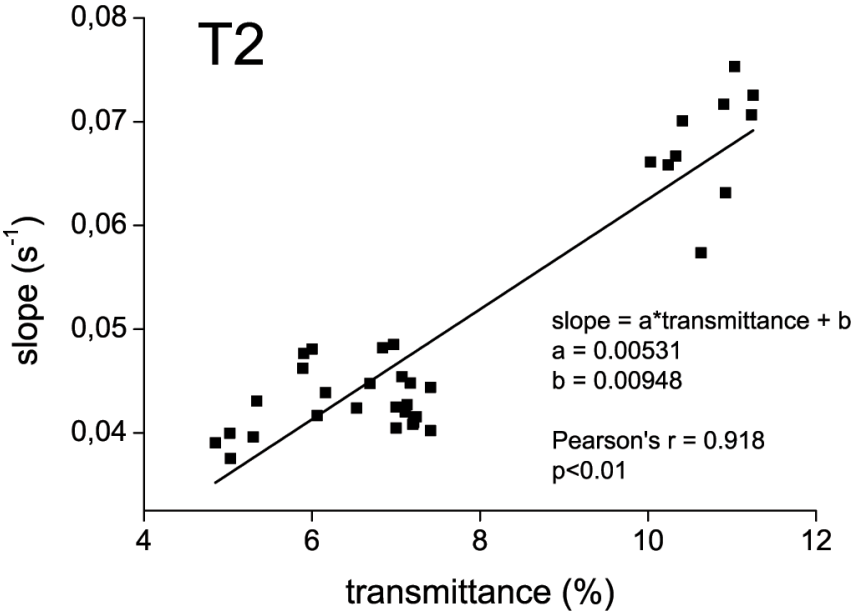
T2
slope (s-1)
transmittance (%)
slope = a*transmittance + b
a = 0.00531
b = 0.00948
Pearson's r = 0.918
p<0.01

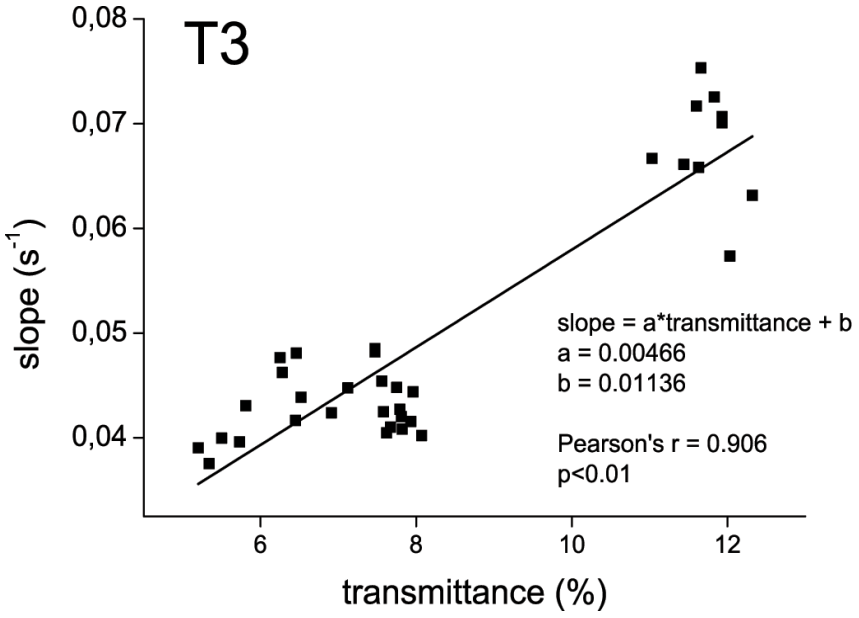

Figure 5. Linear correlation between the slope of the linear part of light transmittance rise and transmittance values at the start of curing (a), end of curing (b) and during an additional illumination (c).

Table 2 shows variables used for describing the polymerization kinetics (duration of the linear transmittance rise, time of the temperature peak and slope of the linear transmittance rise) and DC values immediately after curing and 24 h post-cure. The linear transmittance rise was observed for all of the experimental materials, with notable differences in its duration between the ACP-based and control materials. The ACP-composites presented high immediate DC with insignificant post-cure DC increase, while the controls showed the opposite behavior: low immediate DC and high post-cure DC increase.

Figure 6 is a SEM micrograph of a cured sample of ACP40, showing irregularly shaped ACP agglomerates of approximately 2-5 μm.

Table 2. Variables used for describing polymerization kinetics and degree of conversion immediately after curing and 24 h post-cure.

Material	**duration of the linear transmittance rise (s)**	**time of the temperature peak (s)**	**slope (%/s)**	**DC immediately after curing (%)**	**DC 24 h post-cure (%)**
ACP40	18.98 (0.97) AB	22.19 (0.63) AB	4.10 (0.07) AB	86.4 (1.1) A	86.7 (1.6) A
ACP40-Ba10	20.22 (0.64) A	20.18 (0.77) A+	4.44 (0.28) AB	80.0 (1.9) B	81.3 (1.7) B
ACP40-Si10	19.94 (0.59) A	23.96 (0.65) B	3.99 (0.20) A	81.5 (1.6) B	83.5 (0.7) AB
ACP40-Ba5Si5	17.38 (0.55) C	19.90 (0.31) A	4.55 (0.27) B	80.3 (2.5) B	80.6 (1.5) B
ACP40-Ba9Si1	17.94 (0.48) BC	20.64 (0.23) A	4.45 (0.23) AB	79.5 (0.9) B	80.6 (2.0) B
Ba40	9.36 (0.74) D	22.60 (1.96) AB	6.45 (0.47) C	33.0 (2.9) C	55.5 (2.3) C *
Ba40Si10	6.58 (0.69) E	16.56 (3.34) C	7.14 (0.31) D	33.4 (1.6) C	59.2 (3.5) C *

Standard deviations are given in parentheses.

Same uppercase letters denote statistically homogeneous groups within a column.

Plus sign (+) denotes statistical similarity between values in the first two columns, for a given material.

Asterisk (*) denotes statistically significant post-cure DC increase, for a given material.

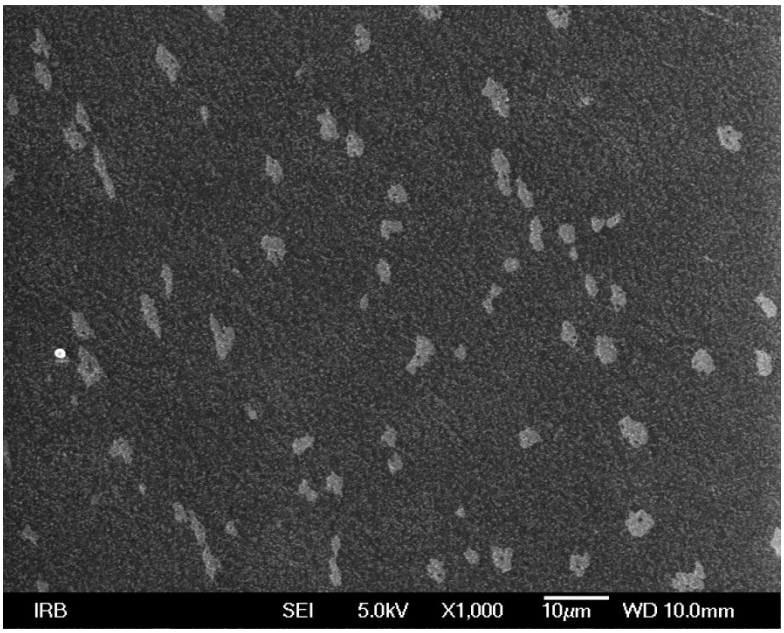

Figure 6. SEM micrograph of ACP40 demonstrating a homogeneous distribution of ACP particles with sizes of 2-5 μm.

4.5 Discussion

4.5.1 The effect of composition on light transmittance

Initial light transmittance values (T1) of the ACP-composites (2.3-2.9%) were lower than that of the commercial reference Tetric EvoCeram (3.8%). However, the ACP-composites presented a considerable transmittance rise during curing, which led to T2 and T3 values similar to or higher than those of Tetric EvoCeram (Figure 3). This indicates that the initially lower potential of the ACP-composites to transmit light improves during the curing to a level comparable to that of the commercial composite. The effect of the addition of inert fillers was the most prominent for material ACP40-Si10 which showed significantly lower light transmittance than the other ACP-composites. Silica fillers exist as agglomerates of different sizes, some of which have the size that maximizes the scattering of curing light (about 0.2 μm for a wavelength of 468 nm) and are responsible for lowering the light transmittance (24). Other combinations of inert fillers slightly decreased the light transmittance, though not statistically significant. It is interesting to note that ACP40, ACP40-Ba10 and ACP40-Ba9Si1 had statistically similar transmittance values within any measurement time (T1, T2 and T3), suggesting that the addition of up to 10 wt% barium glass produced a negligible effect on transmittance.

For all of the experimental composites, T3 was significantly higher than T2, evidencing that post-cure polymerization continued after the initial curing of 30 s (Figure 3). Additional feature that gives information on post-cure behavior is the shape of the curve during an additional illumination – a plateau observed for the ACP-composites (Figure 4a) suggests that the post-cure reaction was mostly finished before the additional illumination, while the curves of the control composites showed a slight slope (Figure 4b) evidencing the continuation of the post-cure reaction. Whether this was caused by the additional illumination or the reaction would continue by itself “in dark” (25) was outside the scope of this work. Nevertheless, real-time light transmittance monitoring appears as a simple means for assessment of the polymerization “completeness” (14).

4.5.2 Polymerization kinetics

Real-time light transmittance measurements enable monitoring of the curing progress. An interesting kinetic feature observed for experimental composites is the linear transmittance rise that lasted for 6.6 - 20.2 s (Figure 4, Table 2). Such kinetic behavior has not been reported in previous studies (10,14-19), which presented light transmittance curves resembling the function f(x)=1-exp(-x) and was shown to be well represented by a sum of two exponential functions (19). The exponential transmittance rise was also demonstrated for the commercial reference Tetric EvoCeram in our study, whose transmittance curves could be described by the function f(t) = 0.0612 + 0.0394 * (1 - exp (-0.2048 t)) + 0.0536 * (1 - exp (-24.2659 t)), where f(t) = transmittance (unitless) and t = time (s). Despite the polymerization progress observed through light transmittance curves cannot be directly translated into conversion, the existence of a linear part in transmittance curves of experimental composites suggests a constant reaction rate during a certain period of polymerization. This is unusual, since the diffusional restrictions that occur very early during methacrylate polymerization are expected to considerably affect the reaction rate through processes known as autoacceleration and autodeceleration (20). However, Dickens et al. have demonstrated that low-viscosity, TEGDMA-rich resins may present a nearly-constant reaction rate throughout a wide range of conversion (26). In their study, Bis-EMA/TEGDMA comonomers with 0-50 mol% of Bis-EMA showed a nearly-constant reaction rate and delayed diffusional restrictions, possibly due to the better network mobility and dominance of cyclization over crosslinking. Our composites had the Bis-EMA content similar to that of Dickens' study (46 mol%) and featured an additional 26 mol% of HEMA. The propensity of monofunctional HEMA to promote linear chain growth instead of crosslinking can even more postpone diffusional restrictions (20) and contribute to the distinct polymerization behavior seen in our composites.

ACP-composites showed longer durations of linear transmittance rise than the controls Ba40 and Ba40Si10 (Table 2), suggesting the later onset of diffusional restrictions in case of the former. Similar to the way in which TEGDMA delays gelation by favoring cyclization over crosslinking (26), the unsilanized ACP particles may be hypothesized to favor high local conversion while hindering the formation of infinite network. Early polymerization of resins containing TEGDMA and HEMA is dominated by cyclization reactions, resulting in poorly crosslinked microgel regions. As polymerization progresses, the microgels become interconnected by crosslinks, leading to macroscopic gelation (20). Unsilanized ACP particles may present obstacles for joining of the microgels, thus hindering crosslinking and delaying

gelation. In contrast, silanized particles are capable of bonding to the growing polymeric network and may allow earlier crosslinking. The earlier onset of diffusional restrictions caused by reactive fillers was demonstrated in a study of composites filled with reactive and nonreactive nanogels (27). Another contributing factor for the observed differences in kinetic behavior may have been comparatively larger particles of ACP filler (Figure 6), which had lower surface area in contact with the resin thus allowing better mobility (28,29). In any case, all of the ACP-composites showed similar duration of the linear transmittance rise (Table 2), demonstrating that the addition of 10% of silanized fillers did not considerably affect their kinetic behavior.

The differences in polymerization kinetics between ACP-composites and controls are furthermore evidenced by the degree of conversion (DC) results obtained immediately and 24 hours after cure. For the ACP-composites, very high DC immediately after curing and a statistically insignificant post-cure DC increase were observed (Table 2), suggesting high mobility of reactive species during curing. In contrast, the controls showed lower initial DC and a significant post-cure DC increase, indicating that severe mobility restrictions occurred much before the composites attained their final conversion. The explanatory hypothesis that this difference may be due to presence of unsilanized particles which enabled better mobility during curing is supported by the studies of rubbers which demonstrated that local mobility and glass transition temperature depends upon the ability of filler particles to form chemical bonds with the matrix (30,31). For dental composites, the effect of reactive particle surfaces on network mobility was suggested by lower conversions of composites containing silanized particles (32,33). Additionally, the fact that commercial composites encompassing a wide range of resin compositions, filler loads and geometries (34) commonly show conversions in the range of 50-75%, contrasting the ACP-composites which attain conversions of 80% or higher (1,21,35-37), supports a probable role of unsilanized particles on polymerization kinetics.

To obtain additional information on polymerization progress, temperature rise was recorded simultaneously with light transmittance (Figure 2). The peak in temperature curve occurs when the temperature buildup ceases due to the sudden decrease in reaction rate that occurs at the onset of vitrification (23). Thus the time of the temperature peak (Table 2) can be used to approximate the glass-point. The glass-point of the ACP-composites was observed at 19.9-24.0 s, while for Ba40 and Ba40Si10 occurred at 22.6 and 16.6 s, respectively. Among the ACP-composites, ACP40-Si10 had the latest occurrence of peak, possibly due to its

comparatively lowest transmittance that reduced the initiation rate, thus delaying vitrification. The influence of other inert filler additions on the time of temperature peak for ACP-composites was statistically insignificant. The early onset of peak for Ba40Si10 suggests the fastest vitrification among all of the materials. A possible explanation is high silanized surface area that may have contributed to more rapid immobilization of the polymerizing matrix (32,33). Much earlier vitrification seen in Ba40Si10 than in Ba40 can be attributed to increased viscosity due to the addition of small silica particles (28). On the other hand, the addition of 10 wt% of silica to ACP-composite did not cause such a pronounced shift in vitrification point. This may have been compensated by large ACP particles with unsilanized surfaces that allowed better mobility, as discussed previously. Comparison of the times of the temperature peak and the duration of linear transmittance rise showed that the largest part of the pre-glass polymerization of ACP-composites was characterized by a linear transmittance rise, which lasted for approximately 17-20 s and ended 0-3 s before vitrification (Table 2). This suggests that the polymerization proceeded with a nearly-constant rate until very close to vitrification. In the case of ACP40-Ba10, the nearly-constant reaction rate lasted throughout the whole pre-glass period. In contrast, the linear part of transmittance rise for the control composites Ba40 and Ba40Si10 ended approximately 10-13 s before the temperature peak, indicating that mobility restrictions occurred at earlier phase of the polymerization.

The linear part of transmittance rise was fitted to a linear function whose slope was assessed as a measure of the polymerization rate. Theoretically, before the onset of diffusional limitations, the polymerization rate is a function of the concentrations of monomer and free radicals (38). For early phase of the polymerization, two assumptions can be made: that the monomer concentration remains constant and that all of the present free radicals are in fact the radicalized initiator. Such simplification yields a constant polymerization rate, which is linearly dependent on the concentration of radicalized initiator (39). Although this approximation is not valid for long time ranges through which we performed linear fitting (7-20 s, Table 2), a good fit throughout the whole range means that the slope remained the same as in the earliest stage of polymerization where the approximation holds. Assuming that slope of the linear part of transmittance rise is a valid measure of the polymerization rate, a relationship between slope and transmittance should exist, as transmittance determines the effective irradiance in the bulk of the sample, which in turn dictates the concentration of radicalized initiator. To examine this relationship, transmittance values of seven experimental composites at the start of curing (T1), end of curing (T2) and during an additional

illumination (T3) were plotted against the slope values and Pearson correlation coefficient was calculated (Figure 5). In a linear function written as y = ax + b, where y=normalized slope and x=transmittance, a values (s^{-1}) were 0.0082, 0.0053 and 0.0047 respectively for T1, T2 and T3. Respective values of Pearson's r were 0.962, 0.918 and 0.906, statistically significant at $p<0.01$. The trend of decreasing a values in the order T1 >T2 > T3 shows that the linear dependence of reaction rate is more steep for earlier transmittance values, while the trend of decreasing r values in the same order shows that earlier transmittance values were more predictive of the reaction rate. Higher correlation for earlier transmittance values is expected, since these values determined the concentration of radicalized initiator.

4.6 Conclusions

Despite the kinetic inferences drawn from light transmittance curves were not confirmed by real-time conversion measurements, we observed a kinetic behavior that has not been reported previously and is suggestive of a rather long period of a nearly-constant reaction rate for composites comprised of Bis-EMA/TEGDMA/HEMA resin and unsilanized ACP particles. Since remineralizing composites usually contain unsilanized particles of various calcium phosphates (8), there are possible consequences relevant to this group of materials. A kinetic behavior with no evidence of autoacceleration suggests slower development of polymerization shrinkage stress and possibly a prolonged pre-gel phase, which is favorable from a clinical standpoint. On the other hand, the final polymeric network may be highly heterogeneous and consist of many poorly interconnected microgel regions (20), resulting in impaired mechanical properties. This indicates the need to further investigate the kinetic behavior of remineralizing composites.

4.7 Acknowledgments

We thank Mira Ristić and Marijan Marciuš from the Division of Materials Chemistry, Ruđer Bošković Institute for the SEM micrographs. We also gratefully acknowledge Drago Skrtic for providing us with the zirconia-hybridized ACP.

4.8 References

1. Skrtic D, Antonucci JM, Eanes ED. Amorphous Calcium Phosphate-Based Bioactive Polymeric Composites for Mineralized Tissue Regeneration. J Res Natl Inst Stand Technol 2003;108(3):167-82.
2. Li F, Wang P, Weir MD, Fouad AF, Xu HH. Evaluation of antibacterial and remineralizing nanocomposite and adhesive in rat tooth cavity model. Acta Biomater 2014;10(6):2804-13.
3. Weir MD, Chow LC, Xu HH. Remineralization of demineralized enamel via calcium phosphate nanocomposite. J Dent Res 2012;91(10):979-84.
4. Skrtic D, Antonucci JM. Dental composites based on amorphous calcium phosphate - resin composition/physicochemical properties study. J Biomater Appl 2007;21(4):375-93.
5. Marovic D, Tarle Z, Hiller KA, Muller R, Ristic M, Rosentritt M, Skrtic D, Schmalz G. Effect of silanized nanosilica addition on remineralizing and mechanical properties of experimental composite materials with amorphous calcium phosphate. Clin Oral Investig 2014;18(3):783-92.
6. Marovic D, Tarle Z, Hiller KA, Muller R, Rosentritt M, Skrtic D, Schmalz G. Reinforcement of experimental composite materials based on amorphous calcium phosphate with inert fillers. Dent Mater 2014;30(9):1052-60.
7. Marovic D, Tarle Z, Ristic M, Music S, Skrtic D, Hiller KA, Schmalz G. Influence of different types of fillers on the degree of conversion of ACP composite resins. Acta Stomatol Croat 2011;45:231-38
8. Xu HH, Weir MD, Sun L, Moreau JL, Takagi S, Chow LC, Antonucci JM. Strong nanocomposites with Ca, PO4, and F release for caries inhibition. J Dent Res 2010;89(1):19-28.
9. Kawaguchi M, Fukushima T, Miyazaki K. The relationship between cure depth and transmission coefficient of visible-light-activated resin composites. J Dent Res 1994;73(2):516-21.
10. Howard B, Wilson ND, Newman SM, Pfeifer CS, Stansbury JW. Relationships between conversion, temperature and optical properties during composite photopolymerization. Acta Biomater 2010;6(6):2053-59.
11. Musanje L, Darvell BW. Curing-light attenuation in filled-resin restorative materials. Dent Mater 2006;22(9):804-17.

12. Shibayama M, Ozeki S, Norisuye T. Real-time dynamic light scattering on gelation and vitrification. Polymer 2005;46(7):2381-88.
13. Seghi RR, Gritz MD, Kim J. Colorimetric changes in composites resulting from visible-light-initiated polymerization. Dent Mater 1990;6(2):133-7.
14. Harrington E, Wilson HJ, Shortall AC. Light-activated restorative materials: a method of determining effective radiation times. J Oral Rehabil 1996;23(3):210-8.
15. Ogunyinka A, Palin WM, Shortall AC, Marquis PM. Photoinitiation chemistry affects light transmission and degree of conversion of curing experimental dental resin composites. Dent Mater 2007;23(7):807-13.
16. Fujita K, Ikemi T, Nishiyama N. Effects of particle size of silica filler on polymerization conversion in a light-curing resin composite. Dent Mater 2011;27(11):1079-85.
17. Shortall AC, Palin WM, Burtscher P. Refractive index mismatch and monomer reactivity influence composite curing depth. J Dent Res 2008;87(1):84-8.
18. Rosentritt M, Shortall AC, Palin WM. Dynamic monitoring of curing photoactive resins: a methods comparison. Dent Mater 2010;26(6):565-70.
19. Ilie N, Durner J. Polymerization kinetic calculations in dental composites: a method comparison analysis. Clin Oral Investig 2014;18(6):1587-96.
20. Andrzejewska E. Photopolymerization kinetics of multifunctional monomers. Prog Polym Sci 2001;26(4):605-65.
21. Par M, Gamulin O, Marovic D, Skenderovic H, Klaric E, Tarle Z. Conversion and temperature rise of remineralizing composites reinforced with inert fillers. J Dent 2016;48:26-33.
22. Emami N, Sjodahl M, Soderholm KJ. How filler properties, filler fraction, sample thickness and light source affect light attenuation in particulate filled resin composites. Dent Mater 2005;21(8):721-30.
23. Atai M, Motevasselian F. Temperature rise and degree of photopolymerization conversion of nanocomposites and conventional dental composites. Clin Oral Investig 2009;13(3):309-16.
24. Clewell DH. Scattering of Light by Pigment Particles. J Opt Soc Am 1941;31:512-17.
25. Pilo R, Cardash HS. Post-irradiation polymerization of different anterior and posterior visible light-activated resin composites. Dent Mater 1992;8(5):299-304.

26. Dickens SH, Stansbury JW, Choi KM, Floyd CJE. Photopolymerization kinetics of methacrylate dental resins. Macromolecules 2003;36(16):6043-53.
27. Moraes RR, Garcia JW, Barros MD, Lewis SH, Pfeifer CS, Liu J, Stansbury JW. Control of polymerization shrinkage and stress in nanogel-modified monomer and composite materials. Dent Mater 2011;27(6):509-19.
28. Beun S, Bailly C, Dabin A, Vreven J, Devaux J, Leloup G. Rheological properties of experimental Bis-GMA/TEGDMA flowable resin composites with various macrofiller/microfiller ratio. Dent Mater 2009;25(2):198-205.
29. Hadis M, Leprince JG, Shortall AC, Devaux J, Leloup G, Palin WM. High irradiance curing and anomalies of exposure reciprocity law in resin-based materials. J Dent 2011;39(8):549-57.
30. Berriot J, Lequeux F, Monnerie L, Montes H, Long D, Sotta P. Filler–elastomer interaction in model filled rubbers, a 1H NMR study. J Non-Cryst Solids 2002;307:719-24.
31. Ou YC, Yu ZZ, Vidal A, Donnet JB. Effects of alkylation of silicas on interfacial interaction and molecular motions between silicas and rubbers. J Appl Polym Sci 1996;59(8):1321-28.
32. Wilson KS, Zhang K, Antonucci JM. Systematic variation of interfacial phase reactivity in dental nanocomposites. Biomaterials 2005;26(25):5095-103.
33. Ferracane JL, Berge HX, Condon JR. In vitro aging of dental composites in water - effect of degree of conversion, filler volume, and filler/matrix coupling. J Biomed Mater Res 1998;42(3):465-72.
34. Ilie N, Hickel R. Investigations on mechanical behaviour of dental composites. Clin Oral Investig 2009;13(4):427-38.
35. Skrtic D, Antonucci JM. Bioactive polymeric composites for tooth mineral regeneration: physicochemical and cellular aspects. J Funct Biomater 2011;2(3):271-307.
36. Skrtic D, Antonucci JM, Liu DW. Ethoxylated bisphenol dimethacrylate-based amorphous calcium phosphate composites. Acta Biomater 2006;2(1):85-94.
37. Tarle Z, Knežević A, Matošević D, Škrtić D, Ristić M, Prskalo K, Musić S. Degree of vinyl conversion in experimental amorphous calcium phosphate composites. J Mol Struct 2009;924:161-5.
38. Watts DC. Reaction kinetics and mechanics in photo-polymerised networks. Dent Mater 2005;21(1):27-35.

39. Steinhaus J, Hausnerova B, Haenel T, Grossgarten M, Moginger B. Curing kinetics of visible light curing dental resin composites investigated by dielectric analysis (DEA). Dent Mater 2014;30(3):372-80.

5.

IMPEDANCE CHANGES DURING SETTING OF AMORPHOUS CALCIUM PHOSPHATE COMPOSITES

Matej Par, Ana Šantić, Ozren Gamulin, Danijela Marovic, Andrea Moguš-Milanković, Zrinka Tarle

Published in Dental Materials 2016;32(11):1312-21, doi: 10.1016/j.dental.2016.07.016

5.1 Abstract

Objectives: To investigate the electrical properties of experimental light-curable composite materials based on amorphous calcium phosphate (ACP) with the admixture of silanized barium glass and silica fillers.

Methods: Short-term setting was investigated by impedance measurements at a frequency of 1 kHz, while for the long-term setting the impedance spectra were measured consecutively over a frequency range of 0.05 Hz to 1 MHz for 24 hours. The analysis of electrical resistivity changes during curing allowed the extraction of relevant kinetic parameters. The impedance results were correlated to the degree of conversion assessed by Raman spectroscopy, water content determined by gravimetry, light transmittance measured by CCD spectrometer and microstructural features observed by scanning electron microscopy.

Results: ACP-based composites have shown higher immediate degree of conversion and less post-cure polymerization than the control composites, but lower polymerization rate. The polymerization rate assessed by impedance measurements correlated well with the light transmittance. The differences in the electrical conductivity values observed among the materials were correlated to the amount of water introduced into composites by the ACP filler. High correlation was found between the degree of conversion and electrical resistivity. Equivalent circuit modeling revealed two electrical contributions for the ACP-based composites and a single contribution for the control composites.

Significance: The impedance spectroscopy has proven a valuable method for gaining insight into various features of ACP-based composites. Better understanding of the properties of ACP-based composites should further the development of these promising bioactive materials.

5.2 Introduction

Incorporation of amorphous calcium phosphate (ACP) fillers in methacrylate resins results in bioactive, ion-releasing composite materials. Their bioactivity is due to the thermodynamic instability of ACP, which in aqueous media spontaneously converts into hydroxyapatite and concomitantly releases calcium and phosphate ions (1). When embedded in the appropriate methacrylate resin, ACP provides a sustained release of calcium and phosphate ions in concentrations sufficient for hydroxyapatite precipitation in dental hard tissues adjacent to the restoration (2, 3). The remineralizing ability of ACP-based composites has been demonstrated *in vitro* (3), *in situ* (4) and in animal model *in vivo* (5). These findings indicate the potential of ACP-based composites for preventing secondary caries, which is considered the main cause for failure of contemporary composite restorations (6).

The major drawbacks of ACP-based composites are poor mechanical properties and high shrinkage stress in comparison to commercial composites (7). To address these issues, ACP-based formulations were introduced with conventional silanized fillers (8, 9). Since the ACP-based composites attain sufficient ion release with 40 wt% of ACP (7), their filler load can be increased by the addition of inert fillers similar to those contained in conventional composites. In this way, a "hybrid" material is composed, which consists of a bioactive part (ACP fillers) and a reinforcing part (inert fillers). When exposed to water, ACP undergoes a dissolution-reprecipitation process converting into hydroxyapatite and releasing ions (10), while the inert fillers remain bonded to the methacrylate network and reinforce the restoration. The admixture of inert fillers (barium glass and silica) has been shown to improve the mechanical properties, without compromising the ion release (8, 9). By fine-tuning the composition of such "hybrid" ACP-based composites, their flexural strength may be enhanced to match the values of commercial resin-modified glass ionomer cements (11) and possibly even commercial composites (12).

Various properties of ACP-based composites have been investigated, but there are no studies examining their electrical properties by means of impedance spectroscopy (IS). Generally, IS is rarely used in investigations of dental composites – only several papers are available, dealing with composite degradation (13), water sorption (14, 15), microleakage (16) and polymerization kinetics (17-19). In particular, Steinhaus et al. (19) have described the kinetics of composite polymerization from the changes of the electrical resistivity as a function of time, $\rho(t)$, using the relation: $\rho(t) = \rho_{init} + B * \Delta t$; where ρ_{init} is the initial resistivity measured

before the curing and Δt is the time period since the start of curing. In the linear range of the resistivity vs. time curve, the resistivity is assumed to be proportional to the rheological viscosity and molecular mass of the growing polymeric chains. Therefore, slope B can be used as a measure of reaction rate during an early stage of polymerization, while polymeric chains grow linearly. Another kinetic parameter in the model is the reaction time constant, τ, contained in the relation: $\Delta\rho(t) = \Delta\rho_{max} * e^{-(\Delta t/\tau)}$ where Δρ(t) is the change of resistivity as a function of time and $\Delta\rho_{max}$ is the total change of resistivity during curing.

All above-mentioned IS studies are performed at a fixed frequency and there are no reports of the electrical properties of dental composites measured in a wide frequency range. This study employs IS to investigate the structural changes occurring during the short-term setting (during light-curing) and long-term setting (up to 24 h post-cure) of five ACP-based and two control composites. The short-term setting is analyzed in terms of impedance (electrical conductivity) changes at a fixed frequency as a function of time, while for the long-term setting the impedance spectra were measured consecutively over a frequency range of 0.05 Hz to 1 MHz for 24 hours. Furthermore, the results obtained by IS are correlated to the degree of conversion, water content, light transmittance and microstructural features.

5.3 Materials and methods

5.3.1 Composite materials

The composition of composite materials is given in Table 1. The synthesis of zirconia-hybridized ACP (Zr-ACP) fillers followed the procedure by Skrtic et al. (20). The resin was blended with fillers in lightproof containers using a dual asymmetric centrifugal mixing system (Speed Mixer TM DAC 150 FVZ, Hauschild & Co KG, Hamm, Germany), followed by deaerating the obtained composite pastes in vacuum for 12 hours.

Table 1. Composition of the experimental composite materials.

	Material	Filler (wt%)	Resin (wt%)		Filler load (vol%)
ACP-based materials	**ACP40**	40% Zr-ACP	60	67% EBPADMA 23% TEGDMA 10% HEMA photoinitiator: 0.2% CQ 0.8% 4E	27.6
	ACP40-Ba10	40% Zr-ACP, 10% Ba-fillers	50		35.1
	ACP40-Si10	40% Zr-ACP, 10% Si-fillers	50		36.6
	ACP40-Ba5Si5	40% Zr-ACP, 5% Ba-fillers, 5% Si-fillers	50		35.9
	ACP40- Ba9Si1	40% Zr-ACP, 9% Ba-fillers, 1% Si-fillers	50		35.3
control materials	**Ba40**	40% Ba-fillers	60		22.0
	Ba40Si10	40% Ba-fillers, 10% Si-fillers	50		31.5

Barium-fillers (Ba): SiO_2 55.0%, BaO 25.0%, B_2O_3 10.0%, Al_2O_3 10.0%, F 2.00%, particle size (d50/d99 (µm)) 0.77/2.28, silanization 6 wt%, product name/manufacturer: GM39923/Schott, Germany.

Silica-fillers (Si): SiO2 ≥ 99.8, primary particle size: 12 nm, silanization 4-6 wt%, product name/manufacturer: Aerosil DT/Evonik Degussa, Germany.

EBPADMA: ethoxylated bisphenol A dimethacrylate, Esstech, PA, USA; TEGDMA: tri-ethylene glycol dimethacrylate, Esstech; HEMA: 2-hydroxyethyl methacrylate, Esstech; CQ: camphorquinone, Aldrich, WI, USA; 4E: ethyl-4- (dimethylamino) benzoate, Aldrich.

5.3.2 Impedance spectroscopy

The samples (n=3) were cast in quartz rings (d=4 mm, h=4 mm), covered by brass electrodes (d=4 mm) and placed in an impedance cell. Complex impedance was measured using an impedance analyzer (Novocontrol Alpha-AN Dielectric Spectrometer, Novocontrol Technologies GmbH & Co. KG, Germany) at 2 V. Measurements at the fixed frequency of 1 kHz and consecutive frequency sweeps from 0.05 Hz to 1 MHz were performed to monitor the short-term and long-term setting, respectively. Frequency sweeps were performed every 5 minutes during the first 3 hours and afterwards at 6 h, 12 h and 24 h.

For light curing of the samples, LED polymerization devices were used (Bluephase G2, Ivoclar-Vivadent, Schaan, Liechtenstein; wavelength range 380–515 nm, intensity 1200 mW/cm^2). The light probes of two polymerization devices were placed immediately adjacent to the quartz rings and parallel to the brass electrodes, diametrically opposite to one another. To assure a thorough curing throughout the sample, the first polymerization device was activated for 30 s, followed by a successive activation of the second one for additional 30 s.

From complex impedance (Z*), the electrical conductivity (σ*) was calculated using the relation $\sigma^*=1/Z^*\cdot h/A$ where h is the height and A is the cross-sectional area of the sample. The short-term setting results were presented as changes of the real part of conductivity, σ', and resistivity ($\rho^*=1/\sigma^*$) as a function of time. The linear part of the resistivity curve was fitted to a straight line ($R^2>0.99$), and curing kinetics were assessed using parameters slope and τ, as described previously by Steinhaus et al. (19). The impedance spectra were analyzed by means of equivalent circuit modeling and parameters were obtained using the complex non-linear least square (CNLLSQ) fitting using ZView software.

5.3.3 Gravimetric analysis

For each material, six discs (d=5 mm, h=2 mm) were polymerized using the Bluephase device for 40 seconds on each side. The samples were weighted to the accuracy of 10^{-4} g with the analytical balance (XS204, Mettler Toledo, Greifensee, Switzerland) immediately after polymerization, after 5 days and 14 days of desiccator storage. The equilibrium occurred after 5 days, thus the water content (wt%) was calculated as: ((mass before drying) – (mass after drying)) / (mass before drying).

5.3.4 Light transmittance

Uncured composite materials were cast into cylindrical Teflon molds (d=6 mm, h=2 mm), covered from both sides with a polyethylene terephthalate (PET) film (0.05 mm thick) and sandwiched between two glass plates (h=1 mm). The curing unit tip was positioned immediately below the glass plate and the spectra were taken from the opposite side of the sample by a CCD array fiber spectrometer HR4000 (Ocean Optics, Dunedin, FL, USA). Transmittance was recorded at the wavelength of 468 nm immediately after activation of the curing unit and five repeats were made for each composite. The ratio of the light intensity passing through the sample and the light intensity passing through the empty sample compartment was calculated as the transmittance (%).

5.3.5 Scanning electron microscopy (SEM)

The light-cured (40 s), disc-shaped samples of 1 mm thickness, unpolished and uncoated were examined with FE-SEM JSM 7000 (JEOL, Peabody, MA, USA).

5.3.6 Raman spectroscopy

Five cylindrical samples (d=3 mm, h=2 mm) were made using a stainless steel mold. Uncured composite was cast into the mold, the mold apertures were covered with a PET film and curing was performed for 40 s through the upper aperture with the Bluephase device. The curing unit tip was positioned at the angle of 90°, immediately adjacent to the mold aperture, contacting the PET film covering the sample. Raman spectra were recorded from the upper sample surface immediately after curing and after 24 h of dark storage in the incubator (Cultura, Ivoclar-Vivadent, Schaan, Liechtenstein) at 37±1°C.

FT-Raman spectroscopy measurements were performed using a Spectrum GX spectrometer (PerkinElmer, Waltham, USA). The excitation was an NdYaG laser at 1064 nm wavelength, with laser power of 400 mW and resolution of 4 cm^{-1}. The exposed sample surface was 0.5 mm in diameter. For each spectrum, 100 scans were recorded. Spectra of the uncured composites (n=5) were recorded in the same manner. The spectra were processed with the Kinetics add-on for Matlab (Mathworks, Natick, Massachusetts, USA).

Degree of conversion calculation was performed by comparing the relative change of the band at 1640 cm^{-1}, representing the aliphatic C=C stretching mode to the aromatic C=C band at 1610 cm^{-1}, before and after polymerization. Peak heights of aliphatic C=C and aromatic C=C bands were used for the conversion calculation by the following equation: conversion = 1 – $R_{polymerized}/R_{unpolymerized}$, where R = (aliphatic C=C peak height) / (aromatic C=C peak height) (21).

It is important to note that the sample geometries differed among the methods due to technical reasons. The curing regimes used for each of the sample geometries were adapted to attain the maximum conversion throughout the bulk of the samples, as confirmed by preliminary measurements. Thus the samples were assumed to be fully and homogeneously polymerized, allowing comparison of the results obtained from different setups. For all the experiments, sample preparation and measurements were done at room temperature of 21±1°C.

5.3.7 Statistical analysis

Descriptive statistics were used to present the data and Pearson's correlation analysis was used to correlate the water content, conversion, filler load and transmittance with impedance data (α=0.05). One-way ANOVA with post-hoc Tukey test was used for comparison of conversion among the composites, while the repeated samples t-test was used for comparison of conversion immediately after curing and 24 h post-cure (α=0.05). Statistical analysis was performed in SPSS 20 (IBM, Armonk, NY, USA)

5.4 Results

Water content (wt%), transmittance (%) and degree of conversion (%) are shown in Table 2. Electrical resistivity data and kinetic parameters slope and τ are shown in Table 3. Parameters of the equivalent circuit models are given in Table 4. The results of correlation analyses are shown in Table 5.

Table 2. Water content, transmittance and degree of conversion

Material	Water content (s.d.) (wt%)	Transmittance (%)	Degree of conversion immediately after curing (s.d.) (%)	Degree of conversion 24 hours post-cure (s.d.) (%)
ACP40	2.0 (0.1)	2.96 (0.10) a	85.3 (2.0) a	88.0 (0.9) a
ACP40-Ba10	1.8 (0.1)	2.91 (0.20) a	81.2 (1.9) b	81.9 (0.9) b
ACP40-Si10	1.4 (0.1)	2.35 (0.21) b	80.0 (1.6) b	82.4 (0.4) b
ACP40-Ba5Si5	1.7 (0.1)	2.85 (0.23) a	80.6 (1.0) b	83.0 (1.5) b
ACP40-Ba9Si1	2.0 (0.1)	3.00 (0.25) a	79.6 (1.0) b	81.3 (1.0) b
Ba40	0.9 (0.1)	5.08 (0.15) c	40.9 (1.8) c	61.1 (0.8) c *
Ba40Si10	1.0 (0.3)	5.19 (0.29) c	38.7 (2.7) c	59.6 (1.8) c *

Lowercase letters indicate statistically homogeneous groups in the same column. Asterisks (*) denote statistically significant 24 h post-cure increase.

Table 3. Electrical resistivity before and after curing, changes of electrical resistivity during the setting and kinetic parameters of the setting reaction.

Material	log (ρ / Ω cm) before curing (s.d.)	log (ρ / Ω cm) immediately after curing (s.d.)	log change of ρ during short-term setting	log change of ρ during long-term setting	Mean slope (s.d.) (10^6 Ωcm/s)	Mean τ (s.d.) (s)
ACP40	6.19 (0.03)	8.51 (0.05)	2.32	0.06	9.2 (1.7)	44.6 (2.1)
ACP40-Ba10	6.33 (0.02)	8.65 (0.05)	2.31	0.58	13.6 (1.8)	39.0 (0.6)
ACP40-Si10	6.15 (0.02)	8.39 (0.05)	2.24	0.73	6.7 (1.2)	44.5 (0.1)
ACP40-Ba5Si5	6.42 (0.01)	8.73 (0.02)	2.30	0.19	16.0 (1.4)	38.3 (1.0)
ACP40-Ba9Si1	6.15 (0.03)	8.41 (0.02)	2.27	0.37	7.5 (0.3)	40.3 (0.4)
Ba40	7.24 (0.01)	9.10 (0.03)	1.86	1.63	29.1 (3.7)	44.8 (3.2)
Ba40Si10	7.50 (0.02)	9.03 (0.03)	1.53	1.88	20.8 (1.2)	40.3 (1.1)

Table 4. Parameters of the equivalent circuit models obtained from the CNLLSQ fitting.

Material	R1 / Ω	CPE1		C1 / F	f_{max1} (Hz)	R2 / Ω	CPE2		C2 / F	f_{max2} (Hz)
		A / $s^{\alpha}\ \Omega^{-1}$	α				A / $s^{\alpha}\ \Omega^{-1}$	α		
ACP40	2.91 E+07	3.20 E-12	0.99	2.92 E-12	1673	1.25 E+08	1.17 E-11	0.86	3.86 E-12	436
ACP40-Ba10	5.88 E+08	3.58 E-12	0.99	3.36 E-12	81	4.33 E+09	5.89 E-12	0.87	3.33 E-12	11
ACP40-Si10	5.07 E+09	4.13 E-12	0.96	3.19 E-12	222	3.15 E+08	2.84 E-12	0.97	2.49 E-12	8
ACP40-Ba5Si5	1.50 E+09	5.81 E-12	0.93	3.52 E-12	222	3.56 E+08	3.90 E-12	0.94	2.81 E-12	30
ACP40- Ba9Si1	1.05 E+09	6.05 E-12	0.94	3.76 E-12	436	1.59 E+08	3.21 E-12	0.96	2.54 E-12	41
Ba40	6.14 E+10	1.50 E-12	0.96	1.32 E-12	4	-	-	-	-	-
Ba40Si10	4.67 E+11	1.43 E-12	0.95	1.42 E-12	0.2	-	-	-	-	-
neat resin	1.43 E+11	1.38 E-12	0.96	1.29 E-12	1	-	-	-	-	-

Table 5. Pearson correlation coefficients and corresponding p-values

Correlation	Pearson's r	p
water content – log (ρ) before curing	0.91	<0.01
water content – log (ρ) 24 h post-cure	0.92	<0.01
conversion – log change of ρ (short-term)	0.96	<0.01
conversion – log change of ρ (long-term)	0.93	<0.01
slope – τ	-	n. s.
slope – filler vol%	-	n. s.
slope – transmittance	0.88	0.01

n. s. = not significant

5.4.1 Short-term setting - impedance measurements at fixed frequency

The real part of electrical conductivity (σ') at 1 kHz as a function of time for all materials investigated is shown in Figure 1a. A representative plot of the electrical resistivity as a function of time for ACP40-Si10 composite is shown in Figure 1b.

The kinetic parameters slope and τ are shown in Table 3. The slope was obtained by linear fitting of the resistivity curves in their linear range (R^2>0.99), while the reaction time constant τ was determined as the time required for the resistivity change to reach a ($1-e^{-1}$ ≈63%) of the total change of resistivity.

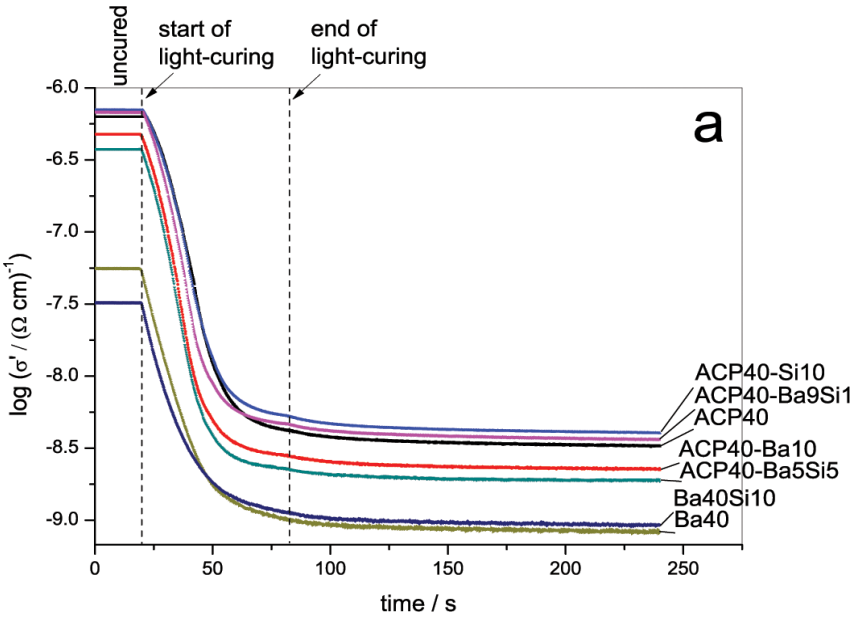

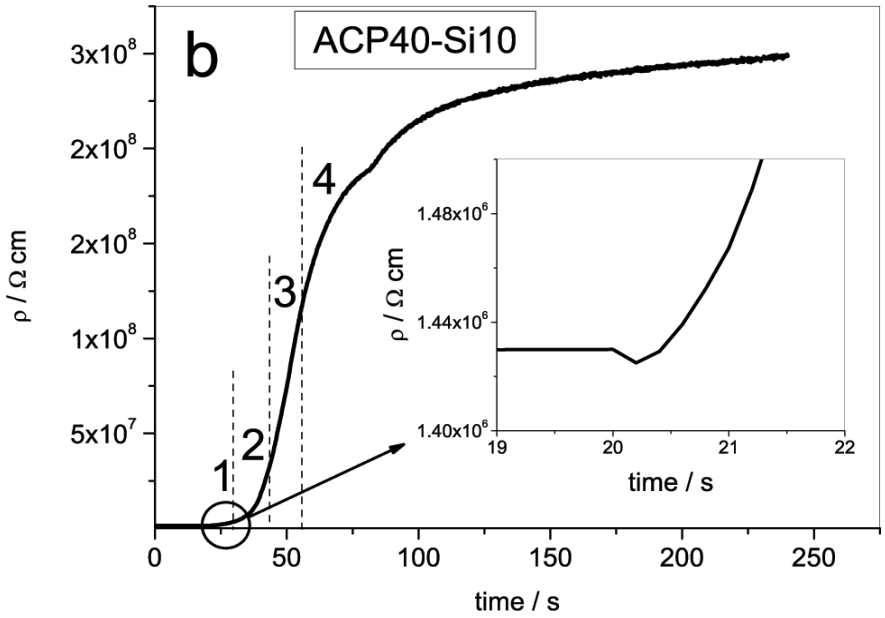

Figure 1. (a) Real part of the electrical conductivity as a function of time; (b) Electrical resistivity as a function of time for ACP40-Si10. Resistivity is presented in a linear scale for extracting kinetic parameters. Numbers refer to the phases of setting described in the text. The inset shows a magnified view of the part of the resistivity curve immediately after activating the polymerization device - a slight drop of resistivity can be observed, lasting for about 0.5 seconds.

5.4.2 Long-term setting - impedance measurements in a wide frequency range

Conductivity spectra for samples ACP40-Ba10 and Ba40Si10 are shown in Figure 2a-b, being representative for ACP-based and control materials, respectively. The initial conductivity drop caused by curing was followed by a more gradual post-cure conductivity decrease, amounting to 0.1-1.9 decades (Table 3). The impedance spectra of cured materials showed a conductivity plateau at low frequencies, while at higher frequencies conductivity increases in a power-law fashion (22).

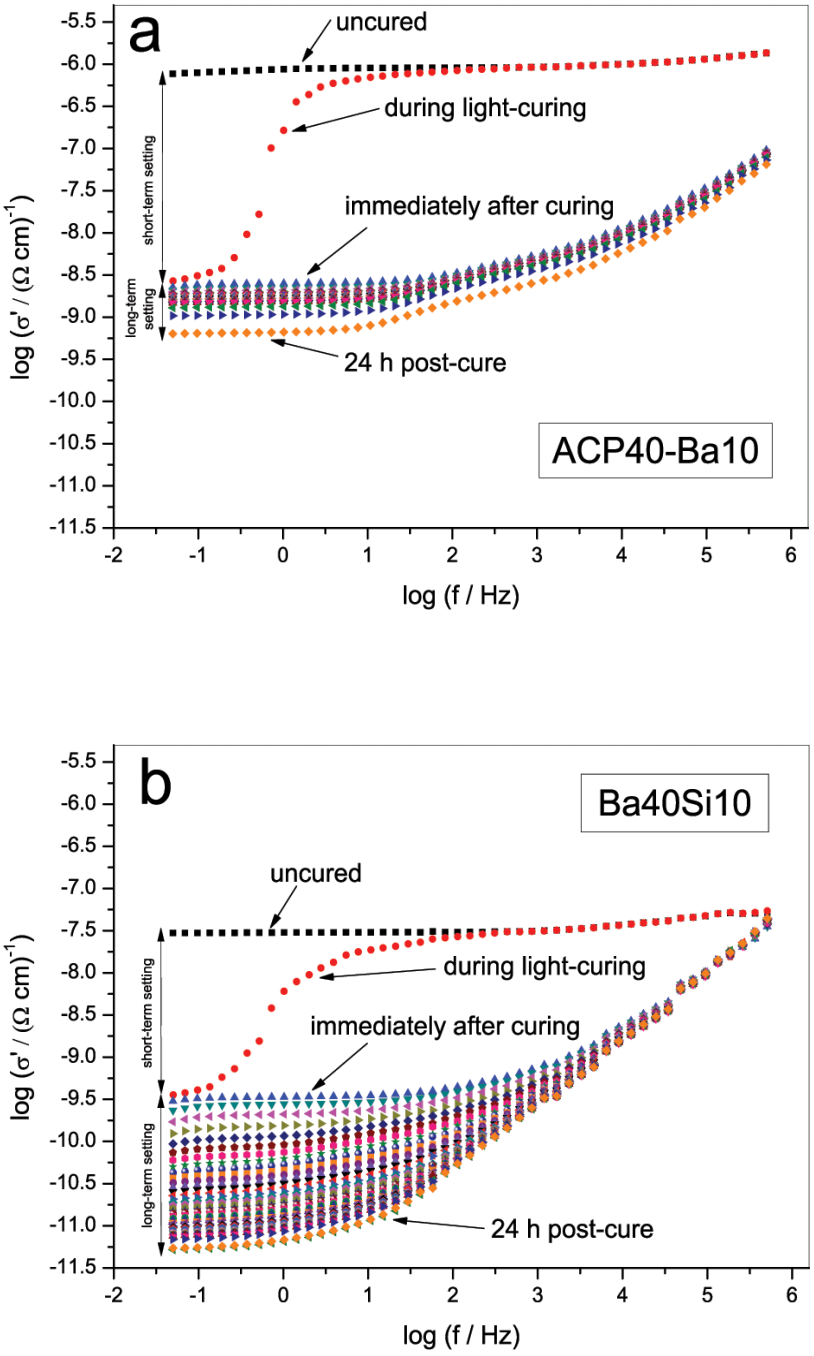

Figure 2. Electrical conductivity spectra for ACP40-Ba10 (a) and Ba40Si10 (b).

The representative complex impedance plots and equivalent electrical circuit models for ACP40-Ba10, Ba40Si10 and neat resin are presented in Figure 3a-c. The impedance spectra of all ACP-based samples showed two poorly resolved impedance arcs while the spectra of control materials and neat resin exhibited a single arc. Thus the corresponding equivalent circuit models for ACP-based and control materials were respectively fitted to a series of two parallel R-CPE (R-resistor, CPE-constant phase element) combinations and a single parallel R-CPE combination.

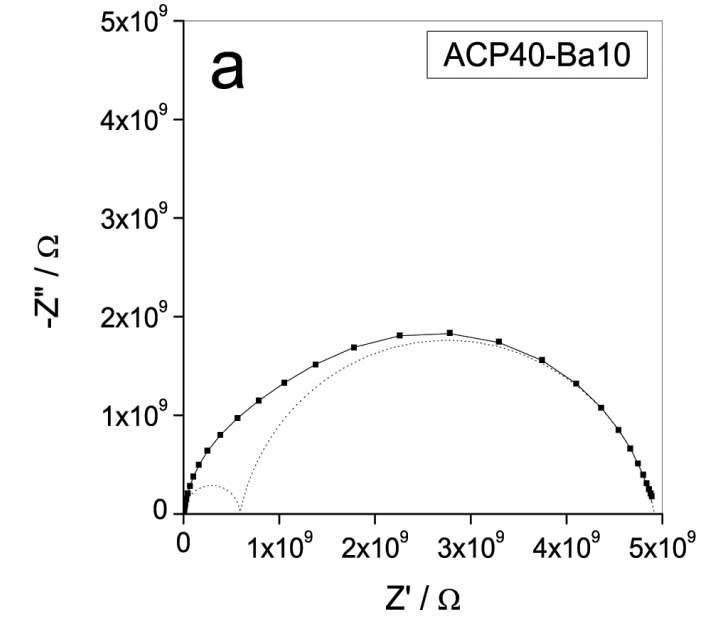

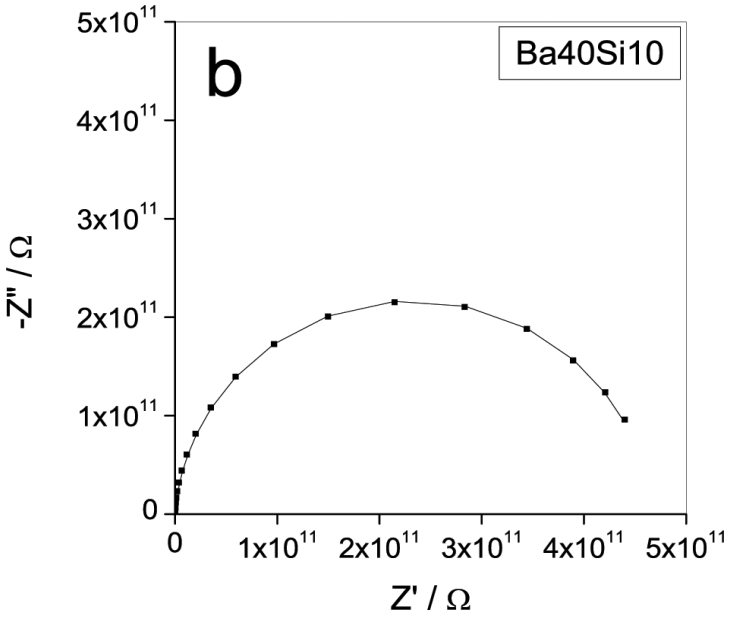

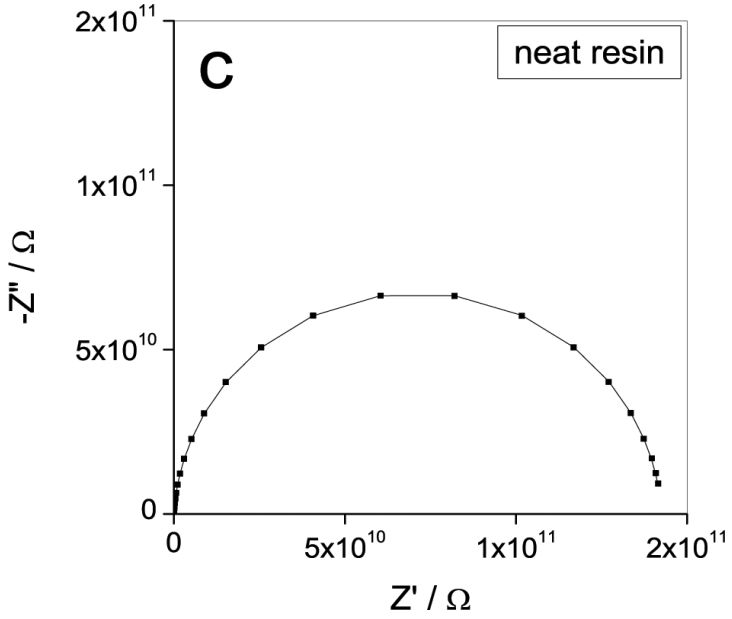

Figure 3. Impedance spectra in a complex plane and equivalent electrical circuit models for ACP40-Ba10 (a), Ba40Si10 (b) and neat resin (c). Since experimental data show the depressed impedance semicircles with the center below the real axis for all samples, the constant-phase elements (CPE) were used for modeling instead of capacitors. The CPE is an empirical impedance function of the type $Z^*_{CPE} = A(i\omega)^{-\alpha}$, where A and α are the constants. The parameter A was translated into real (geometric) capacitance using the equation $C = A(\omega_{max})^{\alpha - 1}$ where ω_{max} represents the frequency maximum in the impedance arc. The points denote experimental values and solid lines correspond to the best fit. The dotted line represents two electrical contributions for the material ACP40-Ba10.

5.4.3 SEM studies

Figure 4 shows the SEM micrographs for materials ACP40 and Ba40. Homogeneously distributed ACP agglomerates of 2-5 μm and smaller Ba fillers of 0.1-1 μm can be observed.

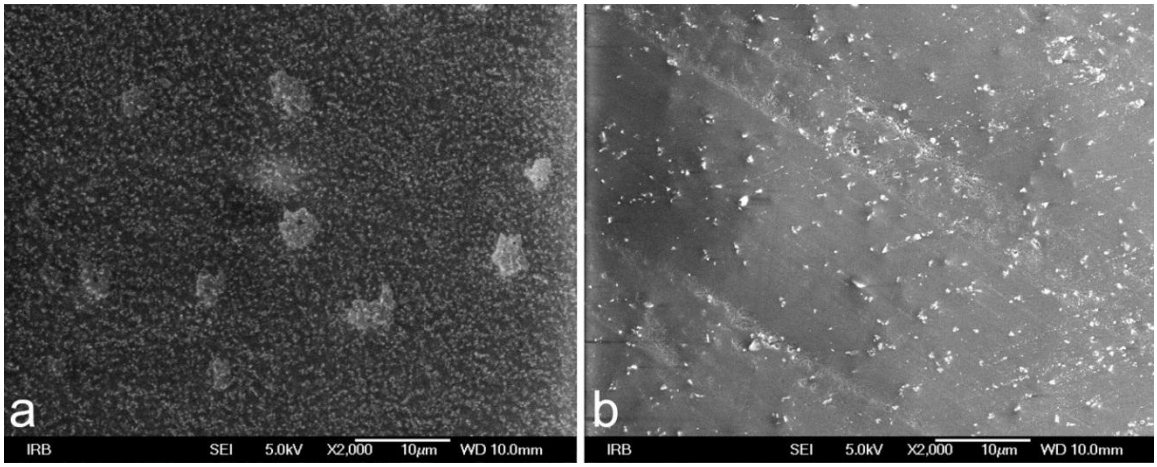

Figure 4. SEM micrographs of the sample surface for ACP40 (a) and Ba40 (b). Material ACP40 shows a homogeneous distribution of ACP agglomerates of 2-5 μm, while the Ba40 filler particles were significantly smaller with a diameter of approximately 0.1-1 μm.

5.5 Discussion

5.5.1 Short-term setting and kinetics of the polymerization reaction

Change of the electrical resistivity during setting is a relevant measure of the polymerization progress, as it reflects the viscosity change (23). As the polymerization advances, resistivity increases because the increasing molecular mass and crosslinking of polymeric chains impair the mobility of charge carriers. Presenting resistivity as a function of time gives a sigmoid curve which can be analyzed through four phases (Figure 1b). Phase (1) occurs shortly after the initiation of curing and represents a slight drop of resistivity that can be attributed to the temperature rise and a transient increase in the ion concentration due to the reaction of camphorquinone and tertiary amine (24). During the phase (2), the resistivity increases significantly as a result of the rapidly growing polymeric chains. Phase (3) begins when the resistivity becomes a linear function of time. It is assumed that in this part the polymerization reaction follows the first order kinetics and this can be used to mathematically model the reaction rate (19, 25). During the phase (4), the linear dependence ceases. This phase corresponds to the onset of vitrification, resulting in diffusion-controlled kinetics and a considerable decrease of the reaction rate. At approximately 80 seconds, a step-like increase

in resistivity can be observed. This is explained by a slight temperature decrease in the sample, since it occurred at the moment the polymerization device was switched off.

Steinhaus et al. have reported a wide range of slope values for commercial composites, ranging from 29 to 559 (10^6 Ω cm/s) (19). In this work, slope values between 6.7 and 29.1 (10^6 Ω cm/s) were observed. A comparatively narrower range of slope values in this study was expected due to the compositional similarity of the materials. For composites based on the same resin and photoinitiator, polymerization kinetics represented by slope should be affected by the differences in filler composition. No significant correlation was found between the slope and filler load, suggesting that the differences in filler load among the materials were too small to measurably affect the reaction kinetics. This is supported by the claim by Atai et al. that the filler load is expected to affect kinetics only in the case of very high particle surface area, attainable by incorporating high filler load of nano-sized particles (26). Despite no significant effect of the filler load on polymerization kinetics, there was a significant correlation ($r=0.88$, $p=0.01$) between the slope and light transmittance. This was expected, since the samples for IS measurements were cured in bulk and the light passing through the sample was attenuated by scattering and absorption (27). Light attenuation in deeper parts of the sample causes lower initiation rate, as less photoinitiator molecules undergo activation to form growth centers for polymeric chains. This is reflected on polymerization kinetics in the early phase of curing, as represented by the slope values. Although it is known that the transmittance of dental composites changes during the polymerization (28), this phenomenon was outside the scope of this paper. Since we focused on the early phase of curing, the transmittance values measured immediately after activating the curing unit were considered appropriate.

The values of the kinetic parameter τ for commercial composites in the range of 16.9-88.4 s have been reported (19), while the values obtained in this work are between 38.3 and 44.8 s. Considering the large discrepancy of slope values between two studies and rather similar values of τ, slope appears as a more sensitive measure of the reaction rate. This can be explained by τ taking into account kinetics of the reaction at times before and after the linear increase of resistivity, i.e. in the range of the resistivity curve where the mathematical model (19) does not hold. This may result in similar τ values for composites with very different chemistries and polymerization kinetics. Additionally, no correlation between τ and slope was found in neither of these two studies.

The impact of differences in experimental setup between this work and work by Steinhaus et al. (19) is the most prominent in the time delay before the onset of a linear resistivity increase. Steinhaus et al. have reported that a linear part occurred at 1-20 seconds after the initiation of curing (19), while in our work it occurred between 20-40 seconds (Figure 1b). Instead of the comb electrodes for measurements at the bottom of thin samples (1 mm) in this work the parallel plate electrodes and two curing units positioned at the sides of the sample were used. Therefore, the effective light path was 4 mm (the diameter of quartz rings) which led to a slower resistivity increase and a delay of the linear part. During the first 20 seconds of curing, a layer of poorly cured material remains at the side of the sample opposite to the curing unit. Since it provides a path of low impedance, no significant increase of resistivity is observed during this period. When the far side of the sample reaches critical conversion (usually about 20 seconds), resistivity increases rapidly and curve readily reaches the linear behavior.

5.5.2 Long-term setting

Since the conductivity of glasses and ceramics usually ranges from $10^{-4} – 10^{-9}$ $(\Omega\ cm)^{-1}$ while that of polymers ranges from $10^{-7} – 10^{-12}$ $(\Omega\ cm)^{-1}$, ElKestawy et al. postulated that glass-filled composite materials should present conductivities in the range of $10^{-9} – 10^{-10}$ $(\Omega\ cm)^{-1}$ (29). Conductivities of completely cured (24 h) control materials in our work agree to these values, while the group of ACP-composites showed conductivities about two orders of magnitude higher. This pattern of differences in conductivity among control and ACP-based materials was maintained also in the uncured materials. Since the ACP filler is not expected to have contributed to such a large conductivity increase, an explanation was sought in the water content of the composites. It is known that precipitated ACP retains a certain amount of water after lyophilization (30) and our results showed that a small amount of water is introduced into the composites by the admixture of ACP (Table 2). A significant ($p<0.01$) positive correlation between log conductivity and water content (wt%) was found for both uncured ($r=0.91$) and cured ($r=0.92$) materials. Thus it appears that the observed differences in conductivity among the tested materials were mostly attributable to their water content. It should be noted that the IS measurements were performed in an isolated system, thus no environmental water uptake was possible.

For all cured samples, conductivity spectra showed a frequency-independent region at lower frequencies (equal to the DC conductivity) followed by a conductivity increase at higher

frequencies, Figure 2a-b. While for the control materials conductivity increases in a power-law fashion (Figure 2b), for ACP-based materials a slight deviation from power-law can be observed in the frequency region of 10 Hz-1 kHz (Figure 2a). A deeper insight into these phenomena can be obtained from the complex impedance plots and equivalent circuit modeling (Figure 3a-c).

Complex impedance plots of composite materials usually exhibit two arcs – the low frequency arc corresponding to the low conductivity continuous resin phase, while the high frequency arc pertains to the more conductive suspended filler phase (31). This pattern was observed for all of the ACP-based materials. Two poorly resolved arcs with capacitances of order of magnitude of 10^{-12} F were detectable in all of the ACP-based materials (Figure 3a, Table 4). The brickwork model for ceramics (32) suggests that an inverse relationship between the thickness of the structural region in the material and its capacitance enables attributing individual arcs to specific regions of the sample. According to this assignment, both arcs observed should correspond to the bulk of the material. However, as the capacitance is a function of the relative permittivity and geometric factor of a particular structural region, it is possible that contributions of these factors result in both regions having the capacitance of order of 10^{-12} F. Unlike ACP-composites, the control composites have shown only one arc whose frequency maximum corresponds to the "low-frequency" arc of the ACP-composites (Figure 3b). Moreover, the impedance arcs for the control composites are very similar to that of the neat resin (Figure 3c). This indicates that the electrical contribution of conventional fillers was indistinguishable from that of the resin, while the ACP-fillers clearly presented as an additional arc. Since the ACP is expected to have similar electrical properties to the conventional fillers, this phenomenon is most probably related to the difference in particle size. Since the conventional fillers were almost one order of magnitude smaller than ACP agglomerates (Figure 4), it is possible that their electrical contribution is very small and therefore not detectable as an additional arc. A similar behavior was shown in a study of ceramics, which explored the dependence of impedance spectra on different particle sizes (33).

Equivalent circuit models for all the materials use the CPEs instead of capacitors, which suggest a distribution of relaxation times. This may be caused by microstructural features that are known to exist in multifunctional methacrylate networks such as microgel regions, differences in conversion and crosslinking throughout the sample and a possible phase

separation (34). Additional cause for such inhomogeneity may be the agglomeration of filler particles.

5.5.3 Degree of conversion and correlation with change of resistivity

The degree of conversion of ACP-based composites immediately after curing was twice that of control composites based on the same resin (Table 2). The conversion in composite materials has been shown to depend on the filler size (35) and filler load (36, 37). These factors determine the interfacial surface area between the resin and filler, affecting local viscosity and polymerization kinetics. Although the ACP-based composites had slightly higher filler load than the control composites, it is possible that the large ACP agglomerates contributed to relatively lower filler surface area, resulting in better monomer mobility and higher final conversion. Additionally, the unsilanized ACP filler may have enhanced the monomer mobility due to the lack of chemical bonding between filler particles and polymeric network, thus allowing higher conversion (36, 38).

The ACP-based composites attained high conversion values immediately after curing with no statistically significant post-cure reaction, while the control composites presented a significant conversion increase 24 h post-cure (Table 2). The fact that the ACP-based composites reached their final conversion immediately after curing further evidences better mobility of monomers and free radicals compared to the control composites. The immediate polymerization to a high extent is favorable in terms of biocompatibility since it implies less unreacted monomer available for leaching out of the restoration.

Composite materials containing only ACP fillers were previously reported to reach higher conversion values than commercial composites, whose conversion ranges from 50 to 75% (7, 20, 39). As discussed earlier, such high conversion may be attributed to the comparatively lower filler load and larger filler particles, as well as better monomer mobility due to the unsilanized filler particles. Upon increasing the filler load of the ACP-based composites by the addition of silanized Ba and Si fillers, a statistically significant decrease of conversion was observed (Table 2). However, this decrease was negligible from clinical aspect, since the ACP-based composites with silanized Ba and Si fillers still attained conversion above the usual range for commercial composites. Additionally, different combinations of inert fillers caused a statistically similar effect on conversion (Table 2), possibly due to the similar filler

vol%. Since the introduction of inert fillers to the ACP-based composites resulted in only minor compromise in conversion, it may be an effective means for improvement of mechanical properties in further research (8, 9).

The correlation of conversion and logarithm of electrical resistivity (Tables 2-3) was examined among all composite formulations for short-term and long-term setting and correlation coefficients of 0.96 and 0.93 were obtained, respectively ($p<0.01$). The correlation of resistivity and conversion measured by infra-red spectroscopy has been reported previously for different polymers at various stages of cure (40, 41). While the cited studies have followed a certain neat resin mixture during the advancement of polymerization, this study demonstrated that the correlation also exists when comparing composite materials of different compositions. However, it must be noted that the tested materials were based on the same methacrylate resin and these conclusions may not apply to composites based on different resins, as they may have very different polymerization kinetics (34). The observed correlation of resistivity and conversion, regardless of the filler composition and ratio, supports the use of impedance methodology as a useful tool for monitoring the extent of cure of composite materials.

5.6 Conclusions

In summary, ACP-based composite materials were investigated by impedance spectroscopy for the first time. The kinetic model by Steinhaus was applied to assess the polymerization rate and slope of the linear part of resistivity curve was found to be a more meaningful measure of the reaction rate than the time constant τ. The reaction kinetics described by the slope showed no correlation with filler vol%, but correlated well with the light transmittance. A significant positive correlation between impedance results and conversion measured by Raman spectroscopy was observed. Differences in conductivity among the tested composites were found to be highly dependent upon the water content introduced by ACP fillers. Equivalent circuit models revealed that the ACP fillers appear as an additional electrical contribution, which is attributable to their particle size. The impedance spectroscopy has proven a valuable method that provided insight into various features of ACP-based composites.

5.7 Acknowledgments

We thank Mira Ristić and Marijan Marciuš from the Division of Materials Chemistry, Ruđer Bošković Institute for the SEM micrographs. We also gratefully acknowledge Hrvoje Skenderović from Institute of Physics, Zagreb for help with the transmittance measurements and Drago Skrtic for providing us with the zirconia-hybridized ACP. This investigation was supported by Croatian Science Foundation (Project 08/31 Evaluation of new bioactive materials and procedures in restorative dental medicine). The authors declare no conflict of interest.

5.8 References

1. Dorozhkin SV. Amorphous calcium (ortho)phosphates. Acta Biomater 2010;6(12):4457-75.
2. Langhorst SE, O'Donnell JN, Skrtic D. In vitro remineralization of enamel by polymeric amorphous calcium phosphate composite: quantitative microradiographic study. Dent Mater 2009;25(7):884-91.
3. Weir MD, Chow LC, Xu HH. Remineralization of demineralized enamel via calcium phosphate nanocomposite. J Dent Res 2012;91(10):979-84.
4. Melo MA, Weir MD, Rodrigues LK, Xu HH. Novel calcium phosphate nanocomposite with caries-inhibition in a human in situ model. Dent Mater 2013;29(2):231-40.
5. Li F, Wang P, Weir MD, Fouad AF, Xu HH. Evaluation of antibacterial and remineralizing nanocomposite and adhesive in rat tooth cavity model. Acta Biomater 2014;10(6):2804-13.
6. Ferracane JL. Resin composite - state of the art. Dent Mater 2011;27(1):29-38.
7. Skrtic D, Antonucci JM. Dental composites based on amorphous calcium phosphate - resin composition/physicochemical properties study. J Biomater Appl 2007;21(4):375-93.
8. Marovic D, Tarle Z, Hiller KA, Muller R, Ristic M, Rosentritt M, et al. Effect of silanized nanosilica addition on remineralizing and mechanical properties of experimental composite materials with amorphous calcium phosphate. Clin Oral Investig 2014;18(3):783-92.

9. Marovic D, Tarle Z, Hiller KA, Muller R, Rosentritt M, Skrtic D, et al. Reinforcement of experimental composite materials based on amorphous calcium phosphate with inert fillers. Dent Mater 2014;30(9):1052-60.
10. Zhang F, Allen AJ, Levine LE, Vaudin MD, Skrtic D, Antonucci JM, et al. Structural and dynamical studies of acid-mediated conversion in amorphous-calcium-phosphate based dental composites. Dent Mater 2014;30(10):1113-25.
11. Xu HH, Moreau JL, Sun L, Chow LC. Nanocomposite containing amorphous calcium phosphate nanoparticles for caries inhibition. Dent Mater 2011;27(8):762-9.
12. Xu HH, Weir MD, Sun L, Ngai S, Takagi S, Chow LC. Effect of filler level and particle size on dental caries-inhibiting Ca-PO(4) composite. J Mater Sci Mater Med 2009;20(8):1771-9.
13. Stoner BR, Piascik JR, Brown B, Wolter SD. A novel array chip to monitor in situ composite degradation using electrochemical impedance spectroscopy. Dent Mater 2011;27(8):811-7.
14. Lagouvardos PE, Pissis P, Kyritsis A, Daoukaki D. Water sorption and water-induced molecular mobility in dental composite resins. J Mater Sci Mater Med 2003;14(9):753-9.
15. Wadgaonkar B, Ito S, Svizero N, Elrod D, Foulger S, Rodgers R, et al. Evaluation of the effect of water-uptake on the impedance of dental resins. Biomaterials 2006;27(17):3287-94.
16. Pradelle-Plasse N, Wenger F, Picard B, Colon P. Evaluation of microleakage of composite resin restorations by an electrochemical technique: the impedance methodology. Dent Mater 2004;20(5):425-34.
17. Lovell LG, Berchtold KA, Elliott JE, Lu H, Bowman CN. Understanding the kinetics and network formation of dimethacrylate dental resins. Polym Advan Technol 2001;12(6):335-45.
18. Rosentritt M, Shortall AC, Palin WM. Dynamic monitoring of curing photoactive resins: a methods comparison. Dent Mater 2010;26(6):565-70.
19. Steinhaus J, Hausnerova B, Haenel T, Grossgarten M, Moginger B. Curing kinetics of visible light curing dental resin composites investigated by dielectric analysis (DEA). Dent Mater 2014;30(3):372-80.
20. Skrtic D, Antonucci JM, Liu DW. Ethoxylated bisphenol dimethacrylate-based amorphous calcium phosphate composites. Acta Biomater 2006;2(1):85-94.

21. Par M, Gamulin O, Marovic D, Klaric E, Tarle Z. Effect of temperature on post-cure polymerization of bulk-fill composites. J Dent 2014;42(10):1255-60.
22. Jonscher AK. The 'universal' dielectric response. Nature 1977;267:673-9.
23. Kranbuehl D, Delos S, Yi E, Mayer J, Jarvie T, Winfree W, et al. Dynamic dielectric analysis: Nondestructive material evaluation and cure cycle monitoring. Polym Eng Sci 1986;26(5):338-45.
24. Jakubiak J, Allonas X, Fouassier JP, Sionkowska A, Andrzejewska E, Linden LA, et al. Camphorquinone–amines photoinitating systems for the initiation of free radical polymerization. Polymer 2003;44(18):5219-26.
25. Bellucci F, Valentino M, Monetta T, Nicodemo L, Kenny J, Nicolais L, et al. Impedance spectroscopy of reactive polymers. J Polym Sci Part B: Polym Phys 1994;32(15):2519-27.
26. Atai M, Watts DC. A new kinetic model for the photopolymerization shrinkage-strain of dental composites and resin-monomers. Dent Mater 2006;22(8):785-91.
27. Emami N, Sjodahl M, Soderholm KJ. How filler properties, filler fraction, sample thickness and light source affect light attenuation in particulate filled resin composites. Dent Mater 2005;21(8):721-30.
28. Harrington E, Wilson HJ, Shortall AC. Light-activated restorative materials: a method of determining effective radiation times. J Oral Rehabil 1996;23(3):210-8.
29. ElKestawy MA, Saafan SA, Shehata MM, Saafan AM. Investigation of the electrical properties of some dental composite restorative materials before and after laser exposure. Dent Mater 2006;22(10):885-95.
30. Combes C, Rey C. Amorphous calcium phosphates: synthesis, properties and uses in biomaterials. Acta Biomater 2010;6(9):3362-78.
31. Lvovich VF. Impedance Spectroscopy: Applications to Electrochemical and Dielectric Phenomena. Hoboken, New Jersey: John Wiley & Sons, Inc; 2012. p. 113-23.
32. Irvine JTS, Sinclair DC, West AR. Electroceramics: Characterization by Impedance Spectroscopy. Adv Mater 1990;2(3):132-8.
33. Dean JS, Harding JH, Sinclair DC, Tanaka I. Simulation of Impedance Spectra for a Full Three-Dimensional Ceramic Microstructure Using a Finite Element Model. J Am Ceram Soc 2014;97(3):885-91.
34. Andrzejewska E. Photopolymerization kinetics of multifunctional monomers. Prog Polym Sci 2001;26(4):605-65.

35. Turssi CP, Ferracane JL, Vogel K. Filler features and their effects on wear and degree of conversion of particulate dental resin composites. Biomaterials 2005;26(24):4932-7.
36. Ferracane JL, Berge HX, Condon JR. In vitro aging of dental composites in water - effect of degree of conversion, filler volume, and filler/matrix coupling. J Biomed Mater Res 1998;42(3):465-72.
37. Halvorson RH, Erickson RL, Davidson CL. The effect of filler and silane content on conversion of resin-based composite. Dent Mater 2003;19(4):327-33.
38. Wilson KS, Zhang K, Antonucci JM. Systematic variation of interfacial phase reactivity in dental nanocomposites. Biomaterials 2005;26(25):5095-103.
39. Peutzfeldt A. Resin composites in dentistry: the monomer systems. Eur J Oral Sci 1997;105(2):97-116.
40. Nahm SH. Use of dielectric spectroscopy for real-time in-situ reaction monitoring. J Coating Tech Res 2006;3(4):257-65.
41. Zahouily K, Decker C, Kaisersberger E, Gruener M. Real-time UV cure monitoring. Eur Coating J 2003(11):245-9.

6. GENERAL DISCUSSION

Studies of bioactive composites are a branch of investigations on dental composites that has recently gained much popularity. Among many different bioactive formulations, ACP-composites show the potential to prevent secondary caries and may be an interesting alternative to contemporary „bio-inert“ composites. This study aimed to investigate various aspects of ACP-composites modified with reinforcing fillers, which demonstrate improved properties in comparison with composites based exclusively on ACP fillers. Specifically, the DC, temperature rise during polymerization, real-time measurements of optical properties as a means of determining polymerization kinetics, and various electrical properties were investigated.

The DC was investigated as a basic property that is essential for mechanical strength and biocompatibility (90, 91). Not only high final DC values (around 80%) were attained for all ACP formulations, but such high values were attained during the light curing period of 20 or 40 s, indicating high biocompatibility immediately after curing. Unlike this curing behavior, most of the contemporary conventional composites present an extensive post-cure reaction that lasts for at least 24 h post-cure (38), evidencing that reactive species are still mobile and may exert a toxic effect. Such DC development was observed in two control composites that were based on the same resin and photoinitiator system as the ACP-composites, but contained only reinforcing and no bioactive fillers. These composites showed the development of the DC typical for commercial composites: low initial DC (cca 40%) followed by a post-cure DC increase during 24 h up to the value of cca 60% (37). In contrast, ACP-composites presented high DC immediately after light curing and no significant post-cure DC increase. Additional important finding is that the addition of silanized fillers comprising barium glass and silica did not impair high DC values, suggesting that modification of ACP-composites with reinforcing fillers may be a feasible strategy to improve their mechanical properties. The DC decline through depth was also measured and it was shown that curing with the irradiance of 1200 mW/cm^2 for 20 s was sufficient for the application in layers of 2 mm thickness. In this regard, the ACP-composites can be layered according to the standard clinical procedure for conventional composites. When light-cured for 40 s with the same irradiance, curing depth was increased to 3 mm.

Among various methods for determining the cure efficiency at depth, vibrational spectroscopies (FTIR and Raman) are the most commonly used (35, 92). The main advantage of these methods is their ability to directly quantify the amount of C=C double bonds in the sample, unlike other methods that rely on indirect assessment of the DC (14). Some

researchers consider FTIR more conventional and appropriate method than Raman spectroscopy, but there are also many reports confirming the usability and adequacy of Raman for DC investigations in dental composites (93, 94). A major complaint to using Raman spectroscopy regards the excitation method for inducing Raman scattering by various types of lasers with high output power. For example, a FT-Raman instrument irradiates the sample surface of approximately 0.2 mm^2 with the laser power of up to 1 W. In comparison, micro-Raman instruments irradiate much smaller sample surfaces (several μm^2) with laser power of about 20 mW (92), thus reaching the irradiance that is two to three orders of magnitude higher compared to that of the FT-Raman instrument. Depending on the absorptivity of the sample, such high irradiances may contribute to a considerable heating and cause chemical changes in the sample. In the case of the cured composites with living radical polymerization, the heating can increase the rate of post-cure polymerization and yield falsely higher DC values (38). Thus Raman spectroscopy could be critiqued for measuring the DC immediately after curing, as the obtained values may be somewhat higher than the true "immediate" values. On the other hand, the effect of heating plays a negligible role after the post-cure reaction was finished, usually 24 h after the light curing. The temperature increase in the irradiated part of the sample may be assessed by comparing the intensities of the Stokes and anti-Stokes Raman shift (95). This could not be done in the present study, as the anti-Stokes scattering is not detected by the FT-Raman spectrometer used. The problem of sample heating by the excitation laser has been expressed for biological samples (96), however it has not yet been investigated for dental composites. This should be done in the future, as Raman spectroscopy continues to be widely employed for the DC measurements.

Another limitation of the used FT-Raman spectrometer was rather low spatial resolution, compared to much more precise micro-Raman instruments (97). However, the attained spatial resolution of about 0.5 mm was considered sufficient for the purpose of measuring the DC at steps of 1 mm. Shortcomings of such low spatial resolution are more pronounced when studying composites with more heterogeneous DC values through depth, e. g. very opaque materials, where the inability to precisely aim a small area of the sample results in a higher experimental uncertainty and reflects as the higher variability of results. This effect is demonstrated in a study of bulk-fill composites that used the same spectrometer and experimental setup as the present study (37), where conventional reference materials demonstrated much higher standard deviations at high layer thicknesses than the more translucent bulk-fill composites. This is due to the steeper decline of the DC through depth

seen in conventional composites and the inability of the FT-Raman setup to limit the sampling area to a sufficiently small size.

Despite all of the listed shortcomings, Raman spectroscopy was considered to be more appropriate for the present study design as it is non-destructive and allowed repeated measurements on the same specimens. This was important for the economical aspect of the study, as using a FTIR spectrometer in either the transmission or ATR mode would necessarily increase total consumption of experimental composites. The transmission mode of FTIR is destructive and would necessitate preparation of a separate sample for each measuring depth. While the ATR mode is non-destructive, it would still increase material consumption, as separate samples would need to be prepared on top of the ATR crystal for each increment thickness. Additionally, ACP-composite samples contained a certain amount of water, as shown by gravimetry and impedance data. Since the vibrational spectrum of water in FTIR spectrum overlaps with the bands of interest for the DC assessment, some artifacts may appear due to the presence of water within the samples. This was the additional reason for choosing the Raman spectroscopy which is much less sensitive to the presence of water.

High immediate DC of experimental ACP-composites suggests a low amount of unreacted monomers available for leaching out of the cured material and thus high biocompatibility (32). It is approximated that only 10% (98) of the unreacted monomers are capable of diffusing out of the cured material, which in the case of the measured DC of 80% gives approximately 2% of the total amount of residual C=C bonds available for exerting a potentially toxic effect. This amount is less than half of that commonly found in commercial composites, which have up to 5% of leachable C=C bonds (assuming the initial DC immediately after cure of about 50%). The residual monomers are not the only species that can exert a potential toxic effect, as other soluble components can also diffuse out of the restoration with aging (98). All composite components are subject to the degradation when exposed to oral environment for prolonged time: polymeric network is cleaved by hydrolysis and enzymatic breakdown, siloxane bonds at the filler/matrix interface are hydrolyzed and components of filler particles are solubilized and eroded (28, 99). Higher DC values, as those found in the experimental ACP-composites, suggest denser polymeric networks and lower mobility of water molecules that are necessary for all of the degradation reactions. Thus higher DC not only leaves less unreacted molecules available for diffusion, but also impairs

the mobility of water and degradation products and in this way contributes to less leaching and better biocompatibility.

In addition to the DC, another property important for biocompatibility is the temperature rise that occurs during light curing (35). Light-curable composites produce much more heat than those chemically cured due to high number of activated growth centers for the polymerization and higher reaction rate. This is especially pronounced when curing with contemporary curing units of high irradiance (more than 1000 mW/cm^2) (100). The polymerization reaction of multifunctional methacrylates features complex kinetics that is characterized by reaction rates not directly governed by the amount of reactants (34). Unlike classical chemical kinetics in which the reaction rate is a function of the concentration of reactants and progressively slows down as the amount of reactants decreases, methacrylate polymerization in very early phase shows the phenomenon of autoacceleration. This occurs because the increasing viscosity of the reaction medium impairs mobility of free radicals on the ends of polymeric chains and reduces the rate of termination. Since the termination rate is reduced and initiation still proceeds due to the activation of new photoinitiator molecules, the overall number of free radicals increases rapidly and yields an increase in the reaction rate in an "autocatalytic" manner. This lasts until the viscosity becomes so extreme that even small monomer molecules cannot reach the reaction sites, and then the reaction rate abruptly decreases in a process known as autodeceleration. Since the polymerization of methacrylate monomers is the exothermic reaction with the heat release of approximately 55 kJ/mol (101), high reaction rate together with high DC values raise the concern of potential biocompatibility issues due to the temperature rise within the bulk of polymerizing composite. Furthermore, the reaction exotherm is superposed to the heating of the high-intensity light curing unit (85). Both effects contribute to the temperature rise within the composite bulk and can potentially harm dental pulp. This makes the temperature rise during light curing an important property to investigate in experimental ACP-based formulations.

Temperature was measured in real-time during the light curing to investigate if the high DC values observed in all experimental composites were accompanied with a high temperature rise (83). In vitro temperature measurements are technically easy to perform, but it is difficult to interpret the clinical significance of the obtained data. Particularly, it is impossible to relate the temperature data obtained in laboratory setting with the intrapulpal temperature rise that would occur if the composite was used clinically. Moreover, there is no consensus about the temperature threshold value that would separate reversible from irreversible pulpal damage

(102, 103). Thus the measured temperature rise was compared to the data for commercial composites that was obtained by other researchers using a similar experimental setup (104, 105). Since the experimental setup for temperature measurements is fairly simple, their data was regarded comparable to the results of this study. It was concluded that the temperature rise produced by ACP-composites falls within the range of established commercial composites, which have a long history of successful clinical use. Therefore the ACP-composites were considered to be no more harmful to the dental pulp with regard to temperature rise than the conventional composites used daily in clinical practice. Additionally, there was a trend of decline in the peak temperature values for composites with reinforcing fillers, suggesting that incorporating even higher amounts of reinforcing fillers as an approach to improve mechanical properties would further diminish the temperature rise. The composites were cured with a LED curing unit of 1200 mW/cm^2 which is today considered as a standard irradiance (106). Dental equipment market offers curing units of much higher irradiance and the heating effect produced by such curing units raises more concerns with regards to pulpal health that the exotherm of the composite polymerization reaction.

The light transmittance of a composite material is determined by light scattering and absorption by chromophores (44). The most part of light attenuation is due to the scattering at filler particles, which depends on the particle geometry and the difference in refractive indices between the resin and the filler. For a giver resin and filler composition, the refractive index mismatch is fixed, thus the light scattering is determined by the size distribution of filler particles. The scattering intensity peaks at approximately half the wavelength of the curing light, i.e. at about 230 nm and decreases with either increasing or decreasing the particle size (107, 108). When formulating new composites, it is easier to control the light scattering if the filler particle size is known and constant. Also, a narrow particle size distribution makes it easier to predict the effect of filler geometry on the scattering effect. Since ACP particles tend to form agglomerates of different sizes, it was difficult to predict their effect on light scattering and overall light transmittance. In addition, the original size of ACP particles probably differs from the final particle size in a blended composite, as strong forces developed during the mixing procedure separate large agglomerates to decrease the final particle size. It is also possible for a mixing procedure to make the particle size distribution narrower, i.e. to yield a more uniform particle size. This effect may depend on the material viscosity, as higher viscosity causes higher shear forces that could tear apart particle

agglomerates. Thus various ACP-formulations might have different sizes of ACP particles depending on their viscosity, even if they were all prepared from the ACP fillers of the same initial size. In short, there were many unknowns about the particle size of ACP fillers and their effect on light scattering in composites could not be predicted. Thus it was necessary to investigate the light transmittance of ACP-composites as an important factor for the efficiency of light curing.

The light transmittance of a composite material must be measured in real-time, as it changes rapidly during the light curing period (16). This occurs due to the change in optical properties of the polymerizing resin, whose refractive index gradually rises as the polymerization advances, thus affecting the resin/filler refractive index mismatch and reflecting on light scattering (109). The resultant light curing efficiency at depth is therefore a function of the dynamical change in light transmittance, rather than of a single fixed transmittance value. This is evident in the transmittance behavior of ACP-composites, whose initial transmittance values were lower than that of the commercial composite, but at some point during the polymerization surpassed the transmittance of the commercial material, to finally reach significantly higher values at the end of the curing period. This is favorable for efficient cuing at depth, as mentioned in the above discussion about the DC decline through various measurement depths.

The fact that light transmittance depends on the change of the resin refractive index throughout the light curing allows monitoring of the reaction kinetics through the transmittance changes (45, 85). Although light transmittance curves are to some extent convoluted with the effect of photoinitiator consumption and the effect of heating, these phenomena were neglected and most of the transmittance changes were assumed to be due to the transition from monomer to polymer (110, 111). In this way, the recorded rise of light transmittance can be regarded as a function of monomer conversion and provide information on polymerization kinetics. Simultaneous real-time measurements of light transmittance and temperature revealed an interesting kinetic behavior that appears unique to ACP-composites and has not been previously detected in commercial materials. The ACP-composites showed a constant reaction rate throughout a rather long period of polymerization, unlike the commercial reference material which showed the evidences of autoacceleration and autodeceleration in very early polymerization phase. Such kinetics was attributed to high amount of unsilanized ACP particles and has implications on other groups of experimental bioactive composites as most of them also contain unsilanized fillers. The kinetic behavior

observed through light transmittance measurements was in line with the DC data that showed high initial DC and practically no post-cure DC increase (49). Slower reaction rate through the most part of the pre-vitrification period allowed higher consumption of monomer, resulting in high immediate DC and leaving less unreacted species for the post-cure reaction. An obvious and apparently not particularly important finding was the correlation of the reaction rate with the light transmittance. However, this served to support the validity of parameters derived from the real-time transmittance data as a measure of the polymerization kinetics.

Impedance spectroscopy generally operates by applying an alternating voltage across the sample and measuring the magnitude of the current response. By dividing the time-dependent voltage with the time-dependent current, the complex impedance ($Z^*=Z'-iZ''$) is obtained (112). Since the complex impedance is a function of frequency, it is measured over a wide frequency range which gives an impedance spectrum. Because various conduction processes have different kinetics, they are dominant at different frequency regions – dipolar properties occur at higher frequencies while the long-range conduction dominates lower frequencies (113). Plotting the magnitudes of Z' and Z'' measured over the wide frequency range in a complex plane (Nyquist plot) and fitting the curve using a non-linear least squares algorithm to equivalent circuit models enables one to separate various conduction mechanisms and assign them to the different structural regions of the sample (114). On the other hand, continuous measurements of the impedance as a function of time at a fixed frequency enable sufficient time resolution that allows the real-time monitoring of the polymerization reaction (48).

Impedance spectroscopy is not routinely used in dental composite investigations and this study demonstrated for the first time that some useful information can be gained by examining composite's electrical properties (49). Real-time monitoring of electrical conductivity enabled assessing two parameters (slope and reaction time constant τ) that served as a measure of polymerization kinetics. This is possible because the electrical conductivity reflects rheological viscosity during a certain part of polymerization and can be considered as a function of the DC. This assumption was confirmed by a good correlation of the conductivity data and the DC data obtained by Raman spectroscopy. The conductivity curve is of a sigmoid shape with inflection points that reflect the major changes in the reaction rate due to autoacceleration and autodeceleration (48). Near the point of vitrification the linearity between the conductivity and DC no longer holds, thus the "middle" linear part of the sigmoid

curve was used for extracting the kinetic parameter slope. Light transmittance data correlated well with the slope, suggesting that optical properties were major determinant of the reaction kinetics for ACP-composites. This is expected, since these materials were compositionally very similar, i.e. based on the same resin and photoinitiator and differing only by 10 wt% of the reinforcing fillers. However, another kinetic parameter representing the reaction time constant, τ, showed no correlation with light transmittance. This is due to a non-linear relationship between the electrical conductivity and DC after the vitrification point. Since the reaction time constant contains information on the reaction kinetics that is well beyond the vitrification point, its value does cannot represent the kinetics during the linear part of the conductivity curve. This explains no correlation between the kinetic parameters slope and τ, since each of them represents polymerization kinetics within different time frames.

While the impedance was measured on a single frequency during light curing to attain higher time resolution, for the long-term setting (up to 24 h) wide range frequency sweeps were performed. The data revealed two distinct electrical contributions which were separated by the equivalent circuit modeling and fitted by the least squares method to assign the electrical contributions to different structural regions within the material. The structural regions differentiated by the analysis were related to differences in particle size between ACP and reinforcing fillers. Additionally, the impedance data was found to be useful for quantifying the amount of water introduced to composited by the ACP fillers. This could be useful in screening the ACP-composites containing ACP produced by "wet chemistry" method in which ACP necessarily retains a certain amount of water after lyophilization (115). The retained water might affect the premature intracomposite ACP conversion, which would impair its bioactivity by reducing the ion-releasing ability, thus shortening the composites' shelf-life.

By investigating various properties of ACP-composites, this study showed that "hybrid" composites containing both bioactive and reinforcing fillers have the potential to be used clinically. Due to inferior mechanical properties (75), the investigated materials are not appropriate for load-bearing restorations, but could be used as temporary filling materials, pit and fissure sealants or liners combined with an overlay of a stronger conventional composite. Recent studies have shown that the mechanical strength of ACP-composites can be considerably improved by decreasing the ACP particle size to the nano-level. The nano-ACP particles have a high surface area to volume ratio and allow sufficient ion release with lower ACP filler loading. This leaves more space for reinforcing, non-degradable glass and silica

fillers and in turn improves mechanical properties. Additionally, the nano-ACP fillers upon their conversion to hydroxyapatite leave much lower porosity in the material structure which is critical for mechanical properties. Both effects greatly improve mechanical properties of ACP-composites based on nano-sized ACP fillers yielding mechanical properties comparable to that of commercial composites.

An important limitation of the experimental setup for impedance measurements is the usage of parallel electrodes which mandated curing the sample from its side through the transparent quartz ring. This caused the inhomogeneity in cure throughout the cylinder of 4 mm radius, and was the reason for the consecutive use of two diametrically positioned curing units. In this way a complete cure was attained after both curing units finished their cycles, but kinetic parameters were different from that obtained by using comb electrodes. The comb electrodes are more appropriate for determining reaction kinetics as they measure electrical properties of a thin layer at the bottom of the sample that is equally distanced from the curing unit tip, unlike the setup with parallel electrodes used in this study (48, 116). The major difference in experimental setup between this study and the study that used the comb electrodes (48) to originally introduce the kinetic parameters derived from impedance data (slope and τ) makes values of these parameters incomparable between two studies. However, the kinetic parameters are well comparable among different materials within a single study. Also, final properties of a completely cured material should not depend much on the experimental setup and are expected to be similar regardless of using the parallel plate or comb electrodes.

ACP fillers used in this study were prepared by the conventional procedure of "wet chemistry" (74). Upon rapid mixing the concentrated aqueous solutions of calcium and phosphate salts, an insoluble calcium phosphate forms that is initially amorphous in structure and becomes crystalline with aging in the solution. If the precipitate is separated from the solution and lyophilized quickly enough, it remains in the amorphous state. Thus obtained ACP could be stable for an indeterminate time, if kept in dry conditions. This is the simplest and technically the least demanding method of ACP production. The shortcoming of ACP obtained by this method is a wide distribution of particle size and dependence of particle size on the preparation conditions. To obtain smaller particles with a more uniform size of 0.2-3 μm, ACP was ball-milled (72). This form of ACP was used many studies to prepare experimental composites which consistently showed good remineralizing capability, but poor mechanical properties (70). The commonly quoted cause of the mechanical properties regularly weaker than those of commercial composites is the lack of silanization of ACP

particles and uncontrolled particle agglomeration causing a wide particle size distribution (8). Mechanical properties were shown to be improved to some extent by the addition of reinforcing fillers in several recent studies (70, 75). Since the ACP-composites investigated in this study are compositionally very similar to those for which mechanical properties were previously investigated, the mechanical tests were not repeated. Instead, this study focused on other properties in order to complement the previous studies on remineralization and mechanical properties. Improvement in mechanical properties would be very beneficial, as it would allow the formulation of "universal" ACP-composites that would be appropriate for any clinical indication, similarly to contemporary microhybrid composites. This could be attained by switching from the wet chemistry of ACP production to the spray drying technique (76) which allows the preparation of nano-sized ACP particles. Many advantages of nano-ACP were reported, among which the most notable is a considerable improvement in mechanical properties (117). Thus the major shortcoming of the "large-particle" ACP-composites used in this study could be overcome by changing the ACP production process and using nano-sized particles which are much smaller and more uniform in size. The transition to smaller ACP particles in order to improve properties in some sense mimics the evolution of conventional composites, which similarly underwent a progressive decrease in the particle size.

At the end of the discussion, some suggestions for future investigations could be listed:

- Study of the effect of pH on the kinetics of ion release. Since the ion release for most of ACP-composites was determined at neutral pH, it would be interesting to explore the effect of decreasing pH on the ion release. It is expected that the ion release would increase at lower pH, which implies that lower amounts of ACP than the currently used 40 wt% could be used. Lower amounts of ACP would allow higher load of reinforcing fillers, thus improving mechanical properties and mitigating the effect of degradation.
- Formulation of ACP-composites based on more hydrophobic resin matrix would be beneficial, as the current materials have rather high water sorption. The increased solubility of ACP at higher pH values may compensate for the lower hydrophilicity of the resin and attain sufficient ion release. In this way, the composites may be non-releasing at the neutral pH and activate the ion release as the pH decreases.
- Real-time DC study should be performed in order to more thoroughly explain the interesting kinetic behavior detected through light transmittance measurements. The observed kinetic behavior should be confirmed by a more direct method (e.g. real-time FTIR), as it may have important implications on polymerization shrinkage development and the final structure of polymeric network.
- Addition of bioactive glass fillers to ACP-composites may stimulate formation of the hydroxyapatite layer on the composite surfaces. Bioactive glasses release calcium and phosphate ions in a similar manner to ACP and additionally have the tendency to form surface hydroxyapatite layers via hydrated silica that acts as crystallization nuclei. Such hydroxyapatite layer could seal the marginal gap, reduce microbial penetration and contribute to the prevention of secondary caries.
- Study of the bond strength of ACP-composites to dentin, to investigate the effect of unsilanized particles prone to degradation on the long-term bond strength. Some preliminary data shows an important effect of the amount of unsilanized particles on the decline in bond strength values.

7. CONCLUSIONS

Within the limitations of this study, it could be concluded that:

- ACP-composites attain very high DC (about 80%) and the DC is not considerably diminished by the addition of inert fillers
- curing efficiency at depth for ACP-composites is comparable to that of conventional composites, with depths of cure of 2-3 mm
- temperature rise produced during light curing of ACP-composites is no more harmful for dental pulp than that of conventional composites
- light transmittance of ACP-composites is in the range of conventional composites
- real-time light transmittance measurements can provide useful information on polymerization kinetics
- ACP-composites have different polymerization kinetics than the materials that contain only reinforcing fillers, with possible consequences on polymerization shrinkage and polymeric network structure
- impedance spectroscopy is a valuable tool for investigating various characteristics of ACP-composites
- impedance data used for describing the extent of polymerization correlates well with the DC data obtained by Raman spectroscopy
- kinetic parameters obtained by impedance measurements correlate well with light transmittance
- impedance measurements could be used to quantify the amount of water introduced to the composite by ACP fillers

8. LITERATURE

1. Ferracane JL. Resin composite--state of the art. Dent Mater 2011;27(1):29-38.
2. Ilie N, Hickel R. Investigations on mechanical behaviour of dental composites. Clin Oral Investig 2009;13(4):427-38.
3. Sarrett DC. Clinical challenges and the relevance of materials testing for posterior composite restorations. Dent Mater 2005;21(1):9-20.
4. Nedeljkovic I, Teughels W, De Munck J, Van Meerbeek B, Van Landuyt KL. Is secondary caries with composites a material-based problem? Dent Mater 2015;31(11):e247-77.
5. Trujillo-Lemon M, Ge J, Lu H, Tanaka J, Stansbury JW. Dimethacrylate derivatives of dimer acid. J Polym Sci Part A: Polym Chem 2006;44(12):3921-9.
6. Ilie N, Hickel R. Macro-, micro- and nano-mechanical investigations on silorane and methacrylate-based composites. Dent Mater 2009;25(6):810-9.
7. Tavassoli Hojati S, Alaghemand H, Hamze F, Ahmadian Babaki F, Rajab-Nia R, Rezvani MB, et al. Antibacterial, physical and mechanical properties of flowable resin composites containing zinc oxide nanoparticles. Dent Mater 2013;29(5):495-505.
8. Skrtic D, Antonucci JM, Eanes ED. Amorphous Calcium Phosphate-Based Bioactive Polymeric Composites for Mineralized Tissue Regeneration. J Res Natl Inst Stand Technol 2003;108(3):167-82.
9. Khvostenko D, Hilton TJ, Ferracane JL, Mitchell JC, Kruzic JJ. Bioactive glass fillers reduce bacterial penetration into marginal gaps for composite restorations. Dent Mater 2016;32(1):73-81.
10. Antonucci JM, Dickens SH, Fowler BO, Xu HH, McDonough WG. Chemistry of Silanes: Interfaces in Dental Polymers and Composites. J Res Natl Inst Stand Technol 2005;110(5):541-58.
11. Kumar N, Khoso NA, Sangi L, Bhangar F, Kalhoro FA. Dental Resin-based Composites: A Transition from Macrofilled to Nanofilled J Pak Dent Assoc 2012;1:39-44.
12. Beun S, Glorieux T, Devaux J, Vreven J, Leloup G. Characterization of nanofilled compared to universal and microfilled composites. Dent Mater 2007;23(1):51-9.

13. Ilie N, Hickel R, Watts DC. Spatial and cure-time distribution of dynamic-mechanical properties of a dimethacrylate nano-composite. Dent Mater 2009;25(3):411-8.
14. Tarle Z, Attin T, Marovic D, Andermatt L, Ristic M, Taubock TT. Influence of irradiation time on subsurface degree of conversion and microhardness of high-viscosity bulk-fill resin composites. Clin Oral Investig 2015;19(4):831-40.
15. Ilie N, Bucuta S, Draenert M. Bulk-fill resin-based composites: an in vitro assessment of their mechanical performance. Oper Dent 2013;38(6):618-25.
16. Bucuta S, Ilie N. Light transmittance and micro-mechanical properties of bulk fill vs. conventional resin based composites. Clin Oral Investig 2014;18(8):1991-2000.
17. Peutzfeldt A. Resin composites in dentistry: the monomer systems. Eur J Oral Sci 1997;105(2):97-116.
18. Rueggeberg FA. From vulcanite to vinyl, a history of resins in restorative dentistry. J Prosthet Dent 2002;87(4):364-79.
19. Awad D, Ilie N. Effect of polymerisation and ageing on the incremental bond strength of ormocer-based dental materials. Clin Oral Investig 2013;17(5):1339-47.
20. Panduric V, Tarle Z, Hameršak Z, Stipetić I, Matosevic D, Negovetić-Mandić V, et al. Detection of HEMA in self-etching adhesive systems with high performance liquid chromatography. J Mol Struct 2009;924-926:358-60.
21. Frauscher KE, Ilie N. Degree of conversion of nano-hybrid resin-based composites with novel and conventional matrix formulation. Clin Oral Investig 2013;17(2):635-42.
22. Stansbury JW. Curing dental resins and composites by photopolymerization. J Esthet Dent 2000;12(6):300-8.
23. Jakubiak J, Allonas X, Fouassier JP, Sionkowska A, Andrzejewska E, Linden LÅ, et al. Camphorquinone–amines photoinitating systems for the initiation of free radical polymerization. Polymer 2003;44(18):5219-26.
24. Santini A, Miletic V, Swift MD, Bradley M. Degree of conversion and microhardness of TPO-containing resin-based composites cured by polywave and monowave LED units. J Dent 2012;40(7):577-84.
25. Par M, Lapas-Barisic M, Gamulin O, Panduric V, Spanovic N, Tarle Z. Long Term Degree of Conversion of two Bulk-Fill Composites. Acta Stomatol Croat 2016;50(4):292-300.

26. Chung KH, Greener EH. Correlation between degree of conversion, filler concentration and mechanical properties of posterior composite resins. J Oral Rehabil 1990;17(5):487-94.
27. Schulze KA, Zaman AA, Söderholm K-JM. Effect of filler fraction on strength, viscosity and porosity of experimental compomer materials. J Dent 2003;31(6):373-82.
28. Drummond JL. Degradation, fatigue, and failure of resin dental composite materials. J Dent Res 2008;87(8):710-9.
29. Lambrechts P, Goovaerts K, Bharadwaj D, De Munck J, Bergmans L, Peumans M, et al. Degradation of tooth structure and restorative materials: A review. Wear 2006;261(9):980-6.
30. Ferracane JL, Berge HX, Condon JR. In vitro aging of dental composites in water - effect of degree of conversion, filler volume, and filler/matrix coupling. J Biomed Mater Res 1998;42(3):465-72.
31. Hashimoto M, Ohno H, Kaga M, Endo K, Sano H, Oguchi H. In vivo degradation of resin-dentin bonds in humans over 1 to 3 years. J Dent Res 2000;79(6):1385-91.
32. Durner J, Obermaier J, Draenert M, Ilie N. Correlation of the degree of conversion with the amount of elutable substances in nano-hybrid dental composites. Dent Mater 2012;28(11):1146-53.
33. Silikas N, Eliades G, Watts DC. Light intensity effects on resin-composite degree of conversion and shrinkage strain. Dent Mater 2000;16(4):292-6.
34. Andrzejewska E. Photopolymerization kinetics of multifunctional monomers. Prog Polym Sci 2001;26(4):605-65.
35. Tarle Z, Knezevic A, Demoli N, Meniga A, Sutaloa J, Unterbrink G, et al. Comparison of composite curing parameters: effects of light source and curing mode on conversion, temperature rise and polymerization shrinkage. Oper Dent 2006;31(2):219-26.
36. Czasch P, Ilie N. In vitro comparison of mechanical properties and degree of cure of bulk fill composites. Clin Oral Investig 2013;17(1):227-35.
37. Par M, Gamulin O, Marovic D, Klaric E, Tarle Z. Raman spectroscopic assessment of degree of conversion of bulk-fill resin composites--changes at 24 hours post cure. Oper Dent 2015;40(3):E92-101.
38. Par M, Gamulin O, Marovic D, Klaric E, Tarle Z. Effect of temperature on post-cure polymerization of bulk-fill composites. J Dent 2014;42(10):1255-60.

39. Stansbury JW, Trujillo-Lemon M, Lu H, Ding X, Lin Y, Ge J. Conversion-dependent shrinkage stress and strain in dental resins and composites. Dent Mater 2005;21(1):56-67.
40. Braga RR, Ferracane JL. Contraction Stress Related to Degree of Conversion and Reaction Kinetics. J Dent Res 2002;81(2):114-8.
41. Ferracane JL. Buonocore Lecture. Placing dental composites--a stressful experience. Oper Dent 2008;33(3):247-57.
42. Schneider LF, Cavalcante LM, Silikas N. Shrinkage Stresses Generated during Resin-Composite Applications: A Review. J Dent Biomech 2010;2010.
43. Braga RR, Ballester RY, Ferracane JL. Factors involved in the development of polymerization shrinkage stress in resin-composites: a systematic review. Dent Mater 2005;21(10):962-70.
44. Arikawa H, Fujii K, Kanie T, Inoue K. Light transmittance characteristics of light-cured composite resins. Dent Mater 1998;14(6):405-11.
45. Ilie N, Durner J. Polymerization kinetic calculations in dental composites: a method comparison analysis. Clin Oral Investig 2014;18(6):1587-96.
46. Alshali RZ, Salim NA, Satterthwaite JD, Silikas N. Long-term sorption and solubility of bulk-fill and conventional resin-composites in water and artificial saliva. J Dent 2015;43(12):1511-8.
47. Skrtic D, Antonucci JM. Dental composites based on amorphous calcium phosphate - resin composition/physicochemical properties study. J Biomater Appl 2007;21(4):375-93.
48. Steinhaus J, Hausnerova B, Haenel T, Grossgarten M, Moginger B. Curing kinetics of visible light curing dental resin composites investigated by dielectric analysis (DEA). Dent Mater 2014;30(3):372-80.
49. Par M, Santic A, Gamulin O, Marovic D, Mogus-Milankovic A, Tarle Z. Impedance changes during setting of amorphous calcium phosphate composites. Dent Mater 2016;32(11):1312-21.
50. Kuper NK, Opdam NJ, Bronkhorst EM, Huysmans MC. The influence of approximal restoration extension on the development of secondary caries. J Dent 2012;40(3):241-7.
51. Mjör IA. Clinical diagnosis of recurrent caries. J Am Dent Assoc 2005;136(10):1426-33.
52. Jokstad A. Secondary caries and microleakage. Dent Mater 2016;32(1):11-25.

53. Ferracane JL. Resin-based composite performance: are there some things we can't predict? Dent Mater 2013;29(1):51-8.
54. Jandt KD, Sigusch BW. Future perspectives of resin-based dental materials. Dent Mater 2009;25(8):1001-6.
55. Cheng L, Weir MD, Xu HH, Kraigsley AM, Lin NJ, Lin-Gibson S, et al. Antibacterial and physical properties of calcium-phosphate and calcium-fluoride nanocomposites with chlorhexidine. Dent Mater 2012;28(5):573-83.
56. Imazato S. Antibacterial properties of resin composites and dentin bonding systems. Dent Mater 2003;19(6):449-57.
57. Antonucci JM, Skrtic D. Fine-Tuning of Polymeric Resins and Their Interfaces with Amorphous Calcium Phosphate. A Strategy for Designing Effective Remineralizing Dental Composites. Polymers 2010;2(4):378-92.
58. Langhorst SE, O'Donnell JN, Skrtic D. In vitro remineralization of enamel by polymeric amorphous calcium phosphate composite: quantitative microradiographic study. Dent Mater 2009;25(7):884-91.
59. Mehdawi I, Neel EA, Valappil SP, Palmer G, Salih V, Pratten J, et al. Development of remineralizing, antibacterial dental materials. Acta Biomater 2009;5(7):2525-39.
60. Chiari MD, Rodrigues MC, Xavier TA, de Souza EM, Arana-Chavez VE, Braga RR. Mechanical properties and ion release from bioactive restorative composites containing glass fillers and calcium phosphate nano-structured particles. Dent Mater 2015;31(6):726-33.
61. Mehdawi IM, Pratten J, Spratt DA, Knowles JC, Young AM. High strength re-mineralizing, antibacterial dental composites with reactive calcium phosphates. Dent Mater 2013;29(4):473-84.
62. Xu HH, Weir MD, Sun L. Calcium and phosphate ion releasing composite: effect of pH on release and mechanical properties. Dent Mater 2009;25(4):535-42.
63. Skrtic D, Antonucci JM, Eanes ED, Eidelman N. Dental composites based on hybrid and surface-modified amorphous calcium phosphates. Biomaterials 2004;25(7-8):1141-50.
64. Qidwai M, Sheraz MA, Ahmed S, Alkhuraif AA, ur Rehman I. Preparation and characterization of bioactive composites and fibers for dental applications. Dent Mater 2014;30(10):e253-63.
65. Dorozhkin SV. Amorphous calcium (ortho)phosphates. Acta Biomater 2010;6(12):4457-75.

66. Zhao J, Liu Y, Sun WB, Zhang H. Amorphous calcium phosphate and its application in dentistry. Chem Cent J 2011;5:40.
67. Zhang F, Allen AJ, Levine LE, Espinal L, Antonucci JM, Skrtic D, et al. Ultra-small-angle X-ray scattering-X-ray photon correlation spectroscopy studies of incipient structural changes in amorphous calcium phosphate-based dental composites. J Biomed Mater Res A 2012;100(5):1293-306.
68. Zhang F, Allen AJ, Levine LE, Vaudin MD, Skrtic D, Antonucci JM, et al. Structural and dynamical studies of acid-mediated conversion in amorphous-calcium-phosphate based dental composites. Dent Mater 2014;30(10):1113-25.
69. Wang L, Nancollas GH. Calcium Orthophosphates: Crystallization and Dissolution. Chem Rev 2008;108(11):4628-69.
70. Marovic D, Tarle Z, Hiller KA, Muller R, Ristic M, Rosentritt M, et al. Effect of silanized nanosilica addition on remineralizing and mechanical properties of experimental composite materials with amorphous calcium phosphate. Clin Oral Investig 2014;18(3):783-92.
71. Skrtic D, Antonucci JM, Eanes ED, Brunworth RT. Silica- and zirconia-hybridized amorphous calcium phosphate: effect on transformation to hydroxyapatite. J Biomed Mater Res 2002;59(4):597-604.
72. Lee SY, Regnault WF, Antonucci JM, Skrtic D. Effect of particle size of an amorphous calcium phosphate filler on the mechanical strength and ion release of polymeric composites. J Biomed Mater Res B Appl Biomater 2007;80(1):11-7.
73. Skrtic D, Antonucci JM, McDonough WG, Liu DW. Effect of chemical structure and composition of the resin phase on mechanical strength and vinyl conversion of amorphous calcium phosphate-based composites. J Biomed Mater Res A 2004;68(4):763-72.
74. Skrtic D, Antonucci JM, Liu DW. Ethoxylated bisphenol dimethacrylate-based amorphous calcium phosphate composites. Acta Biomater 2006;2(1):85-94.
75. Marovic D, Tarle Z, Hiller KA, Muller R, Rosentritt M, Skrtic D, et al. Reinforcement of experimental composite materials based on amorphous calcium phosphate with inert fillers. Dent Mater 2014;30(9):1052-60.
76. Xu HH, Moreau JL, Sun L, Chow LC. Nanocomposite containing amorphous calcium phosphate nanoparticles for caries inhibition. Dent Mater 2011;27(8):762-9.

77. Dunn WJ. Shear bond strength of an amorphous calcium-phosphate-containing orthodontic resin cement. Am J Orthod Dentofacial Orthop 2007;131(2):243-7.
78. Melo MA, Weir MD, Rodrigues LK, Xu HH. Novel calcium phosphate nanocomposite with caries-inhibition in a human in situ model. Dent Mater 2013;29(2):231-40.
79. Li F, Wang P, Weir MD, Fouad AF, Xu HH. Evaluation of antibacterial and remineralizing nanocomposite and adhesive in rat tooth cavity model. Acta Biomater 2014;10(6):2804-13.
80. Boskey AL, Posner AS. Conversion of amorphous calcium phosphate to microcrystalline hydroxyapatite. A pH-dependent, solution-mediated, solid-solid conversion. J Phys Chem 1973;77(19):2313-7.
81. Zhang L, Weir MD, Chow LC, Antonucci JM, Chen J, Xu HH. Novel rechargeable calcium phosphate dental nanocomposite. Dent Mater 2016;32(2):285-93.
82. O'Donnell JN, Skrtic D. Degree of vinyl conversion, polymerization shrinkage and stress development in experimental endodontic composite. J Biomim Biomater Tissue Eng 2009;4:1-12.
83. Par M, Gamulin O, Marovic D, Skenderovic H, Klaric E, Tarle Z. Conversion and temperature rise of remineralizing composites reinforced with inert fillers. J Dent 2016;48:26-33.
84. Antonucci JM, Regnault WF, Skrtic D. Polymerization shrinkage and stress development in amorphous calcium phosphate/urethane dimethacrylate polymeric composites. J Compos Mater 2010;44(3):355.
85. Par M, Marovic D, Skenderovic H, Gamulin O, Klaric E, Tarle Z. Light transmittance and polymerization kinetics of amorphous calcium phosphate composites. Clin Oral Investig 2017;21(4):1173-82.
86. Regnault WF, Icenogle TB, Antonucci JM, Skrtic D. Amorphous calcium phosphate/urethane methacrylate resin composites. I. Physicochemical characterization. J Mater Sci Mater Med 2008;19(2):507-15.
87. Skrtic D, Antonucci JM. Bioactive polymeric composites for tooth mineral regeneration: physicochemical and cellular aspects. J Funct Biomater 2011;2(3):271-307.
88. Xu HH, Weir MD, Sun L, Moreau JL, Takagi S, Chow LC, et al. Strong nanocomposites with Ca, PO(4), and F release for caries inhibition. J Dent Res 2010;89(1):19-28.

89. Eanes ED, Termine JD, Nylen MU. An electron microscopic study of the formation of amorphous calcium phosphate and its transformation to crystalline apatite. Calcif Tissue Res 1973;12(2):143-58.
90. Ferracane JL, Greener EH. The effect of resin formulation on the degree of conversion and mechanical properties of dental restorative resins. J Biomed Mater Res 1986;20(1):121-31.
91. Ilie N, Obermaier J, Durner J. Effect of modulated irradiation time on the degree of conversion and the amount of elutable substances from nano-hybrid resin-based composites. Clin Oral Investig 2014;18(1):97-106.
92. Miletic V, Santini A. Micro-Raman spectroscopic analysis of the degree of conversion of composite resins containing different initiators cured by polywave or monowave LED units. J Dent 2012;40(2):106-13.
93. Pianelli C, Devaux J, Bebelman S, Leloup G. The micro-Raman spectroscopy, a useful tool to determine the degree of conversion of light-activated composite resins. J Biomed Mater Res 1999;48(5):675-81.
94. Li X, Pongprueksa P, Van Meerbeek B, De Munck J. Curing profile of bulk-fill resin-based composites. J Dent 2015;43(6):664-72.
95. Zhang Y, Son H, Zhang J, Kong J, Liu Z. Laser-Heating Effect on Raman Spectra of Individual Suspended Single-Walled Carbon Nanotubes. J Phys Chem 2007;111(5):1988-92.
96. Marigheto NA, Kemsley EK, Potter J, Belton PS, Wilson RH. Effects of sample heating in FT-Raman spectra of biological materials. Spectrochim Acta Part A 1996;52(12):1571-9.
97. Miletic VJ, Santini A. Remaining unreacted methacrylate groups in resin-based composite with respect to sample preparation and storing conditions using micro-Raman spectroscopy. J Biomed Mater Res B Appl Biomater 2008;87(2):468-74.
98. Ferracane JL. Elution of leachable components from composites. J Oral Rehabil 1994;21(4):441-52.
99. Soares LE, Nahorny S, Martin AA. FT-Raman spectroscopy study of organic matrix degradation in nanofilled resin composite. Microsc Microanal 2013;19(2):327-34.
100. Tarle Z, Meniga A, Knezevic A, Sutalo J, Ristic M, Pichler G. Composite conversion and temperature rise using a conventional, plasma arc, and an experimental blue LED curing unit. J Oral Rehabil 2002;29(7):662-7.

101. Antonucci JM, Toth EE. Extent of polymerization of dental resins by differential scanning calorimetry. J Dent Res 1983;62(2):121-5.
102. Zach L, Cohen G. Pulp response to externally applied heat. Oral Surg Oral Med Oral Pathol 1965;19:515-30.
103. Baldissara P, Catapano S, Scotti R. Clinical and histological evaluation of thermal injury thresholds in human teeth: a preliminary study. J Oral Rehabil 1997;24(11):791-801.
104. Atai M, Motevasselian F. Temperature rise and degree of photopolymerization conversion of nanocomposites and conventional dental composites. Clin Oral Investig 2009;13(3):309-16.
105. Uhl A, Mills RW, Jandt KD. Polymerization and light-induced heat of dental composites cured with LED and halogen technology. Biomaterials 2003;24(10):1809-20.
106. Price RB, Ferracane JL, Shortall AC. Light-Curing Units: A Review of What We Need to Know. J Dent Res 2015;94(9):1179-86.
107. Clewell DH. Scattering of Light by Pigment Particles. J Opt Soc Am 1941;31(8):521-7.
108. Ruyter IE, Oysaed H. Conversion in different depths of ultraviolet and visible light activated composite materials. Acta Odontol Scand 1982;40(3):179-92.
109. Harrington E, Wilson HJ, Shortall AC. Light-activated restorative materials: a method of determining effective radiation times. J Oral Rehabil 1996;23(3):210-8.
110. Howard B, Wilson ND, Newman SM, Pfeifer CS, Stansbury JW. Relationships between conversion, temperature and optical properties during composite photopolymerization. Acta Biomater 2010;6(6):2053-9.
111. Seghi RR, Gritz MD, Kim J. Colorimetric changes in composites resulting from visible-light-initiated polymerization. Dent Mater 1992;6(2):133-7.
112. Kidner NJ, Perry NH, Mason TO, Garboczi EJ. The Brick Layer Model Revisited: Introducing the Nano-Grain Composite Model. J Am Ceram Soc 2008;91(6):1733-46.
113. Jonscher AK. Dielectric relaxation in solids. J Phys D: Appl Phys 1999;32(14):R57-R70.
114. Irvine JTS, Sinclair DC, West AR. Electroceramics: Characterization by Impedance Spectroscopy. Adv Mater 1990;2(3):132-8.

115. Combes C, Rey C. Amorphous calcium phosphates: synthesis, properties and uses in biomaterials. Acta Biomater 2010;6(9):3362-78.
116. Steinhaus J, Hausnerova B, Haenel T, Selig D, Duvenbeck F, Moeginger B. Correlation of shear and dielectric ion viscosity of dental resins - Influence of composition, temperature and filler content. Dent Mater 2016;32(7):899-907.
117. Cheng L, Weir MD, Xu HH, Antonucci JM, Kraigsley AM, Lin NJ, et al. Antibacterial amorphous calcium phosphate nanocomposites with a quaternary ammonium dimethacrylate and silver nanoparticles. Dent Mater 2012;28(5):561-72.

9. CURRICULUM VITAE

Matej Par graduated from the School of Dental Medicine in Zagreb in year 2011 with the weighted average grade of 4.95. During the undergraduate study, he was a student assistant for chemistry and physiology, editor of the student journal "Sonda", and coordinator of the student section for research. He was awarded four dean's awards, a rector's award, special rector's award, stipend of the Ministry of science and education, stipend of the city of Zagreb for undergraduate students, and stipend of the city of Zagreb for doctoral students. He spent the period from October 2016 to April 2017 in the study visit at the Ludwig Maximilian University in Munich under the supervision of Prof. Dr. Nicoleta Ilie.

List of publications

Matej Par, Matea Lapas-Barisic, Ozren Gamulin, Vlatko Panduric, Nika Spanovic, Zrinka Tarle. Long Term Degree of Conversion of two Bulk-Fill Composites. Acta Stomatologica Croatica 2016;12:50(4):292-300.

Matej Par, Ana Šantić, Ozren Gamulin, Danijela Marovic, Andrea Moguš-Milanković, Zrinka Tarle. Impedance changes during setting of amorphous calcium phosphate composites. Dental Materials 2016; 32(11):1312-21.

Matej Par, Danijela Marovic, Hrvoje Skenderovic, Ozren Gamulin, Eva Klaric, Zrinka Tarle. Light transmittance and polymerization kinetics of amorphous calcium phosphate composites. Clinical Oral Investigations 2017;21(4):1173-82.

Matej Par, Ozren Gamulin, Danijela Marovic, Hrvoje Skenderovic, Eva Klaric, Zrinka Tarle. Conversion and temperature rise of remineralizing composites reinforced with inert fillers. Journal of Dentistry 2016;48:26-33.

Eva Klaric, Mario Rakic, Ivan Sever, Ognjen Milat, **Matej Par**, Zrinka Tarle. Enamel and Dentin Microhardness and Chemical Composition After Experimental Light-activated Bleaching. Operative Dentistry 2015;40(4):E132-41.

Matej Par, Ozren Gamulin, Danijela Marovic, Eva Klaric, Zrinka Tarle. Raman Spectroscopic Assessment of Degree of Conversion of Bulk-Fill Resin Composites – Changes at 24 Hours Post Cure. Operative Dentistry 2015;40(3):E91-101.

Ante Jordan, Ana Badovinac, Stjepan Špalj, **Matej Par**, Martina Šlaj, Darije Plančak. Factors influencing intensive care nurses' knowledge and attitudes regarding ventilator-associated pneumonia and oral care practice in intubated patients in Croatia. American Journal of Infection Control 2014;42(10):1115-7.

Matej Par, Ozren Gamulin, Danijela Marovic, Eva Klaric, Zrinka Tarle. Effect of temperature on post-cure polymerization of bulk-fill composites. Journal of Dentistry 2014;42(10):1255-60.

Matej Par, Ana Badovinac, Darije Plancak. Oral hygiene is an important factor for prevention of ventilator-associated pneumonia. Acta Clinica Croatica 2014;53(1):72-8.

Eva Klaric, **Matej Par**, Ivona Profeta, Nevenka Kopjar, Ruzica Rozgaj, Vilena Kasuba, Davor Zeljezic, Zrinka Tarle. Genotoxic Effect of Two Bleaching Agents on Oral Mucosa. Cancer Genomics and Proteomics 2013;10(5):209-15.

Eva Klarić, **Matej Par**, Ivona Profeta, Danijela Matošević, Zrinka Tarle. Postoperative sensitivity after two in-office bleaching methods. Acta Stomatologica Croatica 2011;45(2):100-9.